POLITECNICO DI TORINO

in collaboration with

ÉCOLE POLYTECHNIQUE FÉDÉRALE DE LAUSANNE

Master's Degree in Geotechnical Civil Engineering

Hydro-mechanical response of a gas shale upon suction variations: experimental analysis and preliminary modelling

Supervisors:

Prof. Guido Musso, Politecnico di Torino

Prof. Alessio Ferrari, EPFL

Vincenzo Sergio Vespo, Politecnico di Torino

Candidate:

Sara Incollingo

March 2020

" It's called wayfinding, princess. It's not just sails and knots,

it's seeing where you're going in your mind.

Knowing where you are by knowing where you've been."

Mauii

from "Moana-Disney"

Table of Contents

List of Figures

List of Tables

List of Equations

Abstract EN

Shales are a fine-grained and laminated sedimentary geomaterials. Due to their particular features and their large worldwide presence in the Earth's crust, they are of interest in several geo-engineering applications such as oil and gas extraction, CO_2 sequestration and nuclear waste disposal.

In light of the engineering applications many challenges exist related to the characterization of the mechanical behaviour of these geomaterials for which temperature, chemistry and unsaturated conditions play a key role. In particular, it is really important to study and understand how these materials behave in the partially saturated condition in which they are found. It is also relevant to know how their geomechanical proprieties vary due to the changes in water content.

The study conducted in this thesis aims at improving the knowledge on the behaviour of partially water saturated shales involved in the gas extraction by analysing the change in water content and in volume upon suction under free stress conditions.

Due to the peculiar features of gas shales (e.g. low porosity, low permeability and reduced dimensions of pores), the use of the vapour equilibrium technique is required to study the water retention capacity of the tested material.

Advanced experiments were set up with the aim of characterizing the material from a macro scale to a micro scale.

Firstly, the hydro-mechanical response of the tested gas shale was investigated looking at the swelling and shrinkage behaviour experienced due to the change in water content. Then, the microstructural response was studied upon suction variation using micro-CT analyses.

The experimental results obtained in terms of volumetric deformation in free stress conditions during hydraulic loading show a significant anisotropy and irreversibility in the behaviour.

Cracks opening upon water content evolution was observed at the macro scale and then studied further in details at the micro scale, paying attention also to their changes in thickness due to wetting and drying.

In summary, due to the water uptake, a macroscopic expansion was observed associated with the swelling of the clay minerals inside the shale matrix and with the opening of the micro cracks.

On the other hand, due to the water content reduction during drying, a decrease in volume was observed without registering closing of the openings.

Experimental results obtained indicate the response of the material upon suction variation and the relevant role of partial saturation for a reliable and complete understanding in the hydro-mechanical characterization of the tested gas shale.

Furthermore, a preliminary model was developed in order to reproduce the experimental results in terms of changes in water content, due to suction variations, with time.

The numerical analyses were implemented in the Finite Element code COMSOL Multiphysics 5.5, allowing to define suitable values of the vapour diffusion coefficient for the tested gas shales.

In particular, the variation of the tortuosity factor with the imposed total suction steps was studied through back analysis.

This parameter describes the tortuosity variable for the diffusion of the water vapour trough the porous media, and the evolution with suction that was obtained seems to suggest further the importance of the role of crack aperture on the equilibration times.

Keywords: Gas shale, gas extraction, shale characterization, water retention properties, hydro-mechanical behaviour, partial saturation, vapour diffusion, anisotropy, crack opening.

Riassunto IT

Le shales sono geomateriali di origine sedimentaria caratterizzate da una struttura laminata a grana fine. Date le loro peculiari caratteristiche e la loro vasta presenza sulla crosta terrestre, queste sono di interesse per numerose applicazioni ingegneristiche di ambito geo-energetico, come estrazione di olio, gas naturali, stoccaggio di CO_2 e smaltimento di scorie radioattive.

In vista delle applicazioni ingegneristiche, numerose problematiche vengono affrontate con lo scopo di caratterizzare il comportamento di questi geomateriali dove la temperatura, la meccanica, la chimica e la parziale saturazione giocano un ruolo fondamentale. Infatti, quando le shales sono coinvolte in applicazioni geotecniche è molto importante studiarne e comprenderne il loro comportamento dovuto alle condizioni di parziale saturazione nelle quali queste si collocano. Inoltre, è fondamentale conoscere come variano le loro proprietà geomeccaniche dovute alle variazioni di contenuto d'acqua che queste subiscono durante il loro impiego ingegneristico.

Lo studio condotto in questa tesi ha come obiettivo quello di approfondire le conoscenze sul comportamento delle shales sfruttate nell'estrazione di idrocarburi in condizioni di parziale saturazione, analizzando l'evoluzione del contenuto d'acqua e il cambiamento di volume che queste subiscono come conseguenza della variazione di suzione applicata.

Date le loro caratteristiche peculiari, come la bassa permeabilità e porosità e la ridotta dimensione dei pori, la capacità di ritenzione idrica delle shales è studiata mediante la tecnica dell'equilibrio di vapore.

Una serie di esperimenti avanzati sono stati condotti con il fine di studiare il comportamento delle gas shales sia alla scala macroscopica che a quella microscopica.

Inizialmente, l'analisi sperimentale sulla risposta idro-meccanica delle gas shales oggetto di studio è stata condotta ponendo l'attenzione alle deformazioni dovute alla variazione del contenuto d'acqua, guardando ai provini nella loro interezza.

Successivamente è stata analizzata la risposta idro-meccanica alla scala microscopica, attraverso analisi tomografiche micro-CT.

I risultati ottenuti in termini di deformazioni volumetriche mostrano, in assenza di confinamento, un comportamento anisotropo ed irreversibile della shale soggetta a carichi idraulici.

Durante il processo di imbibizione di un provino si è osservata visivamente l'apertura di una fessura naturale, fenomeno studiato nel dettaglio da un punto di vista microscopico attraverso le analisi tomografiche.

In particolare, dalle analisi sperimentali si è evinto che, dato il processo di imbibizione, le shale sono caratterizzate da un comportamento rigonfiante dovuto al processo di idratazione della componente argillosa nella matrice della shale e dall'apertura, osservata al tomografo, delle microfessure del materiale.

Durante il processo di essiccamento invece, i risultati ottenuti indicano un comportamento contraente del materiale senza una chiara diminuzione dell'apertura delle microfessure.

I risultati sperimentali ottenuti durante il percorso di tesi dimostrano l'importanza della parziale saturazione nella caratterizzazione idro-meccanica delle gas shales analizzate.

E' stato inoltre sviluppato un modello numerico preliminare al fine di riprodurre i risultati sperimentali ottenuti in termini di variazione del contenuto d'acqua dovuto ai diversi livelli di suzione totale imposti nel tempo.

Le analisi numeriche condotte, implementate attraverso il software agli Elementi Finiti COMSOL Multiphysics 5.5 hanno permesso di definire dei valori del coefficiente di diffusione per le gas shales oggetto di studio.

In particolare è stata studiata la variazione del parametro di tortuosità al variare della suzione imposta mediante il processo di analisi a ritroso.

Tale parametro tiene in conto della variabile di tortuosità della diffusione del vapore nei mezzi porosi. L' evoluzione di quest'ultimo con la suzione, conferma l'importanza del ruolo dell'apertura delle microfessure sui tempi di equalizzazione.

Parole chiave: Gas shale, estrazione di gas naturale, caratterizzazione della shale, proprietà di ritenzione, comportamento idro-meccanico, parziale saturazione, diffusione del vapore, anisotropia, apertura di fessure.

Introduction

This thesis presents the results of an experimental/numerical study on the hydro-mechanical behaviour of samples of shale.

The study conducted is devoted to improve the knowledge of the behaviour of partially water saturated shales of interest for the gas extraction by analysing the change in water content and in volume upon suction variation in free stress conditions.

In order to understand this complex geomaterial and the protocol of study this report is organised as follows:

Chapter 1 presents an overview of shales. Their origins and main features are discussed and their classification is highlighted from a geological point of view to an engineering practice. According to that, their field applications are presented paying attention to the hydraulic conditions at which they are found.

Chapter 2 presents the basic concepts useful in order to understand the behaviour of unsaturated geomaterials. Firstly, the interactions between different phases are described, the role of suction is presented and then the relationship that links the water content in porous geomaterial and suction is largely discussed. Moreover, in this chapter is reported the theory of the volumetric response of unsaturated geomaterials upon suction variation and a protocol for the study conducted related to the tested gas shale.

In *Chapter 3* the basic geotechnical characterization of the tested gas shales is reported, highlighting the limitations of the experimental methodologies applied when the tested material are shales due to their particular features such as low porosity and low permeability and high-water retention properties. This chapter is recalled several times during this thesis as the initial point of the experimental investigation of concern.

Chapter 4 is dedicated to the analysis of the water retention behaviour of gas shale and it is conducted with the aim of understanding how the changes in relative humidity of the samples affects the water content and the volumetric response of these geomaterials, paying attention to the macro scale. The water retention behaviour is presented in terms of water content and degree of saturation, focusing on the uncertainties related to the determination of the solid density of the material. The hysteresis of the water retention behaviour is highlighted and the irreversibility of the behaviour in free stress conditions.

In *Chapter 5* the change in microstructure using micro-CT analyses of the tested gas shale upon the evolution of the water content is analysed, both in wetting and in drying, and the swelling and shrinkage experienced due to it.

Chapter 6 is dedicated to the numerical analyses conducted in order to reproduce the results obtained during the experimental tests in terms of water content versus time upon total suction variations. The numerical analyses were implemented using the Finite Element code COMSOL Multiphysics 5.5, allowing to define suitable values of the vapour diffusion coefficient for the tested gas shales through back analysis.

Chapter 7 summaries the main outcomes and conclusions of the experimental and numerical studies conducted in this thesis. Further developments and considerations for future work are addressed

1 General Background

The large exploited of shales in several geo-engineering applications due to their particular features and their large worldwide presence in the Earth's crust (≈50-75% of the sedimentary rock of the earth's crust)(Deen 1981), has raised an interest in understanding their geomechanical behaviour, which depends on mechanics, temperature, chemistry and unsaturated conditions.

1.1 Definition of shales and main features

Shales are fine-grained and laminated sedimentary geomaterials and they are commonly associated with clays due to their small grain size. However, shales have a complex nature because with given gas shales, clay content is highly variable form one formation to another and sometimes other minerals such as quartz, calcite and carbonate dominate.

Depending on the contents, the shales colour can vary from black or grey to brown or red. Shales with organic content (≈1.24-21.35%) are known as organic-rich shales or oil/gas shales or black shales.

In order to characterize shales, not only their heterogeneities and anisotropies are taken into account, but also the environmental conditions in which they are found. In fact, if the formation is found from shallow to great depths, diagenetic and burial histories and natural weathering experienced from shales can vary largely. Consequently, they are characterized by an intermediate behaviour between that of a soil in a shallow shale formation where no diagenesis occurred and that of a rock in deep formations, where the degree of cementation plays a key role in the mechanical behaviour and discontinuities may be observed (Underwood 1966).

According to the aforementioned reasons, each time a shale material is involved in a new engineering application, specific studies should be conducted in order to understand its geomechanical behaviour.

Despite that, the most important common properties between shales that are considered fundamental for the application in engineering fields are:

- low porosity (≈10%), pore size (nm range) and low permeability (nD range) that guarantee a good barrier for the geological disposal of radioactive waste and for the CO_2 sequestration
- in the field of gas-oil extraction from unconventional reservoir, the peculiar water retention proprieties of shales determine the capacity to trap gas and oil inside these geomaterials and to avoid, in the field of nuclear waste disposal, the radionuclide migration or any leakage in the CO_2 storage
- the swelling capacity of shales is exploited in case of fracture creation during constructions
- the high strength and stiffness allows excavation of tunnels and underground cavities in safe conditions.

1.2 Classification of Shale

In order to classify shales is important to distinguish between geological and engineering classification, which differ since geologist and engineers have different objectives.

The geological classification of shale takes into account the lithology of this kind of rock, the texture with the grain size distribution, the colour and the degree of cementation that defines its structure. On the other hand, the engineering classification focuses on the strength proprieties of this kind of geomaterial, the stress history experienced, plasticity features, which depend on clay content, and the swelling and shrinkage conditions.

In general, the term shale is used to classify argillaceous geomaterials consisting of claystone, siltstone, mudstone and marl.

1.2.1 Geological classification

The first geological classification of shales was proposed by Wentworth (1922) who distinguished, based on grain size, between argillaceous material and the remaining sedimentary rocks(Wentworth 1922).

In 1953, Ingram proposed a classification of shales based on their breaking characteristics looking at their lithology and introduced the concept of fissility which is the small-scale lamination and ability to separate along the bedding(Ingram 1953). Starting from that point the term shale became available in the literature. A short schematization of shale formation is reported in *Figure 1-1.*

One step further in the geological classification was made by Underwood in 1967 who divided shales in two categories:

- compaction or “soil like” shales that have experienced low or no diagenesis and have been consolidated by the weight of the overlying sediments
- cemented or “rock like” shales that contain cementing materials such as calcareous, siliceous, phosphatic etc.

Moreover, Underwood (1967) defined in details the geological and chemical mineralogical classification of shales, reported in *Table 1-1*, and although many other authors proposed various classification systems, the Underwood’s one still remains the best geological classification system for shales(Yagiz 2001).

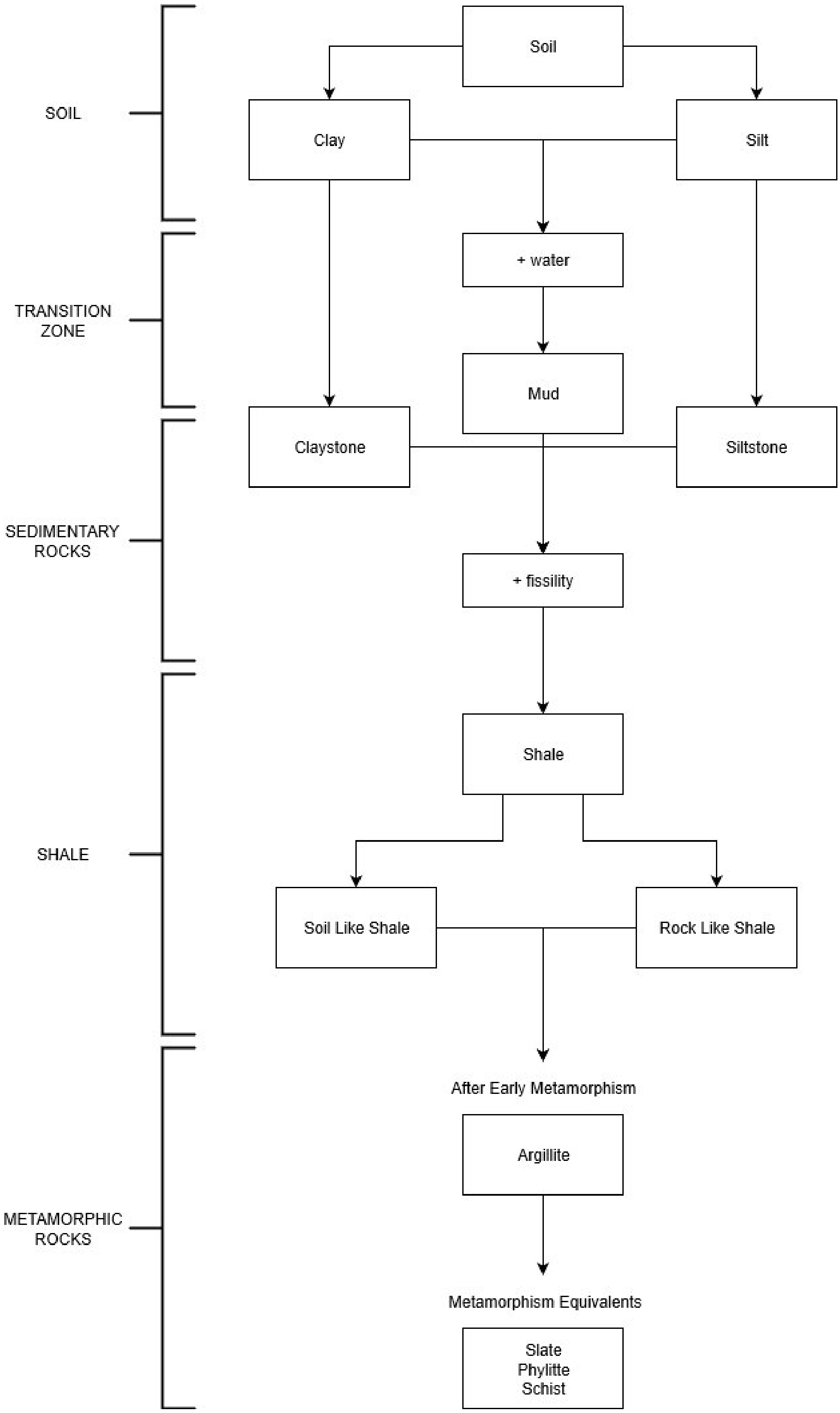

Figure 1-1 Shales and sedimentary rocks, Modified from Underwood 1967

Group	Name	Main Components
"Soil Like" Shale Compacted Shale	Clayey shale	Contain 50% or more clay-sized particles, true clay mineral or clay size particle <0.002mm
	Silty shale	Contain 25% to 45%, silt-sized particles, Silt may be in thin layers between clayey shale bonds
	Sandy shale	Contain 25% to 45%, sand-sized particles, Sand may be in thin layers between clayey shale bonds
	Black shale	Contain organic-rich materials, split into thin semi-flexible sheets
"Rock Like" Shale Cemented Shale	Calcareous shale	Contain 20% to 35% $CaCO_3$ (Marls and shaly chalks contain 35% to 65% $CaCO_3$)
	Siliceous shale	Contain 70% to 85% amorphous silca, often highly siliceous volcanic ash (quartzose shale and detrital quartz)
	Ferruginous shale	Contain 25% to 35% Fe_2O_3 (Potassic shale contain 5% to 10% potash)
	Carbonaceous shale	Carbonaceous materials 3% to 15%, tends to bond constituents together and impart certain degree of toughness
	Clay bonded shale	Welded by re-crystallization of clay minerals or other diagenetic bonds

Table 1-1 Classification of compacted and cemented shale, Yagiz,2001

1.2.2 Engineering classification

As far as the engineering classification is concerned, the large heterogeneity of shales and their particular features such as low permeability, low porosity and their water retention properties make these geomaterials the most difficult rock for sampling and obtaining reliable test data for. Furthermore, in order to study these geomaterials it is impossible to neglect the evidence that their behaviour is affected by water saturation, which makes most of the available experimental methodologies typically used for soils not suitable for shales. Consequently, their classification based on "engineering parameters" remains one of the biggest geotechnical challenges.

The main aspects taking into account in order to classify shales from an engineering point of view regard:

- strength, which is also related to the concept of compacted and cemented shale explained above
- elasticity modules, that vary if the material is subjected to a wetting and drying path due to its water absorption capacity
- permeability and water content, which are related to how well the voids are interconnected and also on the particle size distribution and the clay content of the studied material
- swelling-shrinkage potential, that is related to what kind of clay mineral is contened in the shale and its percentage.

The distinction between compacted and cemented shales is well known since the Underwood's classification. This could be also seen from an engineering point of view because cemented shales present higher strength proprieties than compacted ones, that exhibit lower cohesion (≈15 kPa) and lower friction angle (≈5°). Moreover, strength is also affected by some environmental proprieties, such as moisture content.

In fact, it was observed that an increase in moisture content reduces the Young's modulus. From an experimental point of view this concept was largely studied on a gas shale where it was noticed that wetting the material induced a non-linear decrease of the Young's modulus up to 60% of the elastic modulus measured in dried conditions(Ferrari et al. 2018). In general, uniaxial compressive strength of shales varies from 0,3MPa for weak compaction shales to more than 100MPa for well-cemented shales, but also this parameter is affected by the water saturation and in particular for gas shales a 25% strength reduction was observed when the material was flooded (Ferrari et al. 2018).

As far as the swelling and shrinkage behaviour is concerned, there are many studies in the literature that relate this behaviour to the plastic limit and then to the mineralogy of shales. In fact, it is known that different clay minerals can cause different amounts of swelling. For example, kaolinite and illite are not expansive, whilst montmorillonite expand up to many times its original volume.

1.3 Shale application fields

Due to their particular features, shales are of interest for many applications in the energy-related field. This includes shale gas extraction, CO_2 sequestration and nuclear waste disposal, which represent the hot topics in civil-environment engineering, petroleum engineering and chemical engineering.

1.3.1 Shale gas extraction

According to the International Energy Outlook (IEO) 2019 from the U.S. Energy Information Administration (EIA), natural gas is the world's fastest growing fossil fuel.

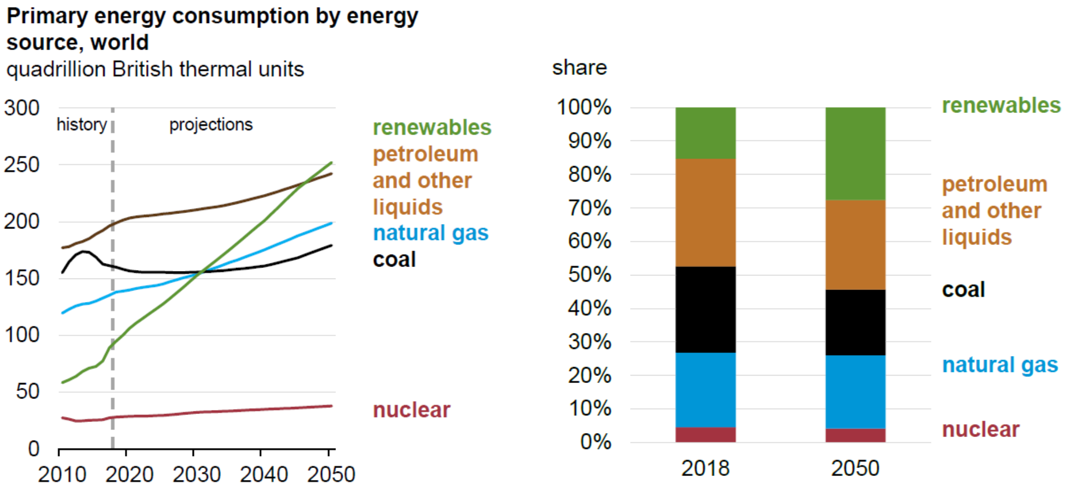

Figure 1-2 Primary energy consumption by energy source, world-from IEO2019

As shown in *Figure 1-2* natural gas consumption is increasing by 1,1% per year, compared with liquids' 0,6% per year growth and coal's 0,4% per year growth.

Moreover, it's possible to observe in *Figure 1-3* that the global natural gas consumption increases more in countries outside the Organization of Economic Cooperation and Development (OECD) especially in the industrial sector, demanding an improvement in oil and natural gas extraction.

The main world producer of natural gas remains the United States, as shown in *Figure 1-4* followed by Middle East and Russia.

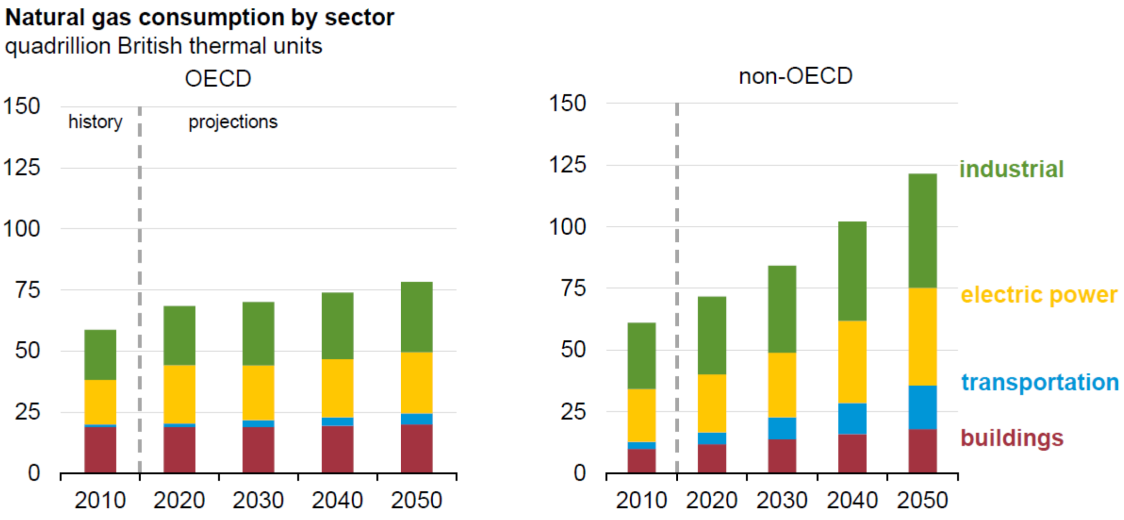

Figure 1-3 Natural gas consumption by sector-from IEO2019

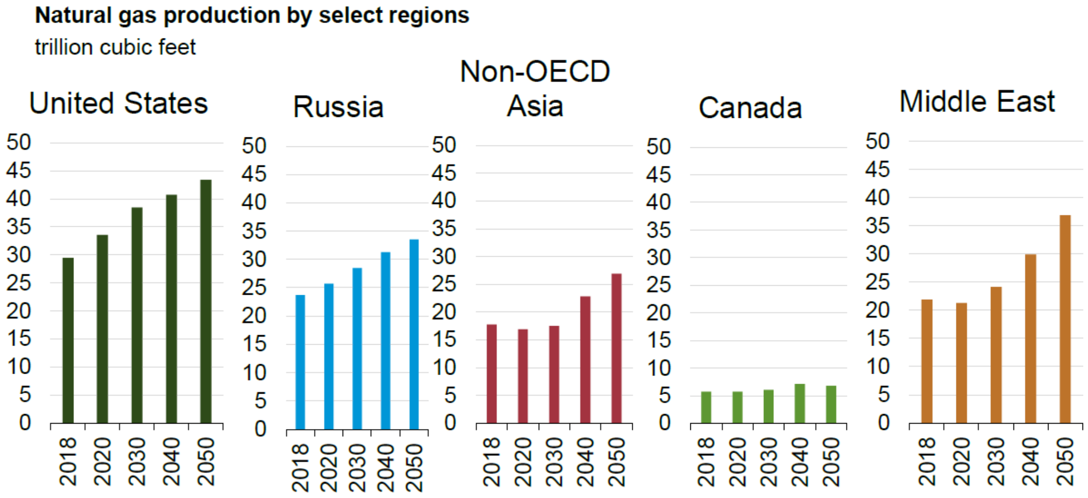

Figure 1-4 Natural gas production by select region-from IEO2019

As regards the United States, shale gas and tight oil can be considered the most important unconventional resources. Shale gas reservoirs in fact are largely exploited in the United States where natural gas extraction is practised majorly from Barnett, Marcellus Eagle Ford and Haynesville shale reservoirs as shown in *Figure 1-5* and *1-6*.

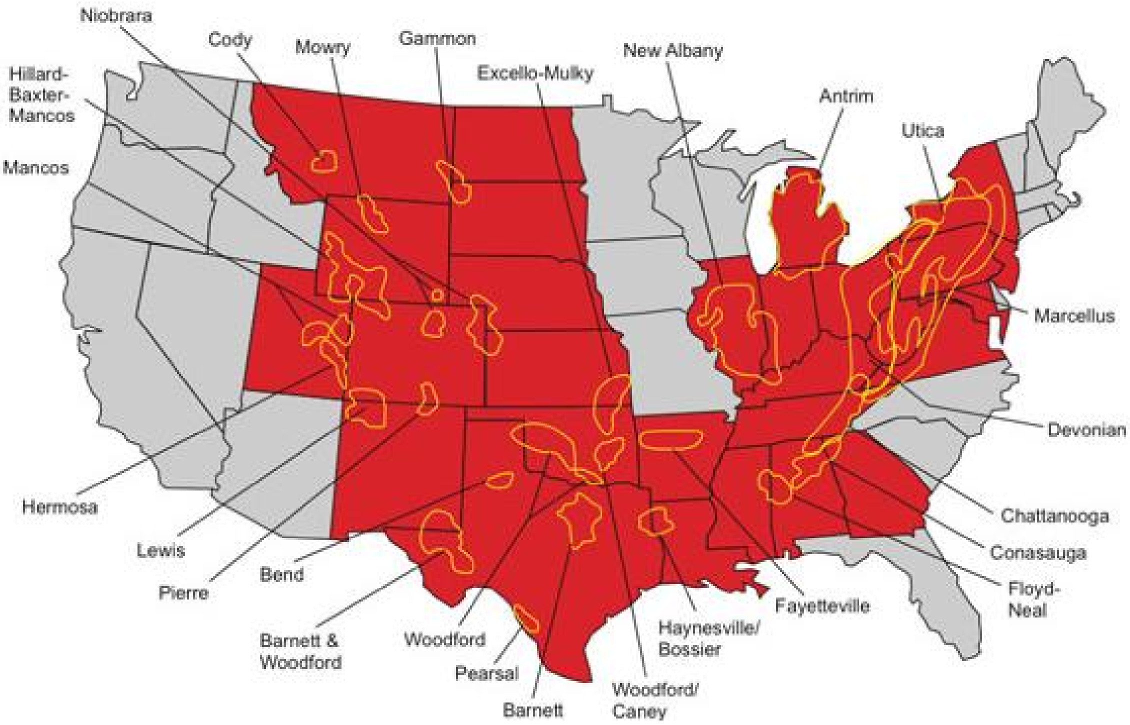

Figure 1-5 Natural gas shale basins in the United States, from T. Boone Pickens' map for shale plays

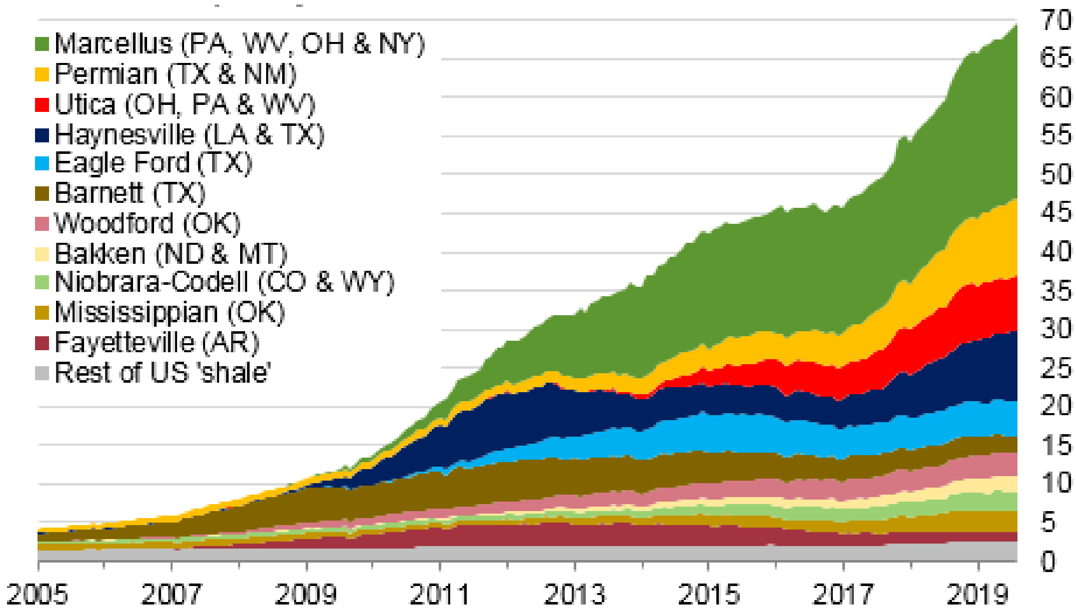

Figure 1-6 Shale gas production from different reservoirs in the United States -from IEO2019

The difference between conventional and unconventional reservoir is due to the main difficulties that derives from the gas extraction.

In some places, natural gas is found in big cracks quite shallow to the ground surface, while in other places, natural gas occurs in small pores within sedimentary rock.

The conventional reservoir is the first case mentioned and the gas extraction can be made by vertical drilling because flows easily up to the surface due to the higher value of permeability and the second one is the unconventional reservoir which is related to low porosity and low permeability and takes into account the main challenges that have to be done in order to produced gas from there*(Figure1-7)*. In fact, in unconventional reservoir hydrocarbons can only be produced through horizontal drilling and multistage fracking, which consist in the injection of millions of cubic meters of water to fracture the material. This technique allows gas release from the rock and permits the gas to flow to and up wells to the surface.

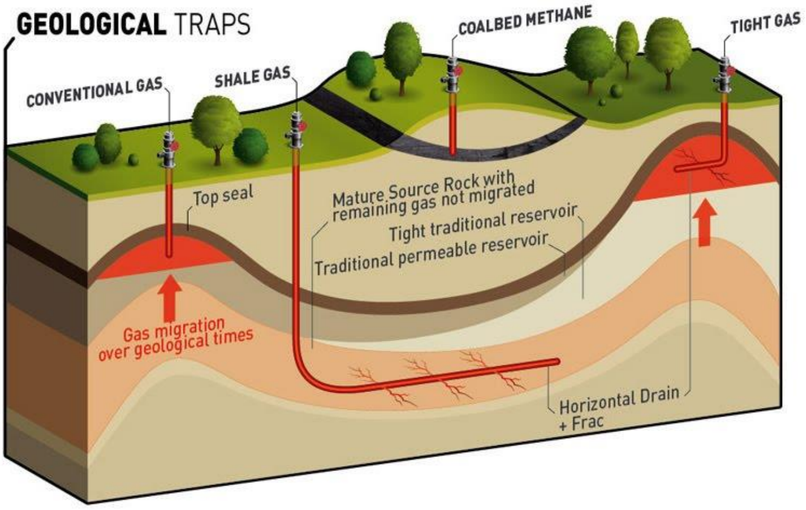

Figure 1-7 Natural gas basin, image from http://www.total.com

The procedure necessary to gain gas from a gas shale reservoir described above, underlines the main problematic issues that geotechnics have to face with in order to understand the behaviour of this geomaterial when it becomes in contact with fracturing water:

- different degree of saturation that induces change in strength proprieties
- swelling potential due to clay content of shale that is responsible for the closure of the wells.

1.3.2 CO_2 sequestration

Due to their particular features, shales are used as a barrier for carbon capture utilization and storage (CCS). They can be regarded as impermeable caprock to prevent CO_2 migration from reservoir and due to their low permeability, low porosity and low hydraulic conductivity they are considered excellent geomaterials for preventing CO_2 leakage after its storage under the ground surface.

The CO_2 sequestration is a critical issue related to environmental engineering whose aim is to block the release of CO_2 into the atmosphere in order to reduce the global warming, by capture it naturally from the atmosphere through biological, chemical and physical processes or by artificial ones that capture CO_2 directly from a gas or a coal-fired power plant and compress it becoming a supercritical fluid before injecting it in the ground surface in order to store it for a long term.

Shales play a key role in this process. Their characteristics can be modified due to the supercritical fluid injected, which leads the geotechnics to understand their behaviour due to the changing in partially saturated condition with the addition of liquid CO_2 in the porous media. Moreover, several studies have reported measurements of swelling in shales' clay minerals induced by CO_2 adsorption, determining a hot topic of studies about the interaction of CO_2 and shale matrix(Liu et al. 2019).

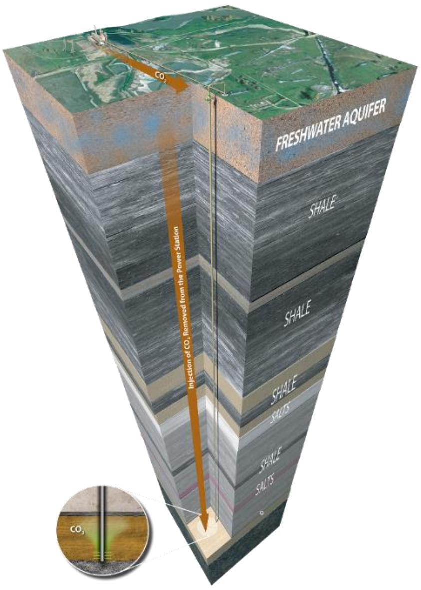

Figure 1-8 Carbon Capture and Storage-image from IEA2015

If on the one hand shales can be regarded as impermeable layer for avoiding the leakage of the CO_2 stored in the reservoir, on the other recent studies demonstrates that organic-rich shales can also treated as both natural gas and CO_2 storage reservoir(Boosari et al. 2015; Liu et al. 2019).

In fact, the supercritical CO_2 or liquid CO_2 can be used as a fracking fluid because it has low viscosity and high diffusivity that makes fracturing with it much superior to hydraulic fracturing in stimulation of shale reservoir. This double aspect (i.e., storage the CO_2 and stimulation of the gas extraction by using the liquid CO_2 in order to create cracks in unconventional reservoir) has attracted a great deal of attention in recent years(Liu et al. 2019).

1.3.3 Nuclear waste disposal

In the last years the underground geological storage is considered the best solution for the nuclear waste disposal produced by nuclear power plants for different countries including Switzerland, Belgium and France(Delage et al. 2010).

A schematic representation of a deep geological repository for radioactive waste is reported in *Figure1-9.*

Repository systems are placed in a stable rock formation, at a sufficient depth in order to protect the environment and people to the radioactive waste that it contains.

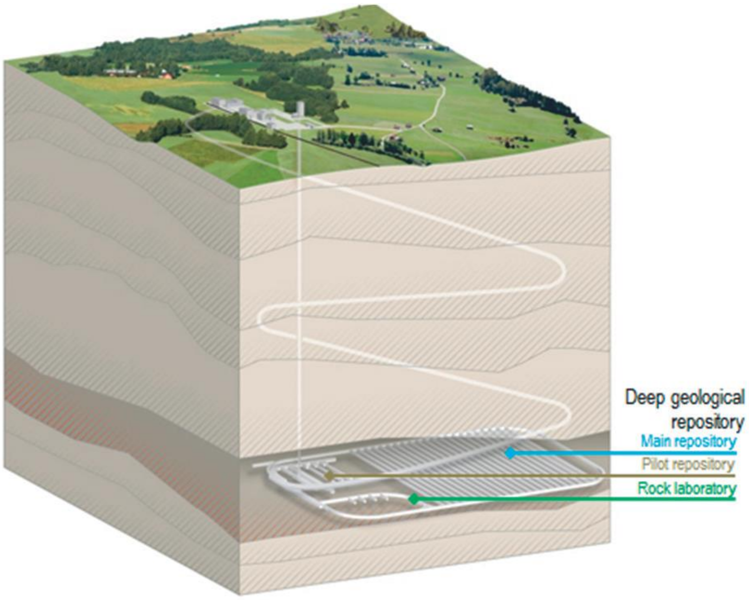

Figure 1-9 Deep geological disposal system for nuclear waste, image from www.ensi.ch

In order to avoid leakage of the waste a multi-barrier system, shown in *Figure 1-10*, is adopted. This is composed by different barrier layers, such as from the interior to the exterior:

- a steel canister which contains the waste
- a layer of sand-bentonite mixture placed around the canister, or more in general a low permeability rock formation
- a shale formation or compacted bentonite which consists in the external barrier of the system.

The shales in this engineering application represent the host rock formation for the repository and the barrier to the radionuclides migration, thanks to their low transport properties that guarantee the sealing of the waste.

Figure 1-10 Multi barrier system for the geological disposal

During the installation of the entire system, starting from the excavation of the tunnel to the storage of the waste, shales experience different levels of hydro-mechanical loadings.

Initially they are subjected to a stress release due to the excavation and they are also exposed to a desiccation due to the ventilation of the tunnel.

Moreover, after the temperature decay of the canister due to the water flow next to the formation a resaturation of the material is expected, that leads to a swelling of the geomaterial, useful to close the fractures, which might be induced by the excavation.

These changes in water saturation and loading bring geotechnics to study the retention proprieties of these material and to quantify their swelling and shrinkage behaviour.

1.4 Objective of this thesis

As it is highlighted in the previous paragraphs of this chapter, when shales are involved in geotechnical fields it is really important to study and understand how these materials behave due to partially saturation condition in which they are found, and how their geomechanical proprieties vary due to changes in water content that they experienced during their engineering application.

The study conducted in this thesis leads to improve the knowledge of the behaviour of partially water saturated shales involved in the gas extraction by analysing the change in water content and in volume upon suction variation in free stress conditions.

2 Shale, unsaturated geomaterial: Protocol of study

In natural occurrence, unsaturated geomaterials are defined as geomaterials with void spaces partially filled with a liquid, commonly referred as water, and partially with a gas which is a mixture of air and water vapour(Tarantino 2013).

Following this approach an unsaturated geomaterial is a media constituted by three phases:

1. solid, the matrix phase
2. liquid, the wetting phase
3. air, the non-wetting phase.

The presence of these two fluids inside the porous material and their interaction with the solid phase highly influences the mechanical and hydraulic response of unsaturated geomaterials.

Sometimes, in order to characterize the behaviour of the unsaturated geomaterials also another phase needs to be taken into account, namely, the air-water interface or the contractile skin that acts like a thin membrane interwoven throughout the voids of the soil, creating a separation between the air and the water phase, determining the ratio of the volume of air to the volume of water in the voids (Fredlund et al. 2012). The presence of this membrane generates capillarity effects that create suction where the pore water pressure is smaller than the atmospheric one. Change in suction strongly influence the behaviour of unsaturated geomaterials, such as deformability, strength and swelling, which is the volume increase due to wetting paths.

However, when considering only the changes in the volume-mass soil properties and not the stress state behaviour of an unsaturated soil, the contractile skin can be considered as a part of the water phase, defining the geomaterial as a three phases media since the volume of the contract skin is small and its mass can be considered as part of the mass of water(Fredlund et al. 2012).

In the following pages of the chapter are reported the basic concepts required to understand the hydro-mechanical behaviour of the unsaturated geomaterials, in terms of suction in unsaturated soil, moisture retention characteristics and swelling and shrinkage capacity.

Moreover, the experimental techniques available in order to determine the hydro-mechanical behaviour of three phases materials are briefly discussed, paying attention to the ones which are suitable for shales.

Finally, the protocol of study is presented.

2.1 Basic concepts of unsaturated geomaterial

As aforementioned, the unsaturated geomaterial is constituted by different phases. In order to understand how the one phase influences the others, it is important to determine in a representative elementary of volume of the geomaterial the volume-mass variables that quantify their presence.

2.1.1 Volume-mass relationships between phases

A schematic representation of an unsaturated geomaterial is reported in *Figure 2-1* where is possible to distinguish the three different phases:

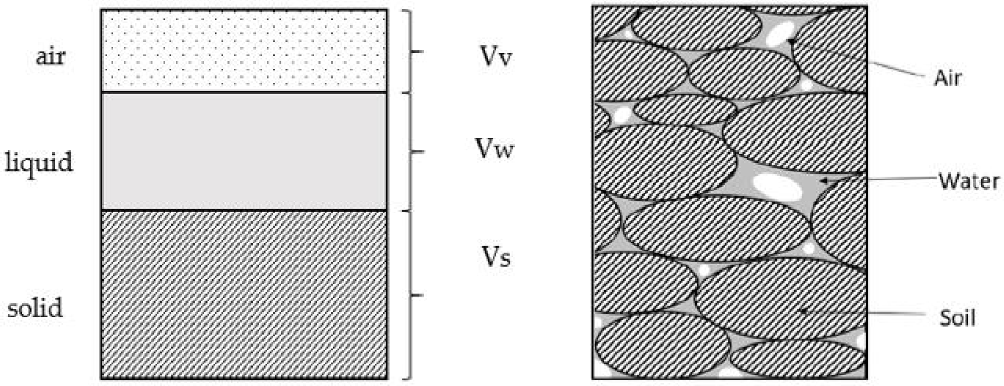

Figure 2-1 Three phases of a geomaterial element

The volume-mass properties that characterize a geomaterial in an engineering practice, according to(Fredlund et al. 1993), are listed below:

- the porosity n, defined as the ratio of the void volume to the total volume

$$n = \frac{V_v}{V} \quad [-] \tag{2-1}$$

Equation 2-1 Definition of porosity

- the void ratio e, defined as the ratio of the void volume to the volume of the solid phase

$$e = \frac{V_v}{V_s} \quad [-] \tag{2-2}$$

Equation 2-2 Definition of void ratio

- the degree of saturation S_r, defined as the ratio of the volume of water to the volume of pores

$$S_r = \frac{V_w}{V_v} \quad [-] \tag{2-3}$$

$$0 < S_r \leq 1$$

Equation 2-3 Definition of degree of saturation

Another common index to quantify the amount of water inside the geomaterial is the volumetric water content θ, defined as the ratio of water volume to the bulk volume of the geomaterial:

$$\theta = \frac{V_w}{V} \quad [-] \tag{2-4}$$

$$0 < \theta \leq n$$

Equation 2-4 Definition of volumetric water content

These two last indexes can be also used to subdivide geomaterials into three groups (Fredlund et al. 1993).

Referring to the degree of saturation it is possible to distinguish geomaterials as:

- dry geomaterials ($S_r = 0$) where there is no presence of water
- saturated geomaterials ($S_r = 1$) where all the voids are filled with water and there is no presence of air
- unsaturated geomaterials ($0 < S_r < 1$), where both air and water are present inside the pores.

At this point it is impossible to avoid the evidence that the amount of water inside of a porous media is a basic parameter in order to define an unsaturated geomaterials.

The liquid phase in general inside the porous media can be grouped into three categories:

- gravitational water, which is the portion of water that can drain due to gravitational forces
- capillary water, which is the water that rises against the gravity forces into "capillary tube"
- adsorbed water, which is a thin film of water that surrounds the solid particles attracted by the surface forces between the molecules of water and soil matrix, which can be removed just by warming the soil up to 100°C (Molfetta 2012).

Even if the volume-mass relationships define the fundamental indexes that revile the relative amount of the three phases in unsaturated geomaterials, in order to understand the hydro-mechanical behaviour of the soil it is important to define how these phases interact one with the other, looking at the interfacial behaviour between liquid-gas and liquid-gas-solid phase, so determining the water retention properties of the material.

2.2 Water retention behaviour of geomaterial

2.2.1 Surface tension

The air-water interface, the contractile skin, possesses a property called surface tension that results from intermolecular forces acting on molecules that are on the interface.

In order to understand this phenomenon is used to consider, as shown in *Figure 2-2* a molecule in the bulk water and one on the air-water interface.

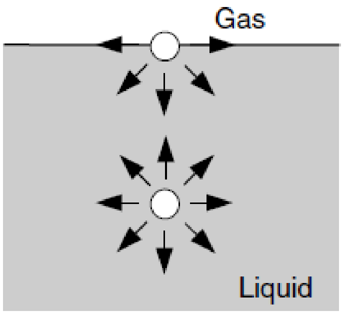

Figure 2-2 Molecules in the bulk liquid and on the contractile skin, (Tarantino 2010)

The molecule in the bulk liquid does not experience any unbalanced force because the forces at which it is subjected are equal in all direction.

On the other hand, a molecule that lays on the interface is subjected to an unbalanced force toward the interior of the water.

In order to get the equilibrium for the contractile skin a tensile pull is generated named surface tension T that causes the contractile skin to behave like a membrane.

Remembering that unsaturated geomaterials are composed by three phases, when the contractile skin is in contact with the solid phase (becoming a gas-liquid-solid interface), it will curve near the solid phase to form a meniscus,as shown in *Figure 2-3* as an example in a simple capillarity system.

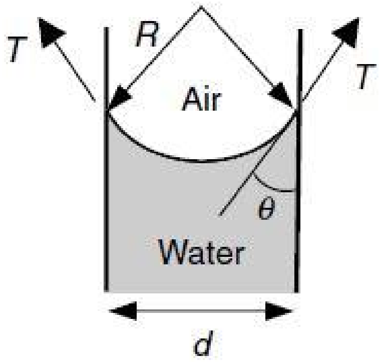

Figure 2-3 Curvature of the gas-liquid-solid interface, (Tarantino 2010)

The angle θ shown in the figure above is the contact angle, or the wetting angle, which is the angle between the solid surface and the gas-liquid interface, measured by the denser fluid. It depends on the properties of the two fluids (air and water), and express the affinity of the fluids for the solid (Bear et al. 2010).

In case of soil particles, the meniscus assumes the shape as shown in *Figure 2-4*, where the solid particles are schematized in the 2D as spherical.

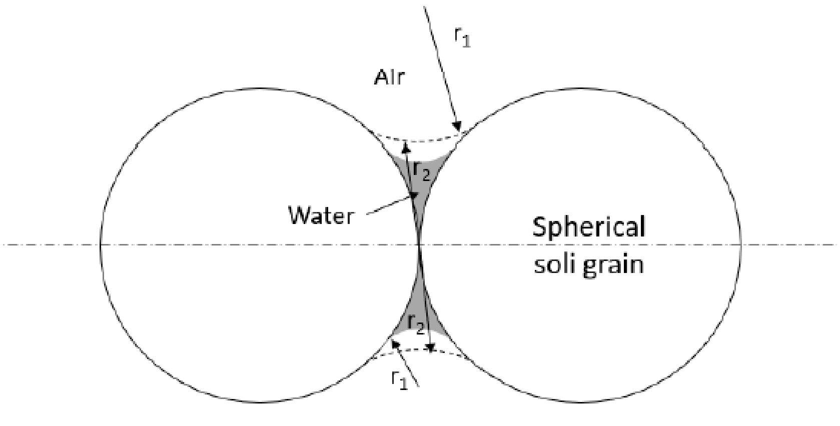

Figure 2-4 Idealized spherical soil grains in unsaturated conditions

The value of the surface tension can be estimated by solving the horizontal equilibrium of the forces acting on the water that connects the grains as:

$$u_a - u_w = T\left(\frac{1}{r_1} - \frac{1}{r_2}\right) \qquad (2\text{-}5)$$

Equation 2-5 Horizontal equilibrium of forces acting on water that connects grains

where r_1 and r_2 are the distances between the particles axis and the radius of the curvature of the water surface.

On the left of *Equation 2-5,* $(u_a - u_w)$ is called matric suction, where u_a is the air pressure in the pores and u_w is the pressure of the water in the pores. Due to the surface tension the pression of the water inside the pores is always lower than the air pressure.

However, the capillarity is not the only responsible for suction in a geomaterial, and water can be attracted in other forms as liquids. In fact, the term suction in unsaturated geomaterials is something much more complex than only capillarity effects, and it is explained as follows.

2.2.2 The role of suction

The soil suction is defined as the free energy of the soil water, or more in general is used as a variable that expresses the pore liquid potential (Fredlund et al. 1993).

The soil suction is composed by two parts(Fredlund et al. 1993; Tarantino 2013):

- the matric suction s, which is associated with the adsorption of water to soil surfaces due to capillarity effects, osmotic mechanisms and electrostatic forces on particle surfaces

- the osmotic suction π, the solute suction, which is associated with the concentration of species in solution.

The sum of the above components is defined as the total suction ψ_t:

$$\psi_t = s + \pi \quad [kPa] \qquad (2\text{-}6)$$

Equation 2-6 Definition of total suction

The total suction could be expressed with the thermodynamic relationship, Kelvin's law as a function of the relative humidity as (Blatz et al. 2008; Fredlund et al. 1993; Romero 2001):

$$\psi_t = -\frac{RT_k}{M_w\left(\frac{1}{\rho_w}\right)}\ln(RH) \quad [kPa] \qquad (2\text{-}7)$$

Equation 2-7 Kelvin's law

where:

R=universal gas constant [J/mol K], 8,314J/mol K

T_K= absolute temperature [K] $T_K = T_C + 273{,}15 \quad (T_C\ temperature\ in\ Celsius)$

M_w = molecular weight of water [kg/kmol], 18,016 kg/kmol

ρ_w= the density of the water [kg/m^3]RH=relative humidity, the ratio between the porewater vapour of the soil and the saturation pressure of the water vapour over a flat surface at the same temperature.

Suction is the key in understanding the behaviour of unsaturated soils, and its effect on soils is studied in terms of amount of retained water (water retention) and of strains.

In order to measure,or impose, the value of suction in geomaterials, a lot of methods are available in literature, and reported in *Table 2-1* with their own field of applicability(Fredlund et al. 1993).

Aim	Name of Device	Suction	Range (kPa)
Techniques to measure the suction	Psychrometers	Total	100-8000
	Filter paper	Total	Entire range
	Tensiometers	Matric	0-90
Techniques to impose the suction	Axis translation	Matric	0-1500
	Vapour Equilibrium	Total	Entire range
	Pore fluid squeezer	Osmotic	Entire range

Table 2-1 Suction measurement

2.2.3 Water Retention Curve

The water retention behaviour of unsaturated geomaterials is expressed as a relationship between the degree of saturation and the suction.

According to that, the graphical view of this relationship is the soil water retention curve, shown in *Figure 2-5*, that expresses all the possible hydraulic states of the material for positive suctions.

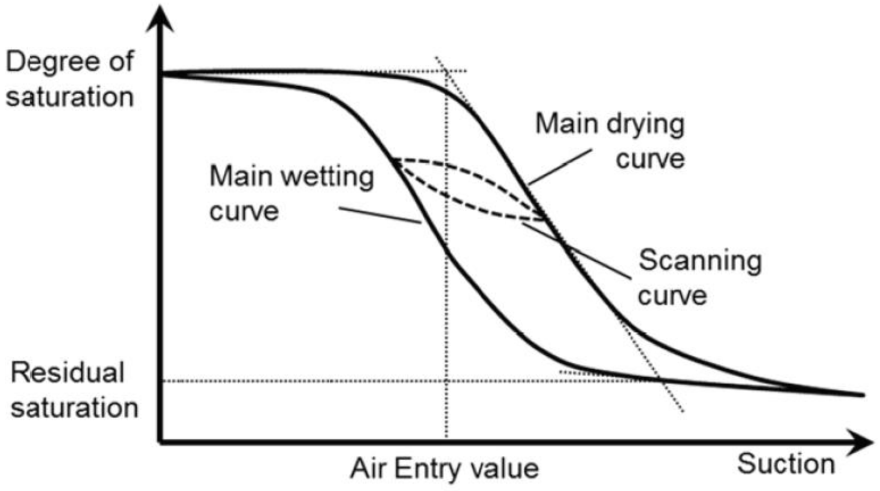

Figure 2-5 Water retention curve, (Favero 2016)

Starting from two different points, it is possible to draw two different hydraulic paths that represent the main drying path (starting from the saturated condition) and the wetting path (starting from the dried condition). All the hydraulic states that are in the middle of these two curves take place inside the hysteresis domain, a region where the water retention behaviour could be considered reversible. If the material is dried and then rewetted (or vice versa), in the hysteresis domain it is possible to define the so called "scanning curves".

A conventional value to identify the water retention curve is the air-entry value, which can be found graphically and represents the value of the negative pressure at which the meniscus of water on the soil particles recedes into the soil allowing air to enter.

The "S" shape of the water retention curve depends on different factors, such as:

- soil structure, dimensions of pores
- clay content
- presence of organic matter in the soil

As shown in *Figure 2-6*, soils such as sand present big and interconnected pores that lead to low air entry values, while soils such as clay have higher air entry value, due to not only the smaller size of pores in comparison with sand soils (that increase the capillarity retention mechanism), but also to the higher specific surface of clay particles, so that strong electro-chemical bond with water that is the dominant factor at high suctions.

As regards shales, and in particular organic shales, the "S" shape of shales in the WRC is not only strongly influenced by the reduced dimension of the pores and their low porosity, but also by the high percentage of organic matter that increases water retention at low suction and reduces the number of pores that are filled with air(Rawls et al. 2003). According to that, shales present very high air entry values, estimated in the range of 10 MPa(Ferrari et al. 2014, 2018).

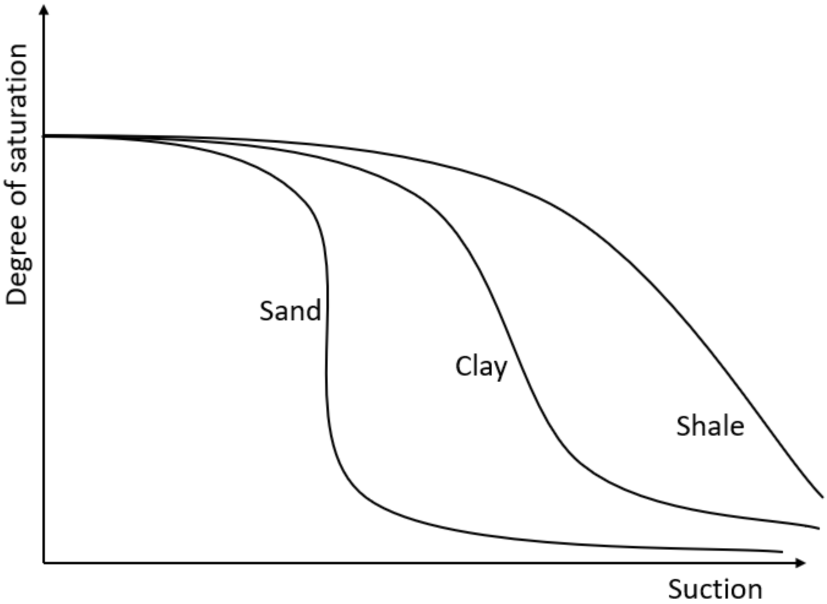

Figure 2-6 Different "S shape" for WRC

2.3 Swelling and shrinkage behaviour of geomaterial

The swelling and shrinkage behaviour of unsaturated geomaterial at constant total stress is related to the change in volume due to the water uptake within the media.

Chen (1988) found that, if the moisture content remains unchanged, no volume change is experienced by the geomaterial(Chen 1988).

Otherwise, a change in moisture content will lead the material to counterbalance the current condition of the soil finding a new configuration state. This configuration that expresses the behaviour of the material is found by a changing in the volume that could be contractive or dilative.

The change in moisture content is strictly related to a change in suction trough *Equation 2-7* and the swelling and the shrinkage behaviour of geomaterial is a consequence to that.

The swelling and shrinkage capacity due to suction variation depends on type of clay minerals and the attractive forces that govern the water uptake in the material, and moreover, it depends on the stress history experienced by the geomaterial(Fredlund et al. 2012).

2.4 Protocol of study for shale

In order to study how the moisture content will change in shales due to suction variations, an experimental study is conducted with the goal of defining the water retention curve of the material.

By applying different wetting paths and drying paths, the volumetric response of the material is studied both from a macroscopic point of view and then from a microscopic one by micro-CT analysis, defining the swelling and the shrinkage behaviour of gas shales.

According to the features of shales presented in *Chapter 1* and *Chapter 2* the following choices are made with the aim of conducting the laboratory experiments:

- due to the capacity to gain and loose water if the material is exposed to different humidity conditions, precautions are taken when the material is treated before, during and after the tests in order to minimize the time of the exposition of the shales in the lab environment
- the material is tested against total suction variation, as the shales have high air-entry values and a wide range of suction values need to be imposed to appreciate the changes in degree of saturation. Accordingly, the vapour equilibrium technique is applied in order to cover this range of suction
- the deformable behaviour of shales due to suction variation is studied both along the direction of the bedding planes and perpendicular to them, in order to analyse the anisotropic response of the material.

3 Characterization of the tested shale

Before conducting any test in the laboratory in order to study the behaviour of shales due to suction variations, a basic characterization of this material is presented in terms of density, porosity and water content.

First an overview of the tested samples is presented, then all the methodologies are reported with the results obtained.

Even if the basic characterization is a routine operation in geotechnical engineering, some precautions need to be taken when the tested material are shales, due to their peculiar features such as heterogeneous composition and low porosity.

According to that some results obtained are discussed in details in this chapter, to understand their reliability due to the limitations of the methodologies applied on shales where the pore size and the microstructure play a key role in the definition and quantification of the parameters studied.

3.1 Tested materials

The gas shale core sample was extracted from the south of America.

As reported in *Table 3-1* the tested material can be considered as a deep shale.

Moreover, as shown in *Figure 3-1*, the material exhibits a laminated structure, cause of cracks' generations, and a dark colour, indication of the presence of organic matter in the material.

Material	Core	Depth [ft]	Depth [m]
Gas Shale	1C	11214,40 - 11214,55	3418,149 - 3418,195

Table 3-1 Summary of the used material

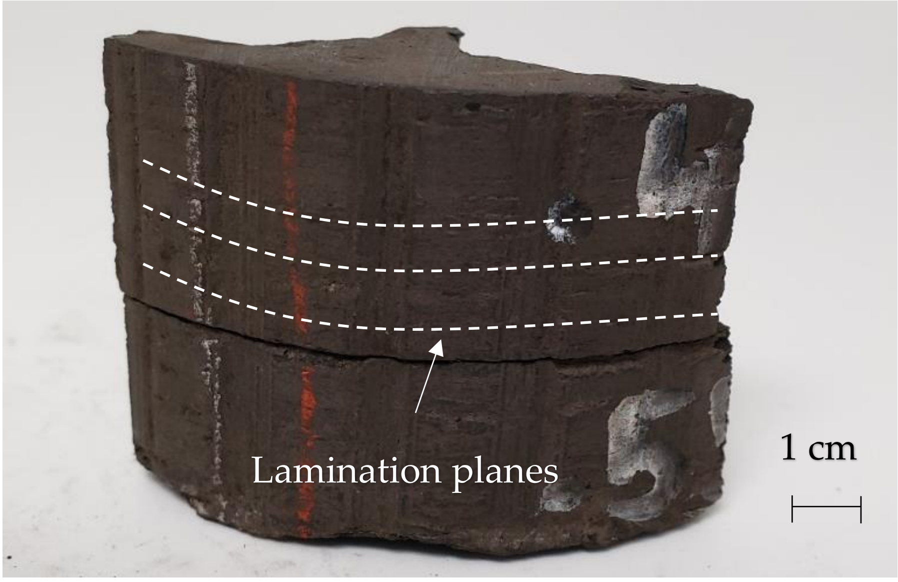

Figure 3-1 Gas shale core sample, lamination planes

As schematized in *Figure 3-2*, after the opening of the received core sample, initially with a mechanical saw there are extracted from the material small cylindrical specimens used in the hydro-mechanical tests, which results are reported later in this thesis.

Later with the remaining material, the carcass, other small samples were realized, which were used to compute the basic characterization of the tested shale, reported in this Chapter.

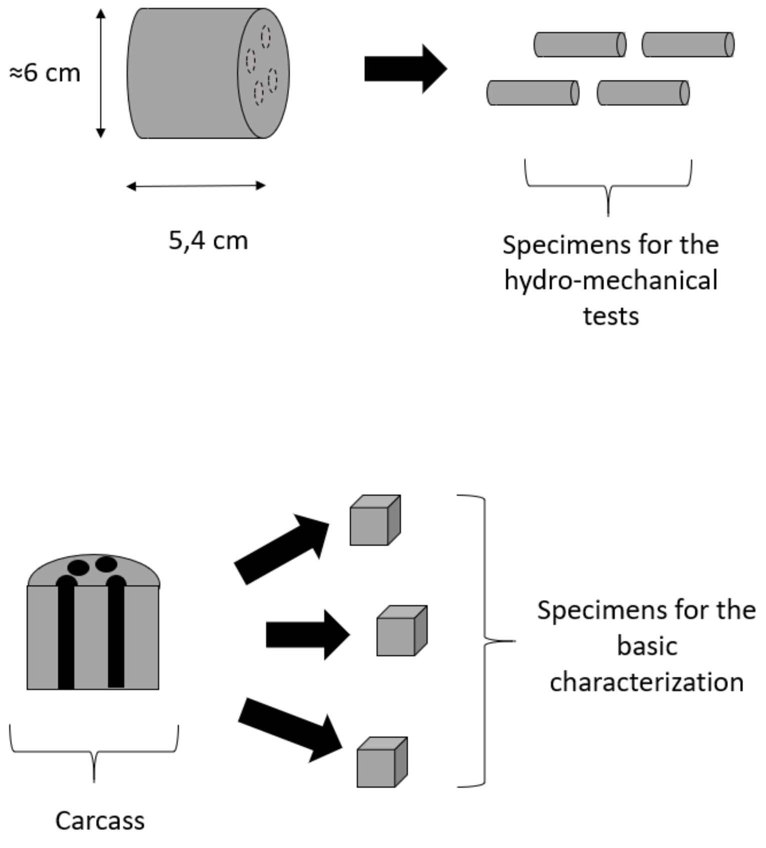

Figure 3-2 Schematization of the tested material

3.2 Basic characterization

In order to determine the basic properties of the gas shale, the carcass, shown in *Figure 3-3*, it was divided into several pieces by cutting it with a mechanical saw.

The parameters directly studied on the samples are listed below:

- the bulk density ρ_b (ratio of the total mass of the material to its total volume)
- the grain density ρ_s (ratio of the solid particles mass to the volume of the solid particles)
- the water content w (ratio of the mass of water to the mass of the solid phase)
- the total organic carbon content TOC (ratio of the mass of organic matter to the mass of the solid phase).

Others parameters obtained in order to characterize the material are:

- the void ratio e, (ratio of the void volume to the volume of the solid phase)
- the porosity n, (ratio of the void volume to the total volume)
- the degree of saturation S_r, (ratio of the volume of water to the volume of pores)

which were derived by the directly measured properties in the laboratory (ρ_b, ρ_s, w), using given phase correlations.

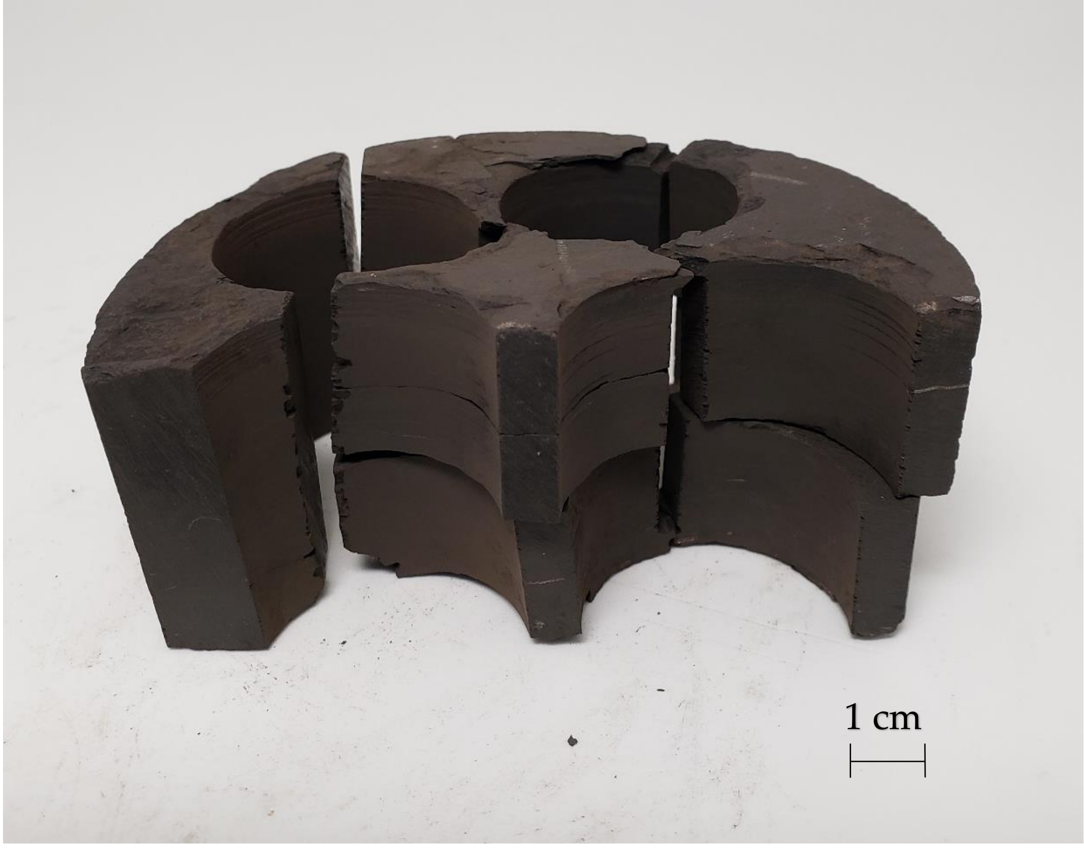

Figure 3-3 Cut of the carcass

The samples used in the basic characterization are divided as follow:

- specimen *1* (on the left side of *Figure 3-3*) is used for the determination of the bulk density
- specimen *UP* and *DOWN* (on the right side of *Figure 3-3*) are used for the determination of the water content, the grain density and the TOC.

Other samples were used to evaluate the grain density of the tested material after their utilization in the Hydro-Mechanical tests (specimen *C* and *E*).

3.2.1 Bulk density

The bulk density ρ_b is defined as the ratio of the total mass of the material to its total volume:

$$\rho_b = \frac{M}{V} \quad [g/cm^3] \tag{3-1}$$

Equation 3-1 Definition of bulk density

This parameter is really important to determine in order to compute the void ratio and the porosity of the material at the initial state before conducting the laboratory tests. In fact, an error on its measurement will affect all the parameters evaluated afterwards.

One of the biggest challenges to measure the bulk density of shales is the determination of the total volume, which is possible to determine it with a caliper if the shape of the tested samples is perfectly regular.

Due to the irregular shapes of the samples that usually take place in a geotechnical laboratory with natural soils, other methods have to be taken into account to measure the total volume of the samples as Archimedes method (fluid displacement method), tomography images or fluid pycnometer.

For the determination of the bulk density it was used the specimen *1*, shown in *Figure 3-4*.

Firstly, it was weighted in order to determine the mass and then the fluid displacement technique was applied to measure its volume.

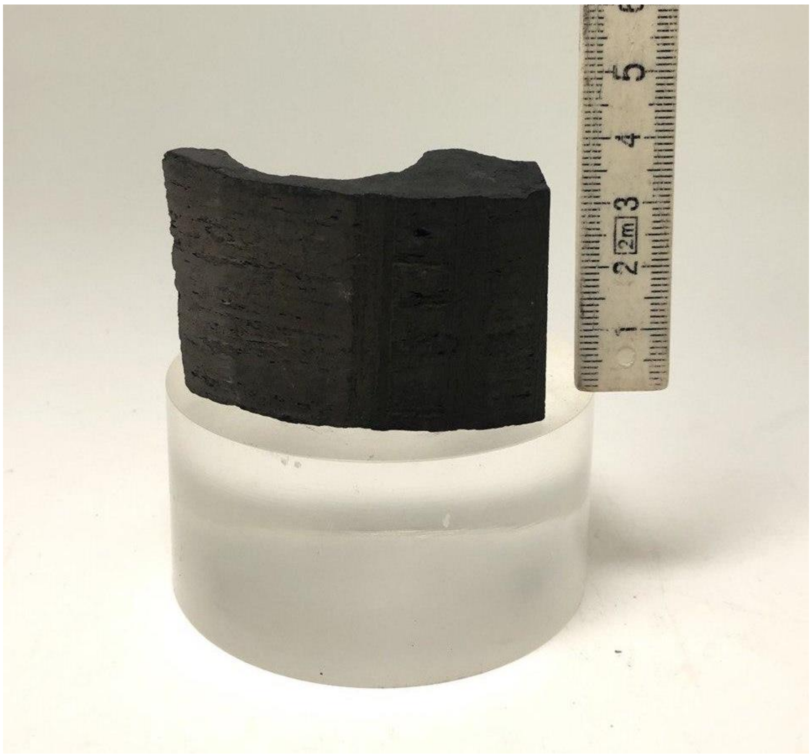

Figure 3-4 Specimen 1

The fluid displacement method was applied using Kerdane, it is an oil from which aromatics are extracted. It was chosen to do the measurement due to its immiscibility in water and its ability to invade the pore spaces filled only with air on the surface of the sample without affecting the soil structure (Péron et al. 2007).

The test was performed at temperature of 22°C, measuring a specific gravity ρ_K of the Kerdane as 0,802 g/cm^3.

After the measurement of its mass at the initial condition, the specimen was put in a Kerdane bath for 1 hour with the aim of filling all the surface air-pore with this fluid. This time was estimated by observation on gas shales: at the beginning of the bath, air bubbles were released from the specimen, after that time this process stopped.

In the meanwhile, a pycnometer as one shown in *Figure 3-5* was weighted filled with Kerdane computing a mass called m_{P1}.

Figure 3-5 Pycnometer used for total volume measurements

After 1 hour of Kerdane bath, the specimen was carefully wiped with absorbent water and weighted again, computing m_2 (mass of the sample with Kerdane and the initial water that there was in the sample at the initial condition).

Then the sample was put in another pycnometer equal to the one used to compute m_{P1} and filled with Kerdane again and then weighted, measuring m_{P2} (mass of pyc.+ wet sample with Kerdane + Kerdane).

The total volume is finally calculated as:

$$V = \left(\frac{m_{P1} + m_2 - m_{P2}}{\rho_K}\right) \quad [cm^3] \tag{3-2}$$

Equation 3-2 Determination of the total volume

from which is possible to compute the initial bulk density ρ_b of the tested shale.

3.2.2 Water content

The water content w is defined as the ratio of the mass of water in the sample to the mass of the solid phase of the sample:

$$w = \frac{M_w}{M_s} \quad [-] \tag{3-3}$$

Equation 3-3 Water content

The specimens used in order to determine the water content werw specimen *UP* and specimen *DOWN* shown respectively in *Figure 3-6* and *Figure 3-7*.

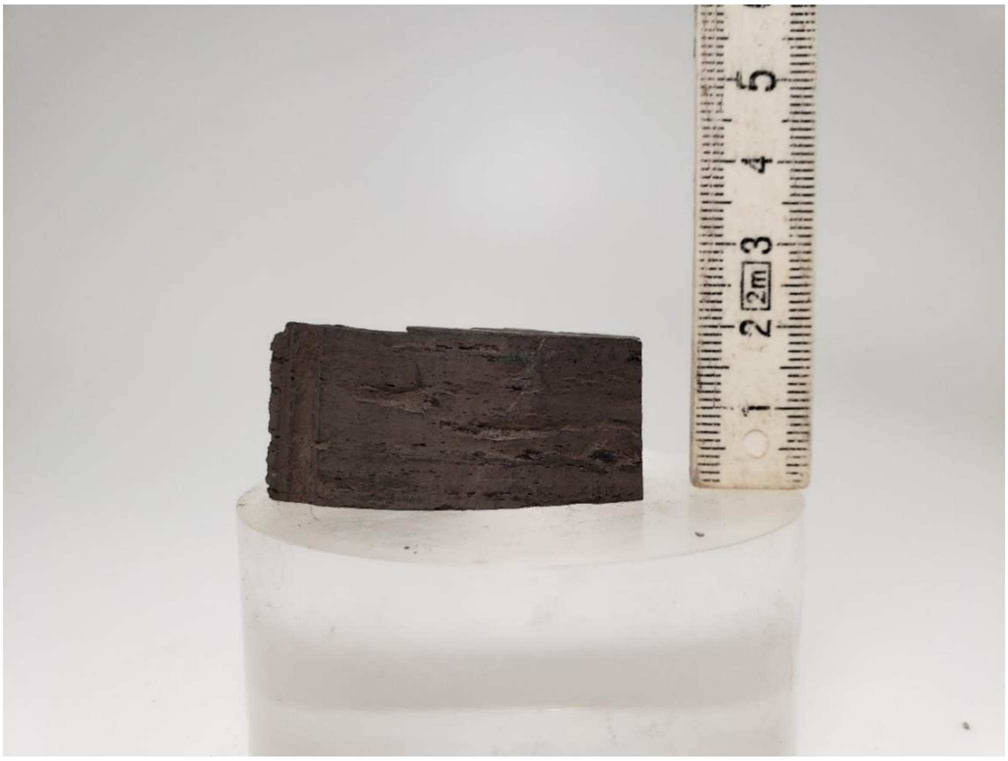

Figure 3-6 Specimen UP, before the oven drying

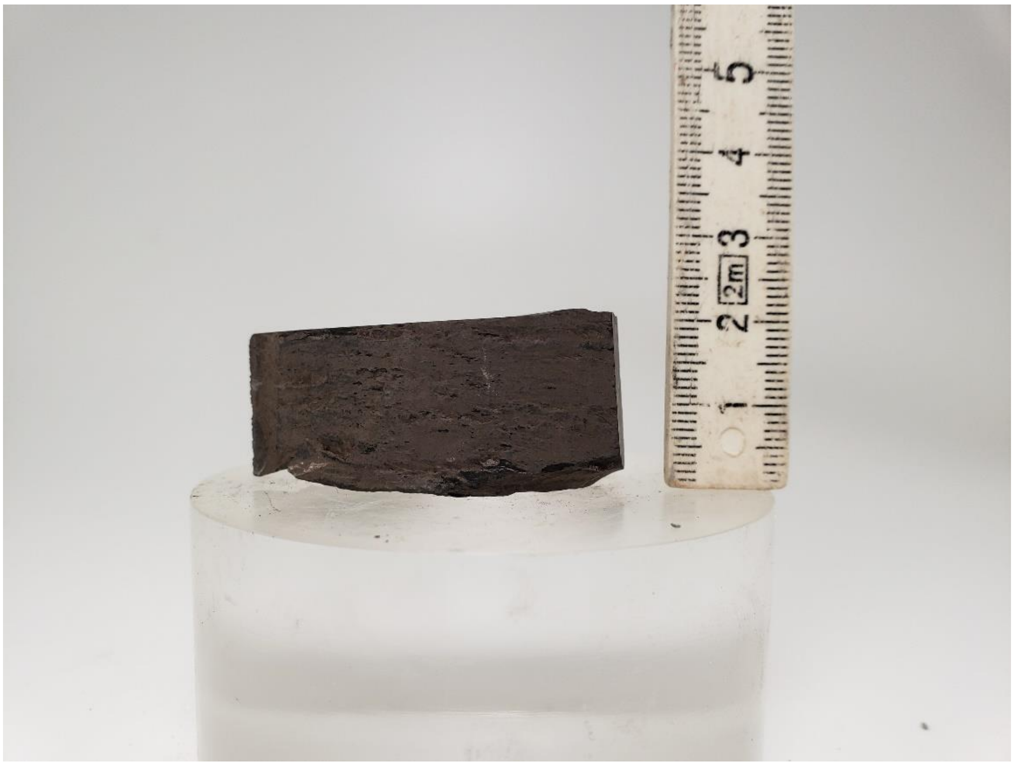

Figure 3-7 Specimen DOWN , before the oven drying

The methodology foresees the drying of the material in the oven at 110° C until a constant dry mass is achieved.

Following the procedure on different gas shales, the tested materials were put in the oven for 7 days before registering the dry mass as it was observed in (Minardi et al. 2016), where this time was considered the required for shales to observe a good stabilization of the dry mass, and not 24 hours as usually prescribed in the standard of soils.

Figure 3-8 shown the mass evolution with time of specimens *UP* and *DOWN*.

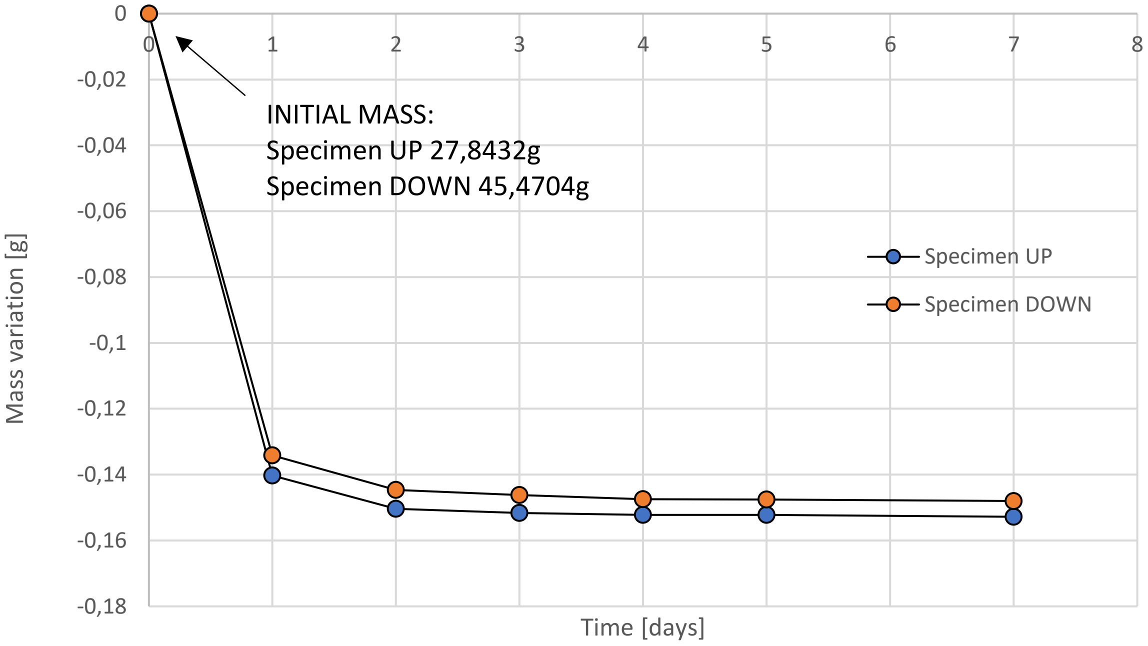

Figure 3-8 Evolution of the dry mass for the two gas shales at 110°C

3.2.3 Total Organic Carbon

The total organic carbon content TOC is defined as the ratio of the organic matter mass to the mass of the solid particles:

$$TOC = \frac{M_o}{M_s} \quad [-] \tag{3-4}$$

Equation 3-4 Definition of the TOC

According to the Swiss Standard SN 670 370 the TOC was determined on the material which was initially oven-dried ad 105°±5°C.

Then it was crushed and sieved at 500 μm and placed in a special oven at 550°C for 1 hour.

After that, before measuring the loss in mass during ignition, the material was put in a desiccator in order to get it cooler at very low relative humidity for 1 hour.

The test was conducted on specimens *UP* and *DOWN* after the measure of the grain density with the helium pycnometer.

The variation of the TOC measured on specimens *UP* and *DOWN* are reported in *Figure 3-9.*

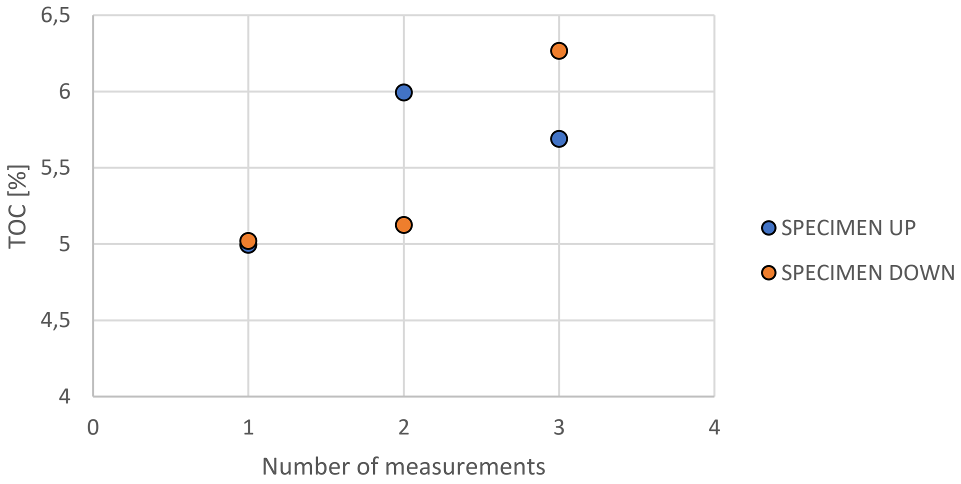

Figure 3-9 Variation of the TOC

3.2.4 Grain density

The grain density ρ_s is defined as the ratio of the solid particles mass to the volume of the solid particles:

$$\rho_s = \frac{M_s}{V_s} \quad [g/cm^3] \tag{3-5}$$

Equation 3-5 Definition of grain density

This value affects all the other parameters obtained by given phase correlations, such as the void ratio, the porosity and the degree of saturation.

Due to this, its estimation is really important in order to characterize the tested material.

Different techniques were used to calculate the grain density, each technique applied is described below, it is presented with its limitation due to the peculiar features of shales.

In details, the tests were conducted with Helium pycnometer and Water pycnometer, following the Swiss Standards on intact specimens, crushed and sieved specimens and on crushed and sieved specimen without the organic matter.

3.2.4.1 Helium Pycnometer

The Helium pycnometer technique was applied on intact specimens and on crushed and sieved specimens with and without organic matter, with the aim of determining the solid density of the tested material.

Before taking the measurements, the specimens involved in these tests were oven-dried at 110°C until a constant mass was achieved.

The Helium Pycnometer used for these tests was the Pycnometer AccuPyc III 1340, its schematic view is shown in *Figure 3-10*.

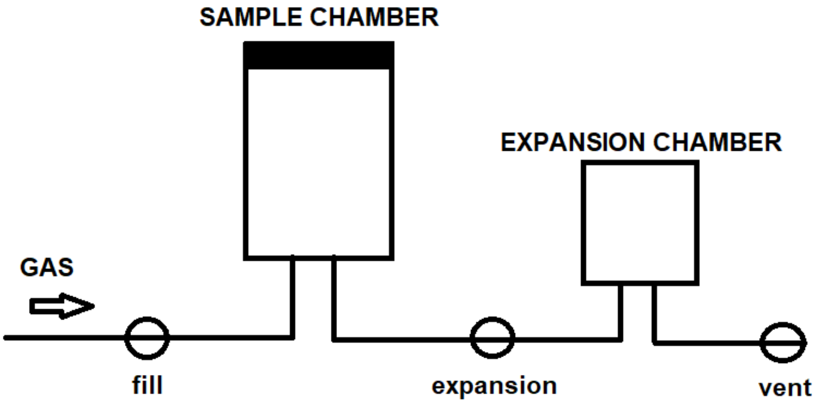

Figure 3-10 Schematic view of the Helium Pycnometer

The instrument operates by measuring the pressure change of Helium in a calibrated volume with the aim of determining the solid volume of the specimen. As input parameter the method requires the specimen weight so density is computed automatically. Once the specimen is placed in the sample chamber, the procedure consists of two stages:

- purges to clean up the specimen and remove air and moisture from the inside of the sample chamber, which are done by cycles of cell filling/expulsion of Helium.
- measurement of the sample volume V_s by filling the sample cell with Helium throughout the fill valve until the equilibrium is reached into the sample chamber and the run fill pressure P_r is measured. Then the expansion valve is opened and the gas flows into the expansion chamber and the final pressure P_f is recorded.

At the end, the volume of the specimen is computed according to:

$$V_s = V_{sample\ chamber} - \frac{V_{expansion\ chamber}}{\frac{P_r}{P_f} - 1} \qquad [cm^3] \qquad (3\text{-}5)$$

Equation 3-6 Determination of the volume of solid particles

where:

$V_{sample\ chamber}$ is the volume of the sample cell [cm^3];

$V_{expansion\ chamber}$ is the volume of the expansion cell [cm^3];

P_r is the run fill pressure [psig];

P_f is the final pressure [psig].

Helium is used because its molecules have a smaller kinematic diameter than other gases and it can penetrate in holes that others cannot, even though it can only enter in the interconnected pores with the external part of the sample (Heller and Zoback 2014) if the tested samples are intact.

The Helium Pycnometer technique was applied to the intact specimen *UP* and specimen *DOWN* after being oven-dried as aforementioned because the water content in the shale impacts on void volume since water blocks some of the pore accessible to Helium and leads to a decrease in void volume, or in other words it leads to an increase of grain density (Bashir et al. 2016).

After the tests, the specimens were grinded and the TOC was removed from the specimens by ignition. The tests were repeated on crushed and sieved specimens without the organic matter.

As regard the measurement on the crushed and sieved specimen with TOC, it was evaluated on another specimen taken at the same depth of specimen *UP*, called specimen *C*, after the oven-dried and the grinding of it.

During all the tests, after being oven-dried, the specimens were put in a desiccator for 1 hour, as shown in *Figure 3-11*, with a silica gel at a very low relative humidity in order to get them cooler and not to allow the temperature to influence the measurements.

Figure 3-11 Desiccator with silica gel

The results obtained in output shown in *Figure 3-12* on intact specimens *UP* and *DOWN* are the measurements of grain density of the samples using cycles of 3 runs by entering in input the value of the dry mass.

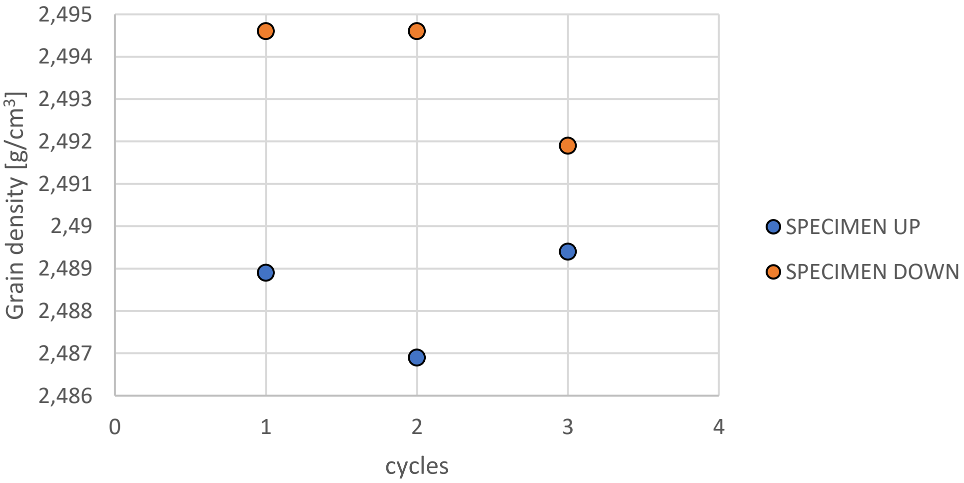

Figure 3-12 Grain density, results from Helium pycnometer, Intact specimens

The results obtained in output shown in *Figure 3-13* on crushed and sieved *UP* and *DOWN* after the ignition are the measurements of grain density of the specimens using cycles of 3 runs by entering in input the value of the dry mass.

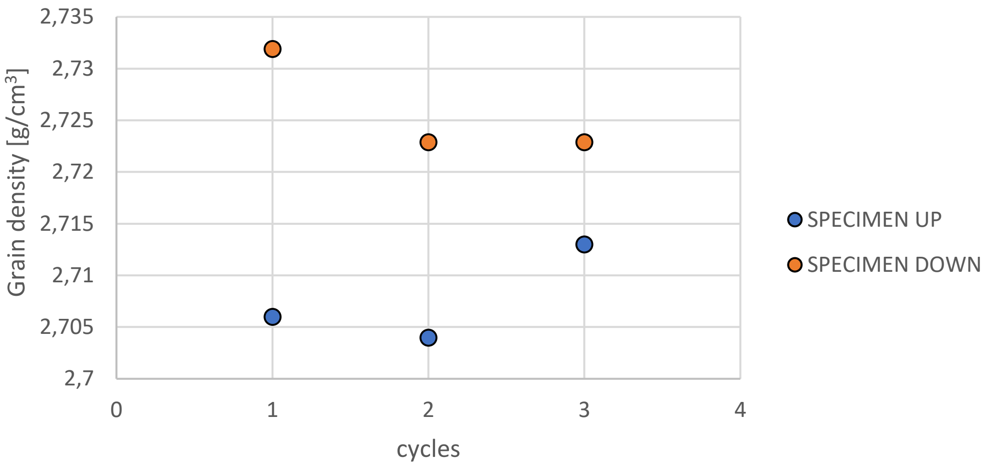

Figure 3-13 Grain density, results from Helium pycnometer, Crushed and sieved specimens without TOC

The results obtained in output shown in *Figure 3-14* on crushed and sieved *C* are the measurements of grain density of the specimen using cycles of 3 runs by entering in input the value of the dry mass.

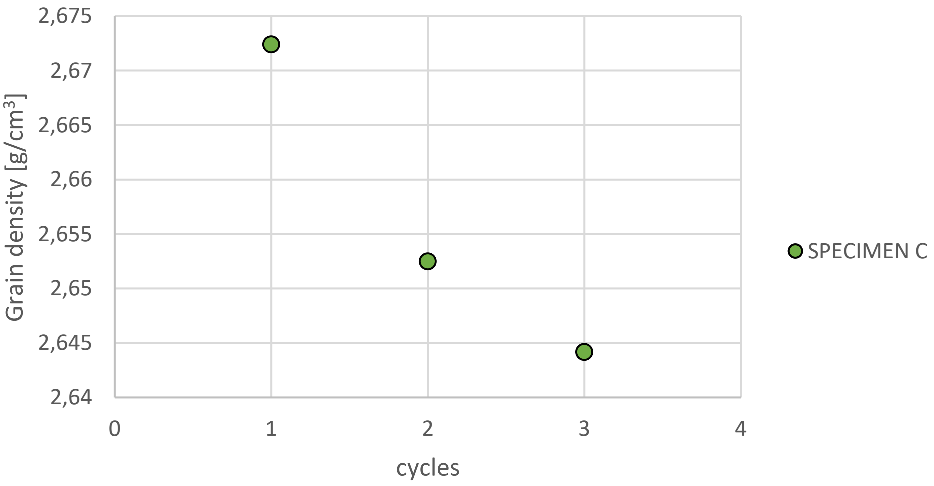

Figure 3-14 Grain density, results from Helium pycnometer, Crushed and sieved specimen

3.2.4.2 Water Pycnometer

The Water pycnometer was applied on specimen *C*, taken at the same depth of specimen *UP* and on specimen *E*, a specimen taken at the same depth of specimen *DOWN* , following the procedure indicated in the standard SN 670 335 on crushed and sieved material passing a 500 µm.

These tests on these two specimens were conducted at the end of their utilization in the Hydro-Mechanical tests, explain later in this thesis.

In order to determine the solid density, the mass of the material was computed by oven-dried the specimens at 110°C, while the volume was measured by using the pycnometer method.

In detailed the following formula was used to compute the grain density:

$$\rho_s = \frac{M_{pm} - M_p}{M_{pm} - M_{pmw} - M_p + M_{pw}} \qquad [g/cm^3] \tag{3-7}$$

Equation 3-7 Grain density, Water Pycnometer

where:

M_{pm} is the mass of the pycnometer with the dried material

M_p is the tare of the pycnometer

M_{pmw} is the mass of the pycnometer filled with dried material and water

M_{pw} is the mass of the pycnometer filled with water.

The results obtained are shown in *Figure 3-15*.

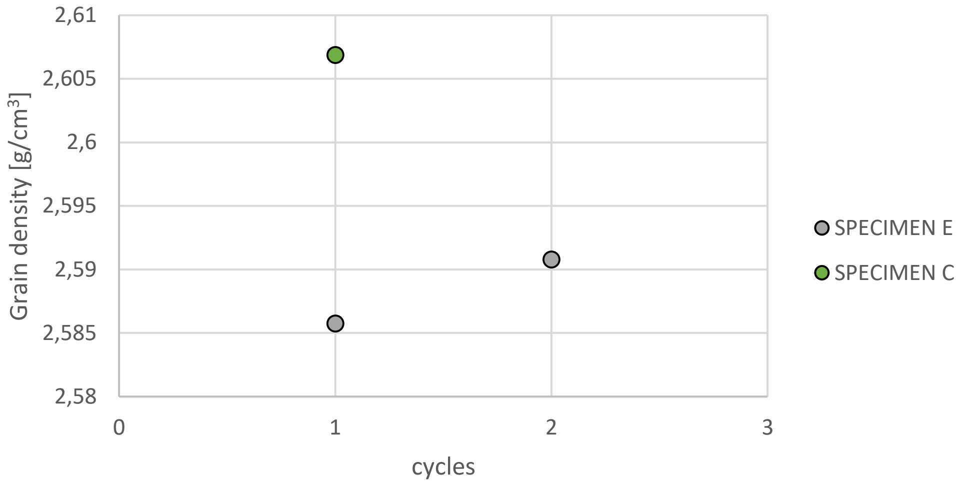

Figure 3-15 Grain density, results from Water pycnometer, Crushed and sieved specimens

If the difference between the results is smaller than 0,02 g/cm^3 the test is considered valid.

The test was then conducted also on the same powder without organic matter used for the determination of the grain density with the Helium pycnometer technique with the aim of determining differences between the two techniques when they are applied on the same material without the carbon content.

3.2.4.3 Challenges with the two techniques

The methodologies presented, pose some challenges when used for gas shales, different difficulties from one technique to the other are found during the tests that affect the result on the parameter studied.

A first difficulty is related to the grinding of the material.

In particular, during the crushing and sieving of the specimens, a lot of powder and ash is generated, loosing this fine component in the final amount of the tested material.

Moreover, even if the scope of the crushing is to separate the grains as much as possible without breaking them, it is possible that some particles remain assembled together and despite the crushing procedure some isolated voids could be present in these particles, affecting the measurement of the grain density.

In addition to that, as regard the procedure conducted with the Water pycnometer on the material continent the organic matter, the difficulty encountered it is referred to a very light material that floats on the surface of the water in the pycnometer, as shown in *Figure 3-16*.

A part of this floating material, most probably hydrophobic, disappear at the end of the boil water bath in which are put the pycnometer for 6 hours, as shown in *Figure 3-17*.

The fraction that still remains when the pycnometer is filled and the flask is put in the neck of the instrument gets out of the pycnometer with the water, loosing that amount of material in the test.

Figure 3-16 Water Pycnometer, floating material before boiling water bath

Figure 3-17 Water Pycnometer, floating material after the boiling water bath

3.2.4.4 Discussion on the results obtained

As aforementioned, the grain density is a key parameter in the basic characterization of the tested material because other fundamental geotechnical parameters are related to it with some given phase relationships, leading to a wrong characterization of the material if this parameter is not evaluated correctly.

All the results obtained in the laboratory using different techniques and for each technique different specimens are reported in *Figure 3-18*. For each technique and tested material, if the test is repeated several times, the results are given as an average of the values obtained.

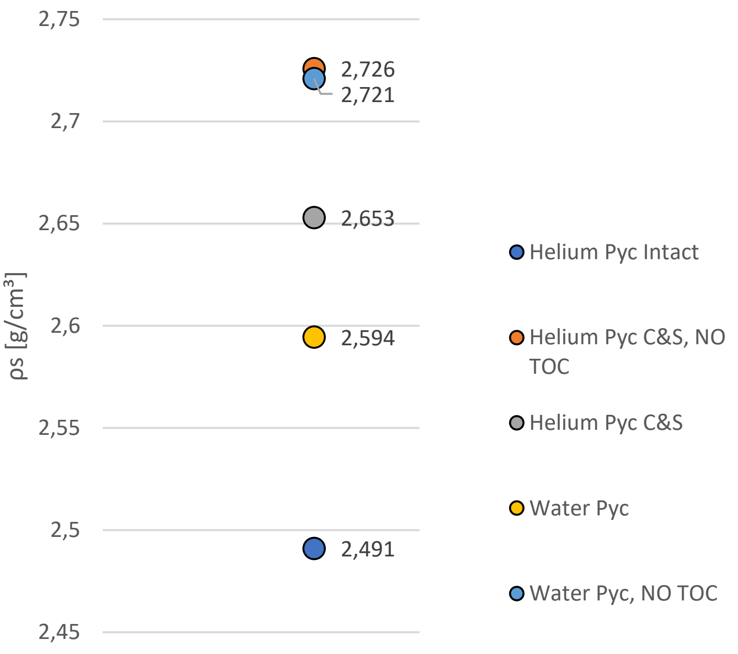

Figure 3-18 Different results of the grain density using different techniques

As it is possible to notice in the *Figure 3-18*, the results obtained differ from each other due to the limitation of the methodologies used on gas shale.

In particular, the smallest value of ρ_s obtained is registered for the intact specimen using the Helium pycnometer. This underestimation is due to the limitation of the Helium to penetrate the specimen, as the pore structure and especially the pore connection has a key role in the determination of the volume of the sample in the chamber of the instrument.

It is possible that some pores inside the specimen are not interconnected with the sample surface, so Helium can not enter within them and the volume registered is greater than the real one this even if the size of the pores, which is in the range of nanometres is higher than the atomic dimension of Helium which is in the range of picometres.

As regard the test conducted on crushed and sieved material using both Water pycnometer and Helium pycnometer, the difference in the grain density results has to be attributed to the underestimation of the volume with the Water pycnometer due to the loss of the floating material observed after the filling of the pycnometer and the insert of the flask.

The highest result obtained is registered on crushed and sieved specimen using both the Helium pycnometer and the Water pycnometer after the ignition of the organic matter. As expected the result obtained is comparable with other shales having the same characteristics but low total organic carbon content (Ferrari et al. 2014; Minardi et al. 2016). This is a confirmation that the presence of the organic matter decreases the value of the grain density.

In this study both the values registered with the Water pycnometer, the most common and reliable technique to evaluate the grain density on shale in literature (Ferrari et al. 2014, 2018; Minardi et al. 2016), and the one with Helium pycnometer on intact specimen are used in order to characterize the hydraulic behaviour of the material.

The solid density related to the intact sample is taken into account in this study even if the value obtained is an underestimation of the solid density of the material due to the reasons aforementioned, but it is a result obtained in order to consider also the variable of the interconnected pores and the structure of them in the sample, which is not studied in detailed further using for example sophisticated techniques such as ESEM images or other microstructural analyses such as for instance MIP and BET.

3.2.5 Void ratio

The void ratio *e* is defined as the ratio of the void volume to the volume of the solid phase (see *Equation 2-2*).

Its determination is performed from the following equation, function of the water content, and the bulk and grain density:

$$e = \frac{\rho_s(1+w)}{\rho_b} - 1 \quad [-] \tag{3-8}$$

Equation 3-8 Determination of the void ratio

3.2.6 Porosity

The porosity n is defined as the ratio of the void volume to the total volume (see *Equation 2-1*).

The porosity is used to quantify the void space in the geomaterial and it is related to the void index as follow:

$$n = \frac{e}{1+e} \quad [-] \tag{3-9}$$

Equation 3-9 Determination of the porosity

3.2.7 Degree of saturation

The degree of saturation S_r is defined as the ratio of the volume of water to the volume of pores (see *Equation 2-3*)

For its determination the following equation based on the void ratio, water content and grain density is used:

$$S_r = \frac{\rho_s w}{\rho_w e} \quad [-] \tag{3-10}$$

Equation 3-10 Determination of the degree of saturation where:

ρ_w is the density of water [g/ cm^3].

3.3 Results

The results obtained from the basic characterization are reported in *Table 3-2* and *Table 3-3*.

As explained before, both the results obtained with the Water Pycnometer and the Helium Pycnometer on intact sample are considered.

	ρ_s	ρ_b	w	e	n	Sr	TOC
	[g/cm³]	[g/cm³]	[%]	[-]	[%]	[%]	[%]
Gas Shale 1C	2,49	2,43	0,54	0,029	2,8	46	5,51

Table 3-2 Results of the basic characterization of the tested material, Solid density Helium Pyc-intact

	ρ_s	ρ_b	w	e	n	Sr	TOC
	[g/cm³]	[g/cm³]	[%]	[-]	[%]	[%]	[%]
Gas Shale 1C	2,59	2,43	0,54	0,071	6,6	20	5,51

Table 3-3 Results of the basic characterization of the tested material, Solid density Water Pyc

As expected, the initial water content, and the value of void ratio and so porosity are very low in gas shales in respect to other soils, leading this geomaterial to have high water retention properties and low permeability.

The high value of organic content found is the reflection of the dark colour of the material.

A value of 3% of the TOC is usual considered as a minimum threshold value for hydrocarbon production(Minardi 2018). The high value found confirms the suitability of the material to be involved in this specific petroleum engineering field.

As aforementioned, the differences related to the values of degree of saturation obtained and reported in *Table 3-2* and *Table 3-3* depend on the solid density measured.

A value of Sr= 20% for the same shale is confirmed in literature at the same depth of retrieval (Hammes et al. 2011). However, the value of the grain density of the material in situ in unknown, since it was not provided by authors.

For the initial degree of saturation, not only the value of the grain density affects the measure, but also the initial water content.

In fact, a previous study on the same shale conducted (Minardi 2018), leads to the same grain density measured with the Water pycnometer, but in that case a degree of saturation estimated at 40%. This difference is due to the initial water content that in that case was higher than the one registered and reported in this thesis and the porosity was estimated at 5%.

The results obtained in this part of the laboratory tests represent the initial condition of the tested material and also the starting point for understanding the behaviour of this shale in other experimental tests explained in the following chapters of this thesis.

4 Macro Hydro-Mechanical Behaviour of the tested shale

Water saturation plays a key role on the behaviour of gas shales due to their sensitivity to changes in water content.

It is important to recall that in their native state, gas shales are partially water-saturated due to the presence of natural gas trapped in their pore space.

In situ changes in water saturation could happen because of the interaction of the material with the fracturing fluids and of the gas extraction process. When the material arrives in the laboratory further changes in water content could happen due to the core extraction, exposition of the material in different humidity conditions and specimen's preparation process.

The water sensitivity of gas shales derives from their mineralogical composition. In fact, gas shales are considered clay-rich materials and it is known that changes in water content for clayey materials will cause swelling or shrinkage depending on the wetting or drying processes experienced respectively(Ewy 2014; Ferrari et al. 2018; Minardi et al. 2016; Pham et al. 2007)

This study is dedicated to the analysis of the water retention behaviour of a gas shale and it is conducted with the aim of understanding how the changes in relative

humidity on samples will affect the water content and the volumetric response of this geomaterial, starting from some considerations based on previous experimental analysis.

4.1 Materials and methods

The developed experimental technique for studying the water retention properties of gas shales is based on the control of the relative humidity (total suction).

Different hydraulic paths were considered in order to study the response in term of water uptake and volumetric deformation during the wetting and drying episodes.

The following section provides details on the tested material, experimental methodology, specimens preparation and wetting and drying paths applied.

4.1.1 Experimental methodology

Due to the particular features of gas shales, such as low permeability and reduced dimensions of pores, the water retention properties of these geomaterials are very high. In order to appreciate changes in water content due to changes in suction, high values of suction are necessary to be imposed to the samples.

As explained in *Chapter 2*, in order to study different hydraulic paths on the tested specimens, the values of total suction (relative humidity) were imposed through the vapour equilibrium technique (VET), which is the available technique to impose the total suction and covering a wide range of high suctions.

Moreover, the vapour equilibrium technique, as it imposes the total suction, it is considered the most suitable technique for gas shales because due to their small amount of water at the initial stage, it would be extremely difficult having a control/direct measurement of the amount of exchanged water (Minardi 2018).

Following this approach, the technique consists in controlling the relative humidity of a closed system with respect to vapour in isothermal conditions (Blatz et al. 2008; Pintado et al. 2009; Romero 2001).

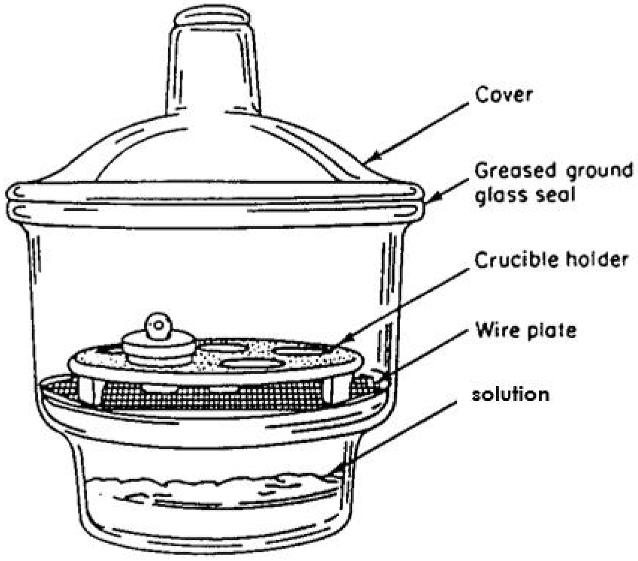

Figure 4-1 Desiccator, image from www.tutorsglobe.com

The specimens are placed in a desiccator on a porous disk that suspends them in the vapour environment above the chemical solutions, as shown in *Figure 4-1*.

Different values of relative humidity can be imposed by changing the salt solution inside the desiccator.

Different salts are used in order to impose different steps of wetting and drying through vapour diffusion.

Indeed, a flux of water exchange between the liquid and the vapour phases occurs in the desiccator until equilibrium is reached, which means that pore fluid and water vapour have the same chemical potential.

4.1.1.1 Previous research on shales

The configuration of the water retention test in free stress conditions conducted in previous researches on shales foresees the use of the vapour equilibrium technique on two "twins' samples", as shown in *Figure 4-2*(Minardi et al. 2016).

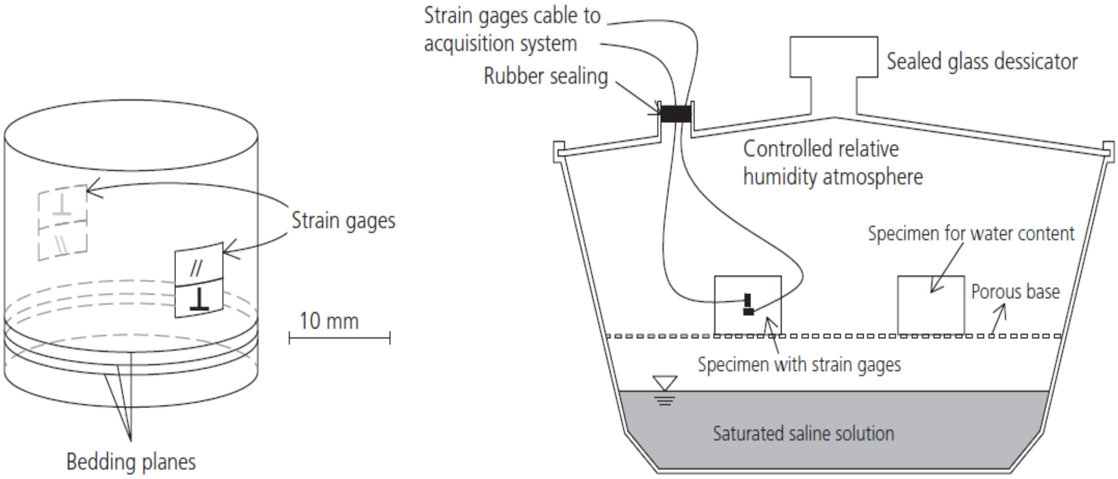

Figure 4-2 Previous experimental setup on shales, Minardi et al. 2016

In particular, to analyse the behaviour of the tested shales due to suction variations, it was set up an advanced testing methodology that combined the total suction control with the deformative response of the material in the two orthogonal directions using two strain gauges, one direction parallel to the bedding planes and the other perpendicular to them.

For those tests, cylindrical specimens of 25mm of diameter and 20mm in height and strain gauges of 4mm of thickness were used.

In details, on one specimen, the mass evolution during the tests was measured for the determination of the water uptake upon suction variations, while the deformative response was registered on the other one.

The underlying assumptions of those tests were that the two specimens, taken at the same depth, behaved exactly in the same way, defining them "twins' samples".

In other words, it was assumed that they had the same characteristics in terms of water uptake capacity, and microstructure, without any further investigation.

4.1.1.2 Research plan for the tested shale

In these presented laboratory analyses on gas shales, it was set up an advanced experiment using the vapour equilibrium technique.

In order to control the relative humidity at which specimens were put in with the aim of quantify the response of the material to suction variations, different salts solutions were used.

The salts used for the saline solution are listed in *Table 4-1* with their relative humidity and nominal total suction at 25°C(Romero 2001).

For the tests presented, the value of relative humidity of the solutions was directly measured by the chilled-mirror psychrometer (Decagon WP4C), and then converted with the psychrometric law (*Equation 2-7*) into their total suction, summarized in *Table 4-1*.

Salt		**Relative Humidity [%]**	**Nominal Total Suction [MPa]**	**Measured Total Suction [MPa]**
Potassium sulphate	$K_2(SO)_4$	97	4	3,96
Potassium chloride	KCl	84	24	22,60
Magnesium nitrate hexahydrate	$Mg(NO_3)_2 \cdot 6H_2O$	53	87	82,50
Lithium iodide trihydrate	$LiI \cdot 3H_2O$	18	235	232,80
Lithium bromide dihydrate	$LiBr \cdot 2H_2O$	6	386	357,42

Table 4-1 Salts used for solutions

During the test, the specimens in the desiccator were weighted regularly with a precise scale of four digits. It was assumed that the equalization of a specimen to the imposed value of total suction was reached when no mass variation was registered.

According to that, periodically the specimens were taken out the desiccator and their weights were recorded. This operation was done as quick as possible (few seconds), in order to minimize the exposition of the specimens to a different relative humidity.

The mass of water exchanged at each step was then back calculated at the end of the wetting and drying paths by computing the dry mass of the specimens after oven-drying them at 110°C, until a constant mass was reached.

The dry mass was subtracted to the one measured at each step to determine the mass of water held by the specimen.

The water uptake was finally quantified by using the water content, which expresses the ratio between the mass of water and the solid mass of the samples.

As regards the volumetric response of the material, this was computed using a different experimental set up from the previous researches, because of the reasons explained as follows.

Calling into question the same behaviour assumption on "twins' samples", the change in mass due to the water uptake and the deformative response of the material was registered on the same specimen tested for the water content determinations.

According to this, strain gauges were not glued on the specimens tested, in order to not affect the mass measurements, and the deformations were performed using a digital micrometre, shown in *Figure 4-3.*

Figure 4-3 Digital micrometre used for the estimation of the deformations

The deformations were computed taking 25 measurements on the height of the specimen in order to measure the perpendicular deformation of the bedding planes and 25 measurements on the diameter in different positions: 10 on the top of the specimen, 5 in the middle and 10 at the bottom of the specimen with the aim of measuring the parallel deformation of the bedding planes.

The volumetric deformation of the specimens was then evaluated using geometrical correlations by averaging the measurements directly taken.

4.1.2 Tested materials

The tested materials are specimens extracted by the 1C core sample at a depth of 3418,149-3418,195 m.

With a mechanical saw, four cylinders with a diameter of 25mm among the length of the core sample were obtained.

When the core was cut in small cylinders perpendicular to the bedding planes of the material, these were divided into smaller cylinders in height by the natural division of them along the bedding planes due to the fissility of the material.

This natural process, leads to obtain samples with irregular shape at the top and at the bottom of the specimens.

A schematic representation of the specimens obtained along the depth and used during the presented following laboratory tests is shown in *Figure 4-4.*

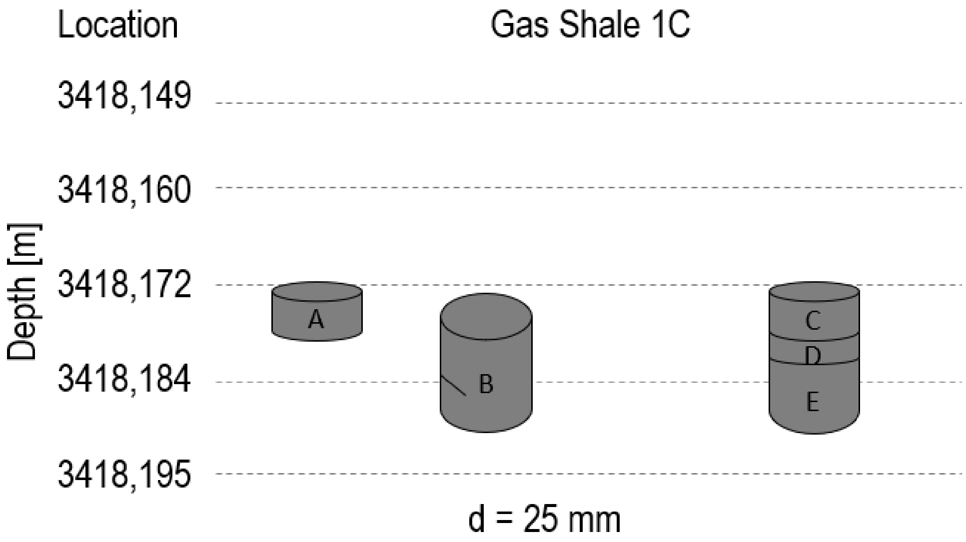

Figure 4-4 Specimens for the macroscopic behaviour

The initial properties of the material are reported in *Chapter 3*.

As it is possible to notice in *Figure 4-4*, specimen *B* presented on one side an external crack. The presence of this crack and the behaviour of the sample B due to that, as a result of the water uptake, is largely discussed later in this chapter.

4.1.3 Specimens preparation

After the cut of the core, the resulted samples are strongly characterized by an irregular shape at the top and at the bottom of the cylinder.

However, having the aim of measuring the total volume at each wetting and drying path with a micrometre, a regular cylindrical shape was required.

With the aim of obtaining it without damage the material and due to the small size of the specimens (≈6-20 mm in height) the surfaces of all the specimens were grinded gently using two different sand papers with two different roughness, one more smoothly than the other: P600, P240.

Even if this procedure was conducted paying attention to grind slowly in order not to generate heat, and wearing latex gloves to minimize water transfer due to hand contact, the specimens got dryer because during their preparation they were exposed to the environmental conditions for nearly 2 hours (time required for the preparation).

As an example, it is reported in *Figure 4-3* specimen *D* before and after the grinding.

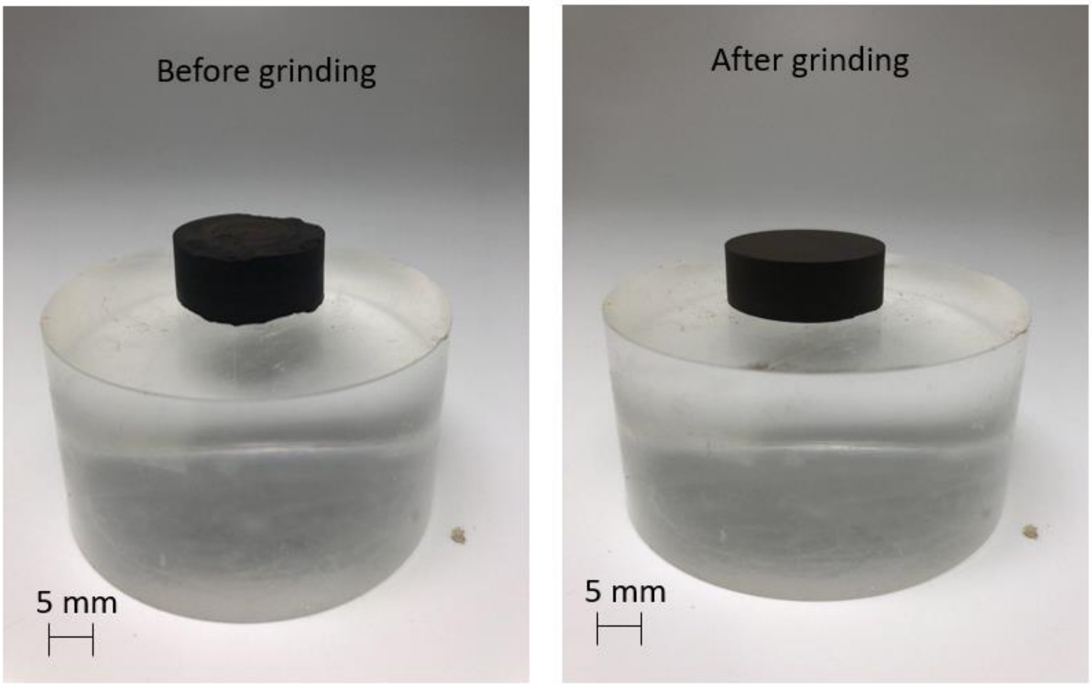

Figure 4-5 Specimen D before and after grinding

One of the most challenging difficulty that has found during the grinding of the material using sand papers was the natural lamination of the samples that represents a key role due to the reduced dimension in height of the tested specimens.

In the case of specimen *A*, it leaded to an interruption of the specimen preparation in order to not damage the specimen. In fact, it was observed an impossibility to continue the grinding as the pressure applied on the specimen to do it leaded the material to break it among the fissility planes. As a result, specimen *A* was not perfectly regular as shown in *Figure 4-6*.

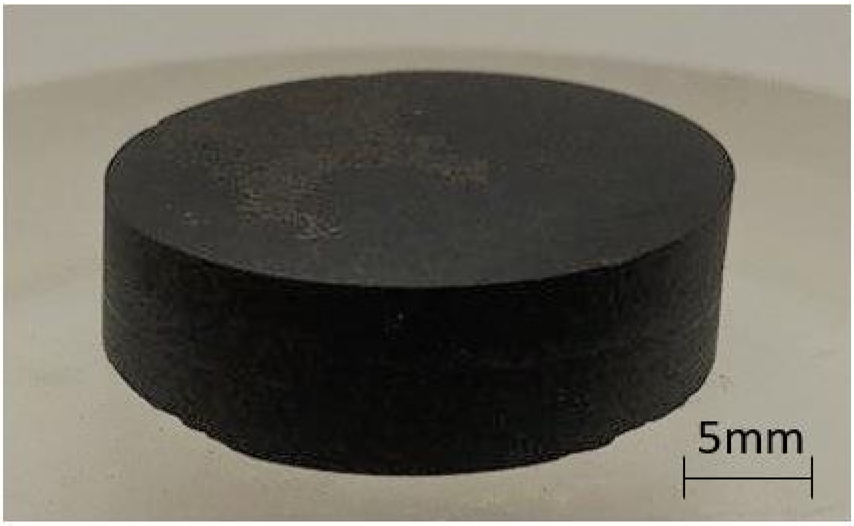

Figure 4-6 Specimen A, after grinding

At the initial conditions, after the first equalization at ψ = 82,5 MPa, the dimensions of the reshaped specimens were the ones reported in *Table 4-2* where the standard deviation calculated on the diameter and the standard deviation on the height measurements are also indicated.

Sample	**Dimensions [mm] at 82,5 MPa**			
	D	σ_D	H	σ_H
A	25,599	0,027	7,443	0,127
B	25,535	0,040	25,439	0,044
C	25,569	0,027	9,039	0,029
D	25,632	0,018	6,535	0,090
E	25,596	0,028	15,283	0,060

Table 4-2 Specimens' dimensions after the first equalization at ψ= 82,5 MPa

As it is possible to notice in *Table 4-2*, the experimental methodology chosen to measure the deformative response of the specimens, it is supported also paying attention to the dimensions of the specimens.

In fact, the heights of the tested gas shale specimens do not allow to glue the strain gauges because there is no enough space to do it on the lateral surface of them.

As regard specimen *B* which is the only sample whose dimensions are comparable with one of the samples used in the previous researches, the presence of the lateral crack poses the choice of the position of the strain gauges hard.

In fact, the strain gauges give a continuous (in time) measurement of the deformations, but a punctual one, making the choice of their position on the sample very challenging, with the risk of not registering some evident deformations such as the one expected in presence of a crack.

To overcame all this issues, and to determine an average macro deformative response of the material, the micrometre analysis measurements becomes the appropriate choice for the tested gas shale.

4.1.4 Testing procedures: applied wetting and drying paths

To investigate the impact of suction on the water uptake response and to the deformative behaviour of the material, different wetting and drying paths were adopted for each specimen, after the first equalization of the specimens at ψ = 82,5 MPa.

This value was chosen to impose a first equalization step close to the one of the free air of the laboratory, at which the samples are exposed when prepared.

The different paths chosen for the specimens are reported in *Table 4-3* and *4-4*, distinguishing respectively between specimens studied mainly on the wetting loading (*A* and *B*) and on the drying one (*C, D* and *E*), defining in some cases some drying/wetting loadings back to the initial condition in order to define the hysteresis of the hydraulic behaviour of the tested gas shale.

Wetting Paths					
Sample	**#0**	**#1**	**#2**	**#3**	**#4**
A	82,50 MPa	22,60 MPa	3,96 MPa	22,60 MPa	82,50 MPa
B	82,50 MPa	22,60 MPa	3,96 MPa	-	-

Table 4-3 Wetting Paths, Specimens A and B

Drying Paths				
Sample	**#0**	**#1**	**#2**	**#3**
C	82,50 MPa	232,80 MPa	357,42 MPa	232,80 MPa
D	82,50 MPa	232,80 MPa	357,42 MPa	-
E	82,50 MPa	232,80 MPa	357,42 MPa	232,80 MPa

Table 4-4 Drying Paths, Specimens C, D and E

4.2 Impact of suction variation

In this section, the results for the specimens of the tested gas shale are reported in terms of water content along time and upon suction variations.

The volumetric response of the material, in time and in change of suction, is reported paying attention to the irreversibility registered on specimens that are reported at the initial conditions after the drying and the wetting paths experienced.

4.2.1 Evolution of the water content

The results of the tests conducted on the gas shale object of this study are reported in terms of water uptake due to the change in suction.

The equalization time, or the time needed to have a stable water content, was found to range between six and twenty days.

This time is required due to the dimensions of the samples and the peculiar features of the tested shale, where the low porosity and low permeability play a key role in the water retention capacity of the material and on determining the low rate of exchange of water mass.

Longer times were required at low suctions imposed along the wetting path. This is not sursprising, since the conductivity of vapour in the specimens decreases with the increase of the pore filling with liquid water.

4.2.1.1 Wetting paths

In this section the results in terms of changing in water during time and the water retention curve expressed in water content versus total suction of specimens *A* and *B*, both along wetting paths, are reported.

At the end of the equalization time at 3,96 MPa, specimen *A* was brought back to the initial value of suction, with the aim of studying the hysteretic hydraulic behaviour of the material after experiencing of wetting.

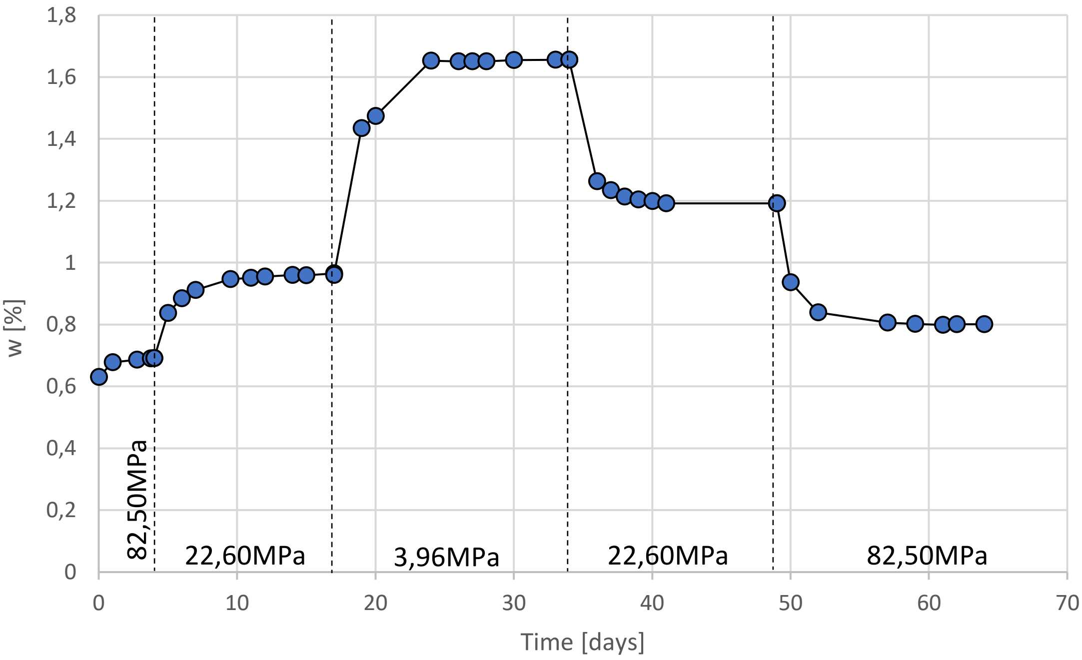

Figure 4-7 Evolution in time of the water content, Specimen A

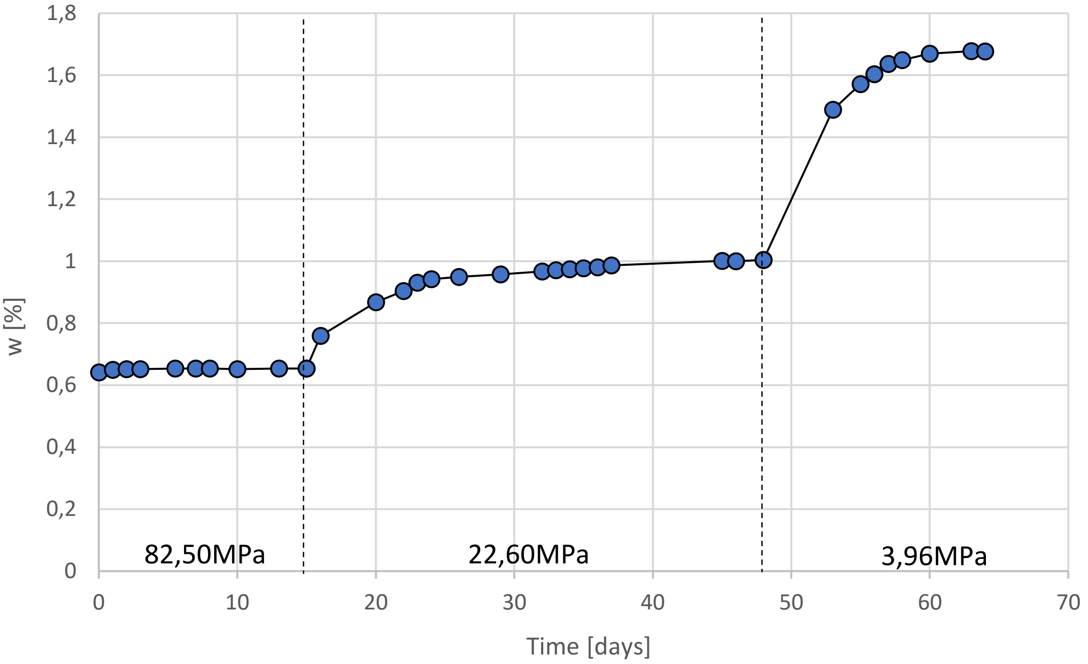

Figure 4-8 Evolution in time of the water content, Specimen B

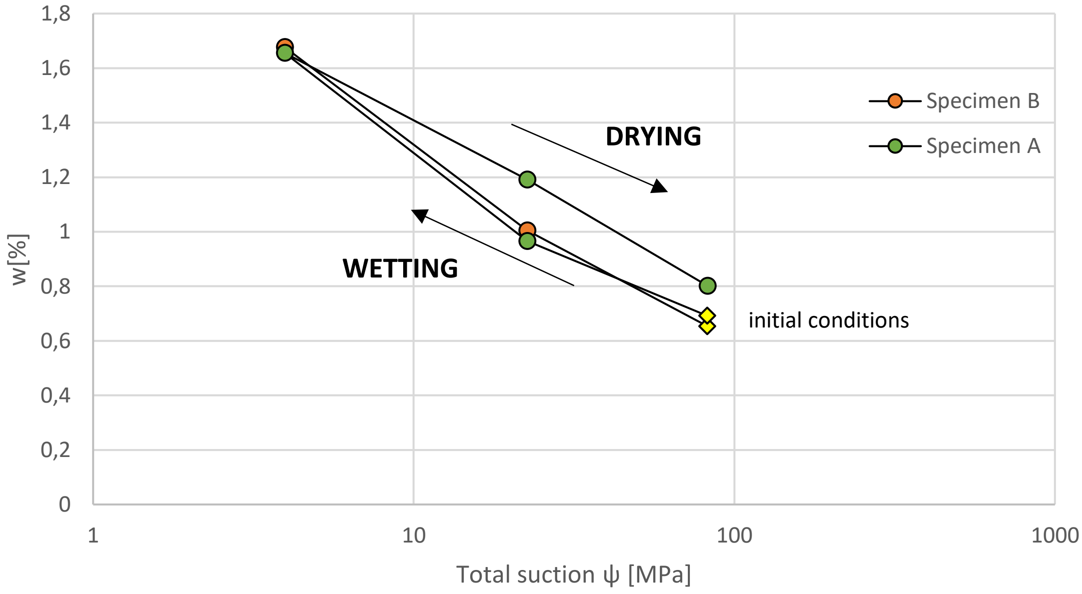

Figure 4-9 Water retention curve in wetting

As it is possible to notice in *Figure 4-7* and *4-8*, both the specimens gained water during the first equalization to the initial condition imposed of 82,5 MPa.

This water uptake after the first equalization time to 82,5 MPa results higher in specimen *A* than in specimen *B*, which means that at the initial condition after the specimens preparation specimen *A* was equalized at a value of total suction higher than the one registered on specimen *B* and in general it showed a value of total suction higher than 82,5 MPa.

This is probably due to the difficulties encountered during the preparation of specimen *A* that required much more time during which the specimen was exposed to the laboratory environment with more pressure applied on the sand papers to grind it which generating heat. Hence, as expected, at the initial condition the material was dryer.

Despite this, in general the water content variation due to the first equalization for both the specimens was smaller than the overall response of the tested material in the whole wetting cycle.

Paying attention to specimen *A*, it was at the end of the last wetting path brought back to the initial condition of suction following the same steps but in reverse.

At the end of the wetting and drying cycles imposed on specimen *A*, a hysteresis of the water retention curve emerged.

In fact, the water content at the end of the wetting cycle it was not the same as the one at the starting point. The difference registered in water content was $\Delta w = 0{,}12\%$.

Moreover at the value of suction $\psi = 3{,}96$ MPa, it is observed on all the specimens studied some condensed drops of water on the surface of the specimens, as shown in

Figure 4-10, suggesting that the water uptake mechanism at that level of suction is not only due to the water vapour molecules diffusion, but also other phenomena could be taken into account.

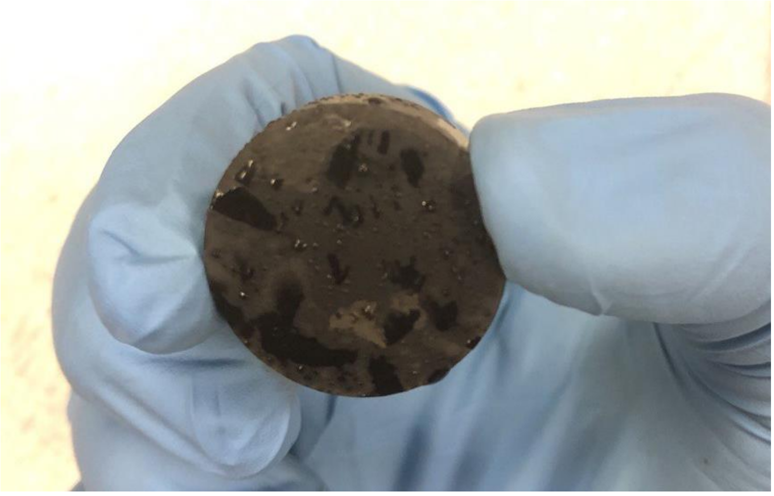

Figure 4-10 Experimental observation at 3,96 MPa

In fact, it is well known that as the partial vapour pressure increase (low values of total suction) a sharp variation of the water content can be observed which can be appointed to the capillary condensation that happens in the small pores of the tested material.

According to (Fisher at al. 1981; Monson 2008), this mechanism could also happen in the tested gas shale at relative humidity lower than 100%.

4.2.1.2 Drying paths

In this section are reported the results in terms of changes in water content along time and the water retention curve expressed in terms of water content versus total suction of specimens *C, D* and *E*, along the drying paths.

At the end of the equalization time for ψ = 357,42 MPa, the specimens *C* and *D* were brought back to the previous imposed total suction (ψ = 232,80 MPa), with the aim of studying the hysteretic hydraulic behaviour of the material after the experience of drying.

Also in these cases, during the first equalization time all the specimens experienced a water uptake, as a result of the specimens preparations.

As regard the evolution of the water content on specimens *C* and *E*, which were both brought back to one step in wetting after the drying paths, this recovered the same water content at the same level of suction. In other words, for both specimens significant hysteretic behaviour was recorded.

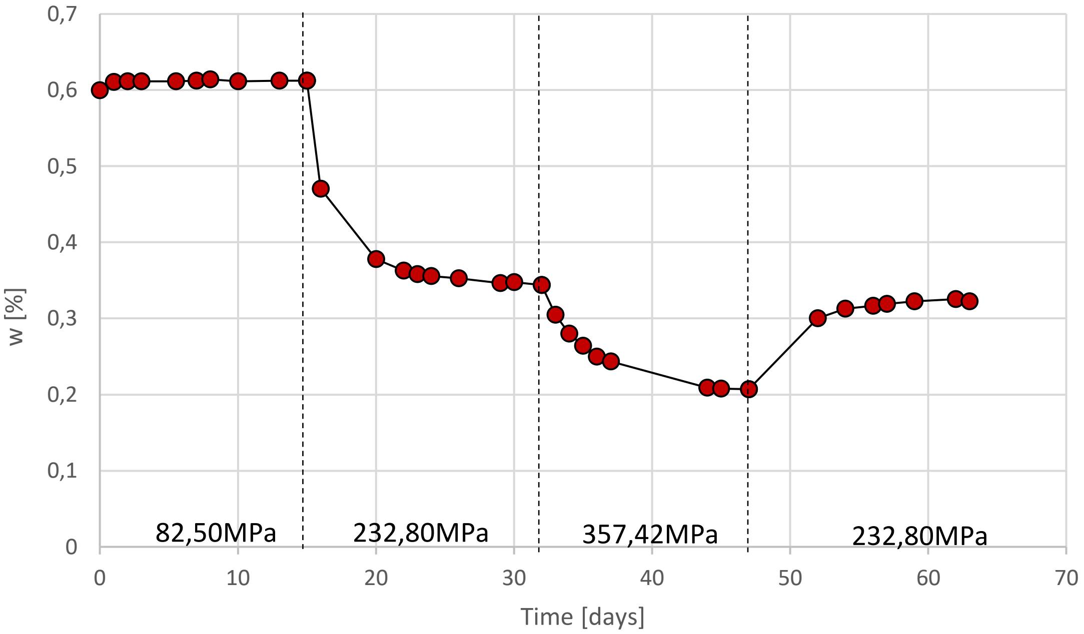

Figure 4-11 Evolution in time of the water content, Specimen C

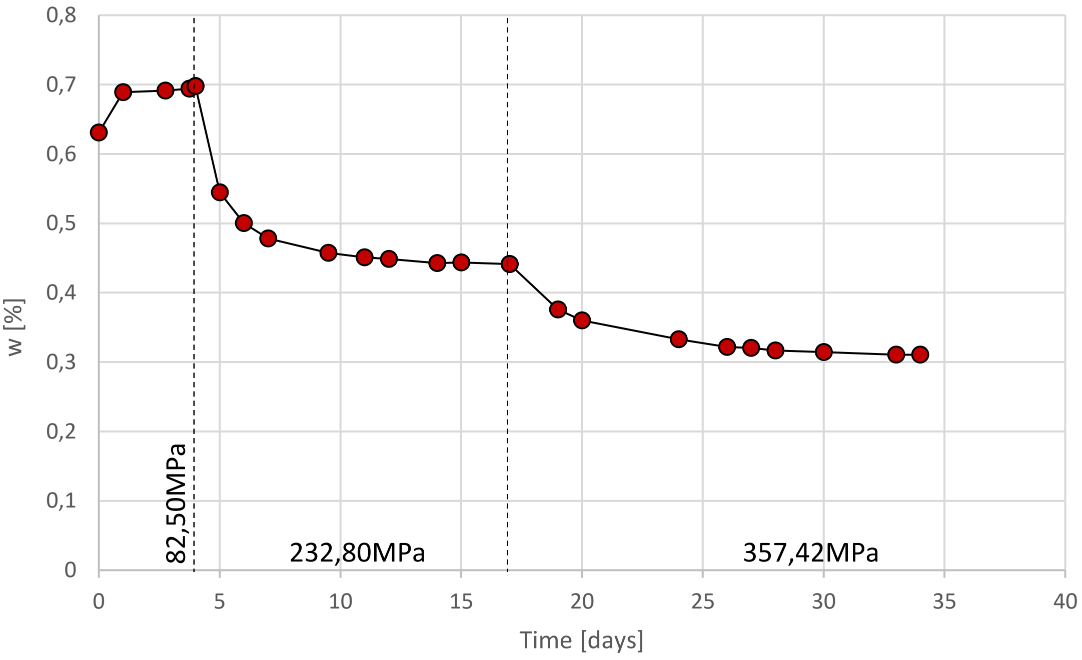

Figure 4-12 Evolution in time of the water content, Specimen D

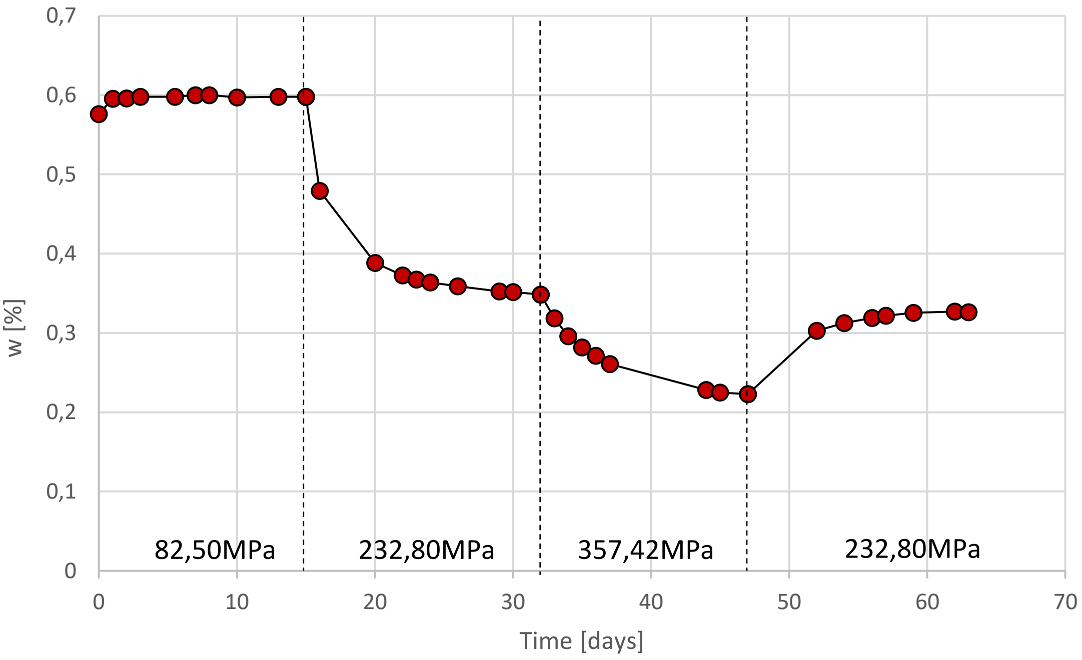

Figure 4-13 Evolution in time of the water content, Specimen E

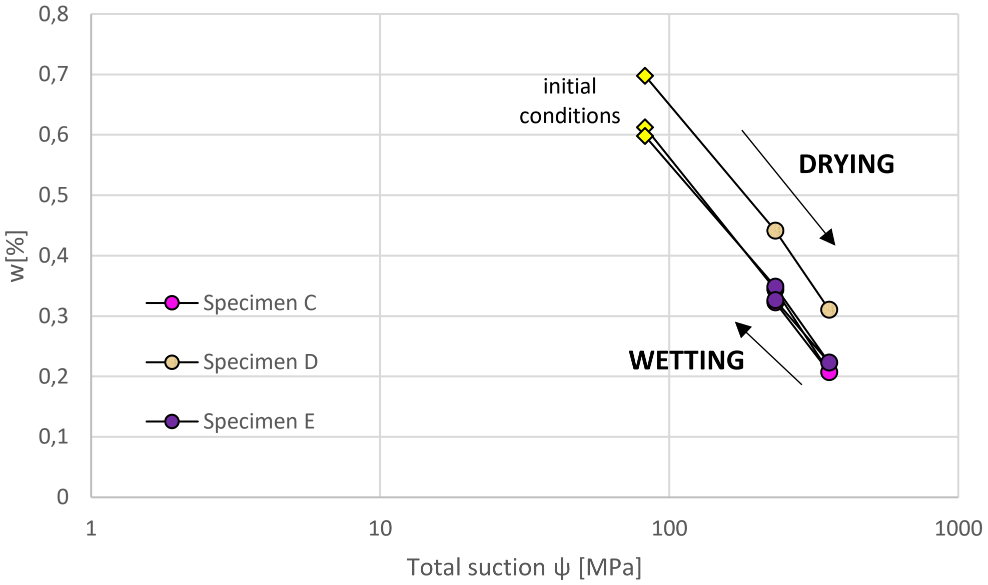

Figure 4-14 Water retention curve in drying

4.2.1.3 Water retention curve in term of water content

By plotting together all the collected data in terms of water content upon suction variation after oven-drying all the specimens, it is possible to define the water retention behaviour of the tested gas shale as shown in *Figure 4-15*.

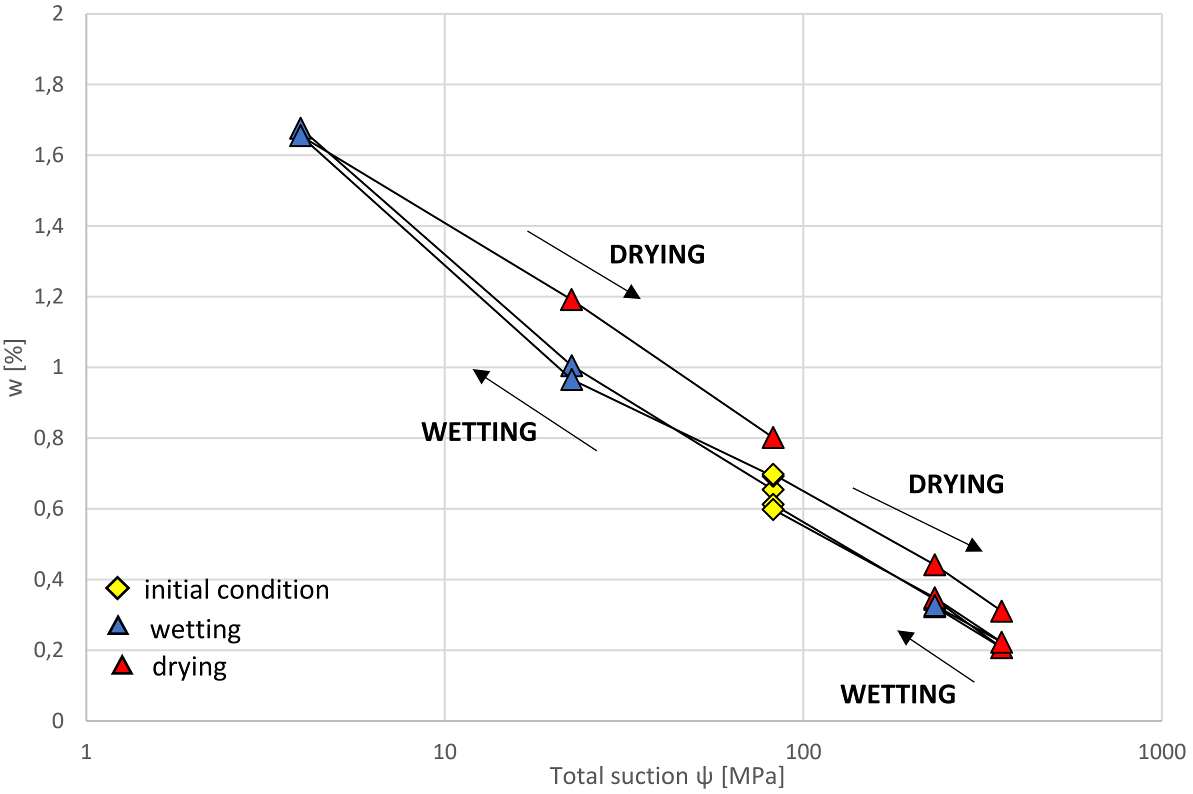

Figure 4-15 Water retention curve of the tested gas shale

Starting from the initial conditions (yellow points in the graph), it is possible to follow the hydraulic paths that all the specimens experienced.

The variability at the initial condition has to be attributed to the different time required in order to prepare the specimens, which caused different initial suctions on all the specimens.

4.2.2 Deformative response

Swelling and shrinkage of shales is a well-known aspect for the wellbore instability, and represent one of the main topics of study in order to understand the volumetric behaviour of this geomaterial when it is faced with drilling fluid or water in general.

The results of the tests conducted on the gas shale object of this study are reported in terms of deformative response due to the change in suction applied by the vapour equilibrium technique.

The sign convention adopted in these analyses for the strains is:

- negative for expansion
- positive for compression.

The values of strains presented are referred to the initial configuration obtained with the first equalization at ψ = 82,50 MPa.

In this section all the results obtain in terms of volumetric strain and perpendicular and parallel strains to the bedding planes are presented.

The lamination planes of the tested gas shale were found to have a strong impact on the deformative response of the material. Indeed, they are the main cause of the anisotropy of shales, as largely discuss later in this section.

4.2.2.1 Results along the wetting cycle

In this section the results in terms of deformations upon suction variation of specimens *A* and *B*, both along the wetting paths are reported.

At the end of the equalization time for ψ = 3,96 MPa, specimen *A* was brought back to the initial suction with the aim of studying the irreversible behaviour of the material after the experience of wetting.

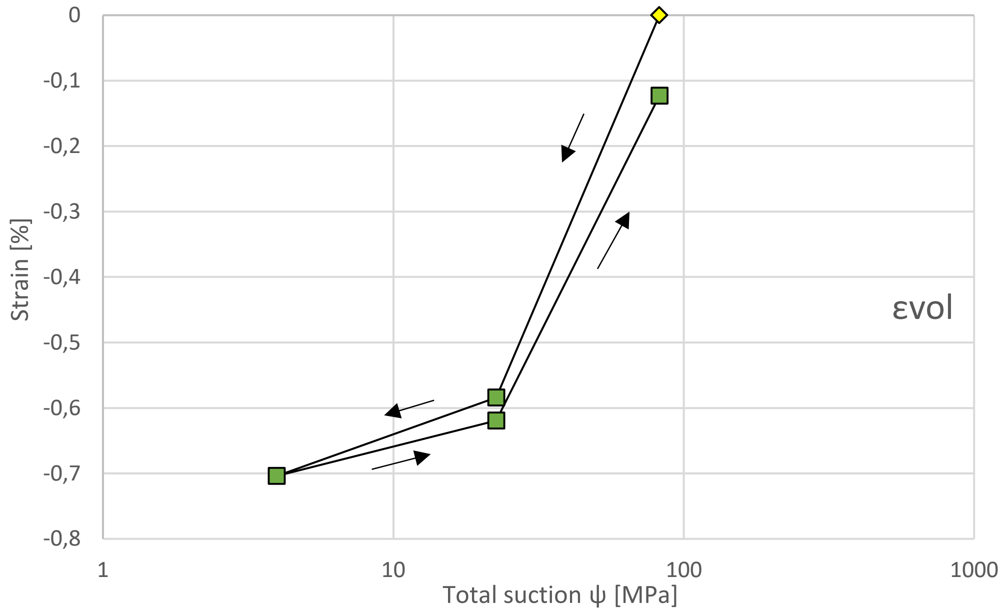

Figure 4-16 Volumetric strain evolution versus suction, Specimen A

As it is shown in *Figure 4-16*, the unrecovered volumetric deformation after the wetting of specimen A is about 0,12%.

This unrecovered strain is due to the increase in the microcracks that characterize the material. In fact, the swelling of the specimen during the water uptake might have induced a change in the microstructure of the material (Liu et al. 2016; Makhanov et al. 2012; Wan et al. 2013) , which is not visible without further investigations looking inside the specimen.

The results obtained show how in free stress conditions, the desiccation process after the wetting paths is not able to recover the strains experienced during the imbibition. Hence it is expected that the microcracks created during the water uptake do not close during the drying process.

As regard the deformative response of specimen *B, Figure 4-17* reports the swelling behaviour of the specimen at the first wetting step.

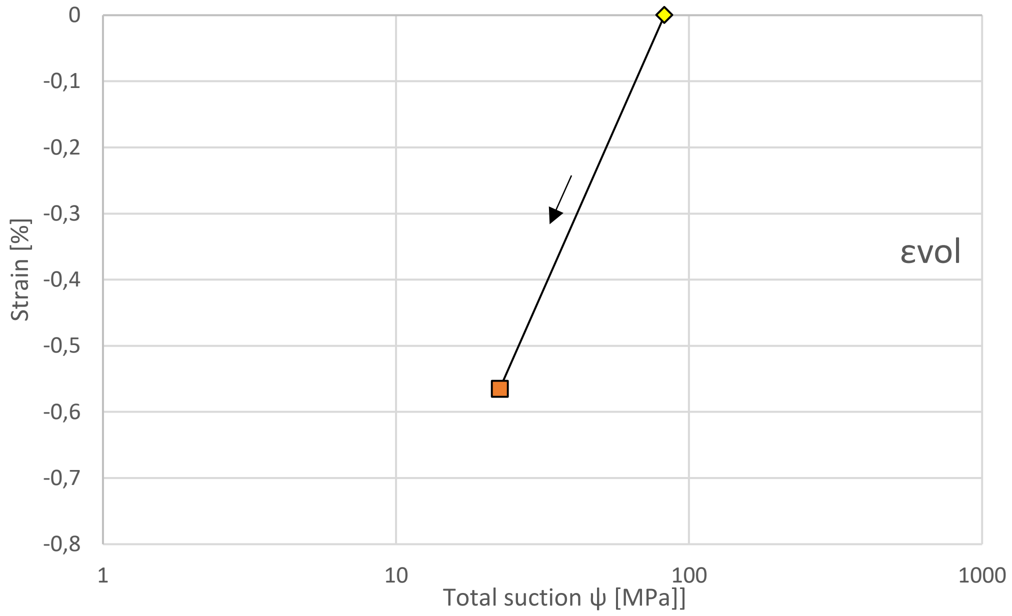

Figure 4-17 Volumetric strain evolution versus suction, Specimen B

It is important to recall that specimen *B* has a crack on one lateral side since its initial conditions.

According to this, one of the evidences of the macroscopic cracks increasing due to the hydraulic load of the tested shale, it is observed on specimen *B*.

Due to the wetting paths experienced on the specimen and the water uptake, it is possible to notice that the original crack extends during the wetting steps, as shown in a zoom in *Figure 4-18.*

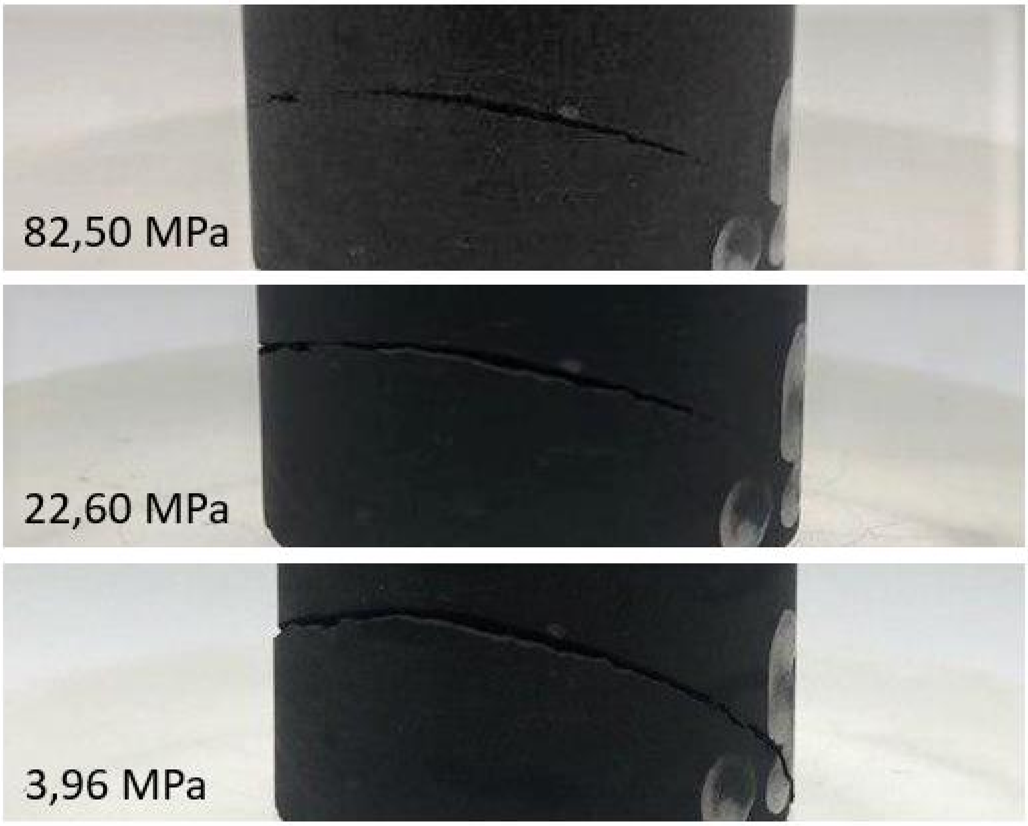

Figure 4-18 Crack generation on specimen B

The cracks in fact, represents a preferential path of the water vapour to enter inside the material.

Due to the attractive forces that there are on clays minerals water vapour molecules are adsorbed on the crack surface initially on a monolayer adsorption and then on multilayer and this leads the opening in the crack in order to pander the water uptake.

At the end of the equalization time for $\psi = 3{,}96$ MPa, the crack has propagated as much as the specimen is divided into two parts along it, as shown in *Figure 4-18*.

This made the volume measurements on specimen *B* at the end of the last wetting step impossible.

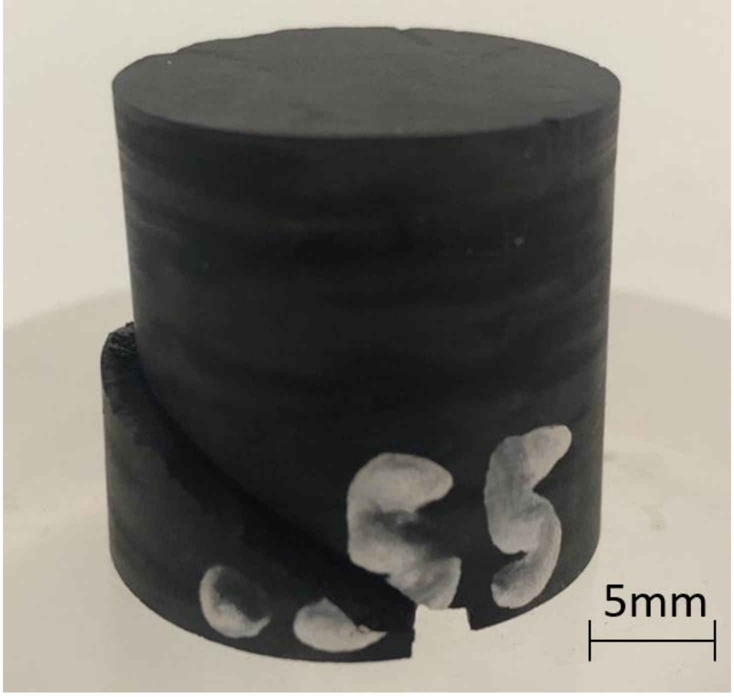

Figure 4-19 Breaking of specimen B at 3,96 MPa

Notwithstanding, the lack of measurements on specimen *B* after the equalization at 3,96 MPa, it is possible to assume that the deformative response could be more or less the same as the one experienced on specimen *A*.

This assumptions is made possible by comparing the strains registered at the first step in wetting for both the specimens *A* and *B* which result exactly the same as shown in *Figure 4-16* and *4-17*.

4.2.2.2 Results along the drying cycle

The deformative response was also monitored along the drying process on specimens *C*, *D* and *E*.

At the end of the equalization with ψ = 357,42 MPa, specimen *C* and *E* were brought back to ψ = 232,80 MPa with the aim of studying the irreversible behaviour of the material after drying.

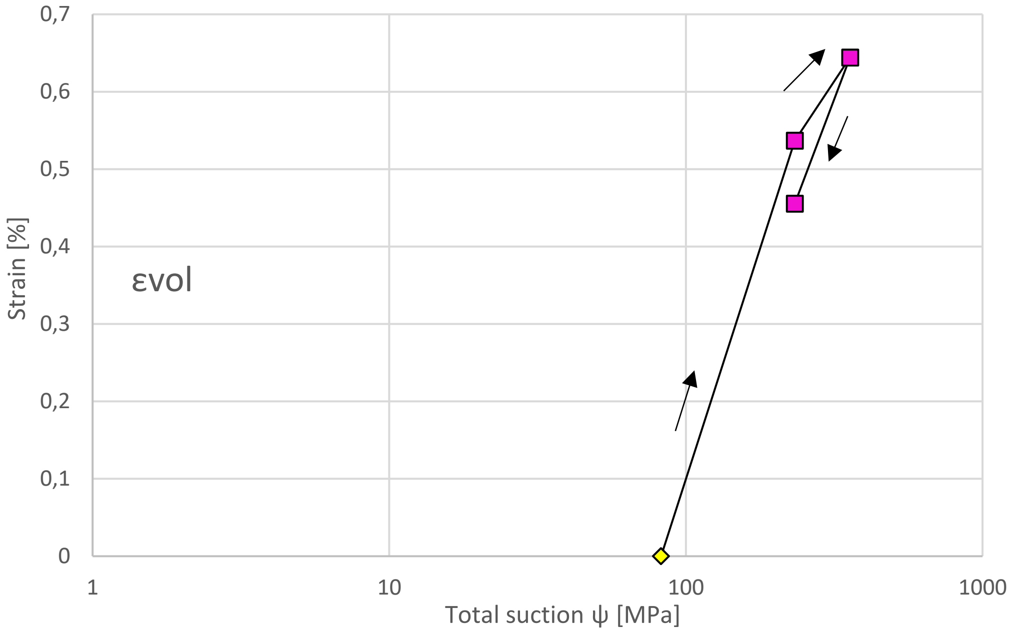

Figure 4-20 Volumetric strain evolution versus suction, Specimen C

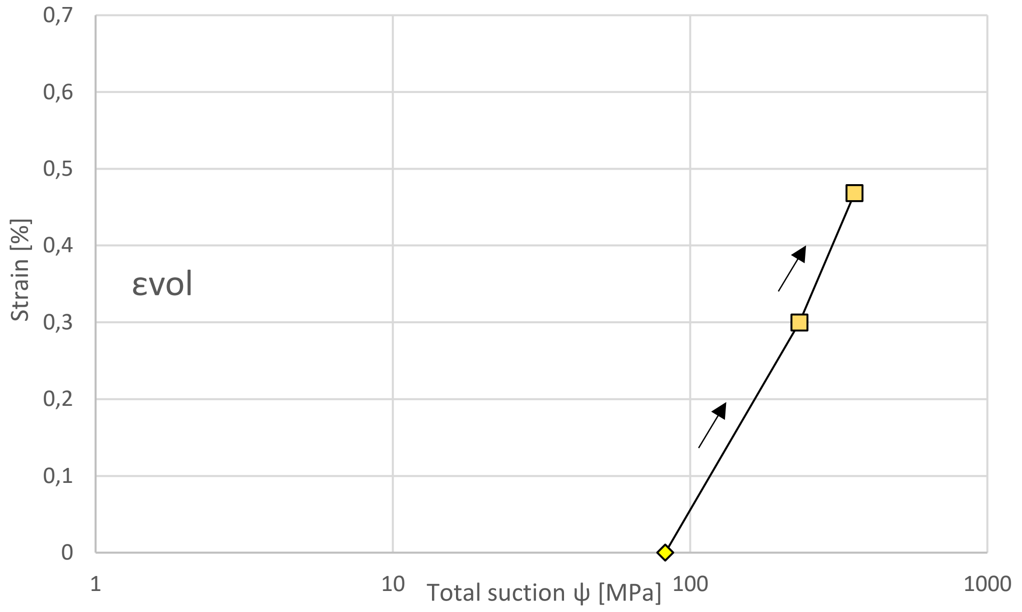

Figure 4-21 Volumetric strain evolution versus suction, Specimen D

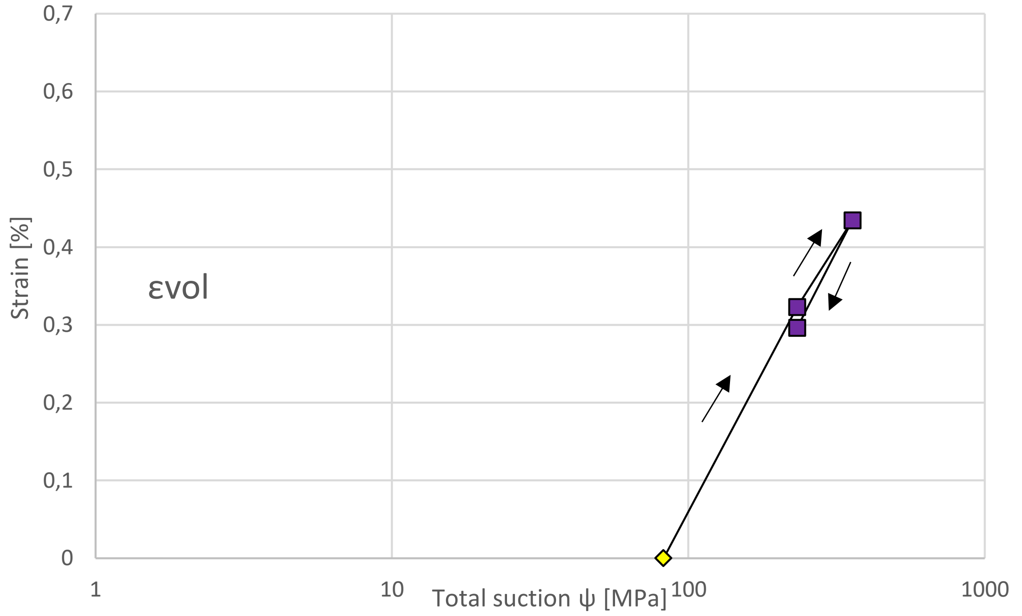

Figure 4-22 Volumetric strain evolution versus suction, Specimen E

As it is possible to observe in *Figure 4-20*, *4-21* and *4-22*, focusing on the first hydraulic step, the shrinkage experienced is much smaller compared with the swelling observed on specimens *A* and *B* at their first step of loading even if the range of suction experienced from the initial condition is about the double in drying than in wetting.

In fact starting from 82,50 MPa to 232,80 MPa (gap od nearly 150 MPa of total suction) the specimens experienced a volumetric deformation of 0,3-0,5% with a change in water content of 0,2% while in wetting from 82,50 MPa to 22,80MPa (gap of nearly 60 MPa of total suction) the samples experienced a volumetric deformation of 0,5-0,6% with a change in water content of 0,3%.

These experimental results confirm the high retention properties of gas shale, where in order to see changes in volume or in water content expecially in the drying path is necessary to apply very high value of total suction.

As regard the hysteretic behaviour experienced after the drying process of specimens *C* and *E*, the amount of the uncovered volumetric strain is about 0,3-0,4%, which also in this case it can be attributed to a change in the microstructure of the geomaterial.

4.2.2.3 Anisotropy of the tested shale

As aforementioned, the lamination structure of shale plays a key role in their hydro-mechanical behaviour, determining the degree of anisotropy.

As regards the swelling and shrinkage response of the tested material, the response of all the specimens upon hydraulic loading is strongly anisotropic, as shown in *Figure 4-23, 4-24, 4-25, 4-26* and *4-27*.

The anisotropy is clearly related to the presence of the bedding planes.

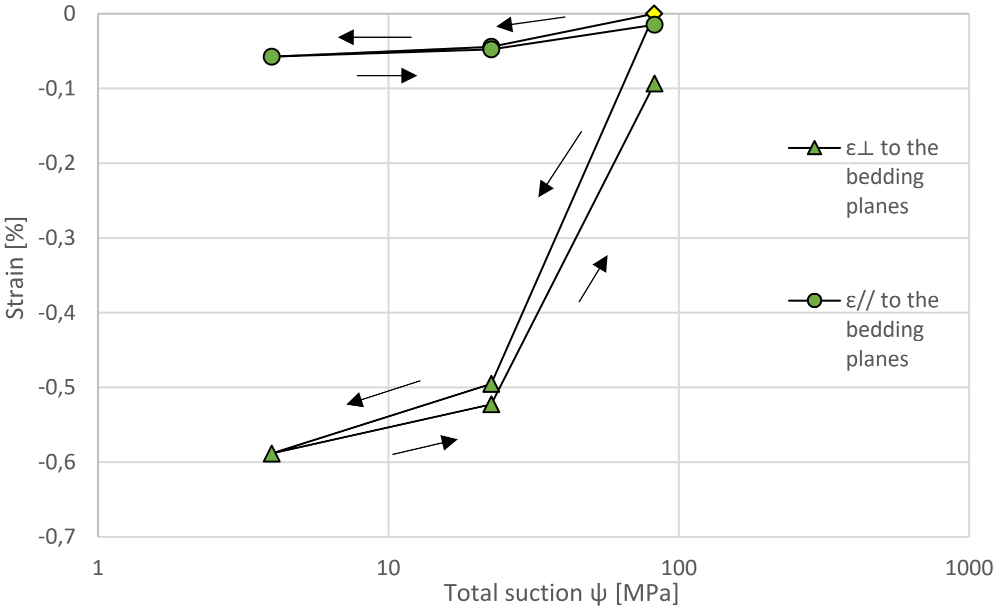

Figure 4-23 Strain determined by total suction changes, Specimen A

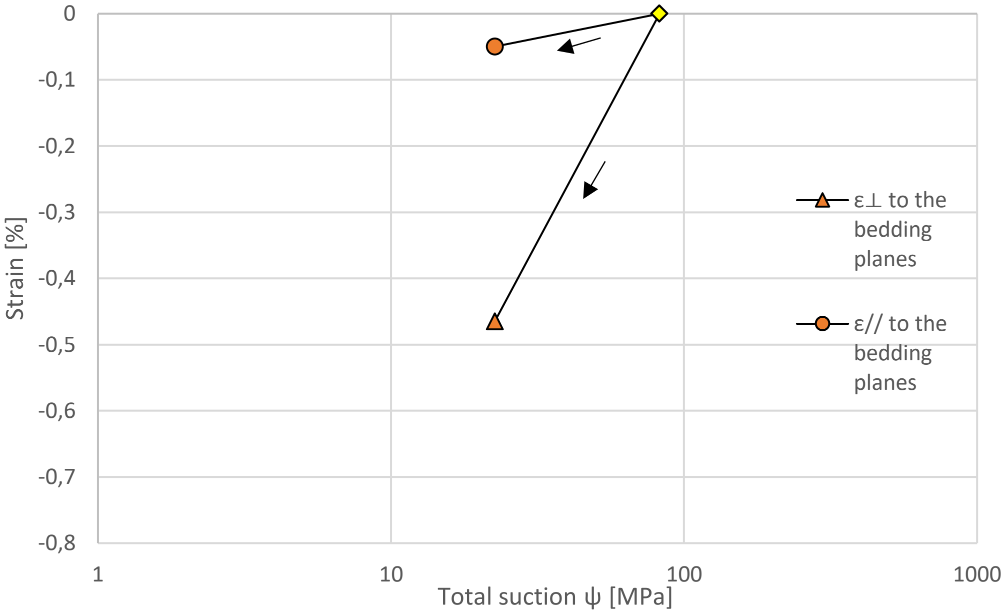

Figure 4-24 Strain determined by total suction changes, Specimen B

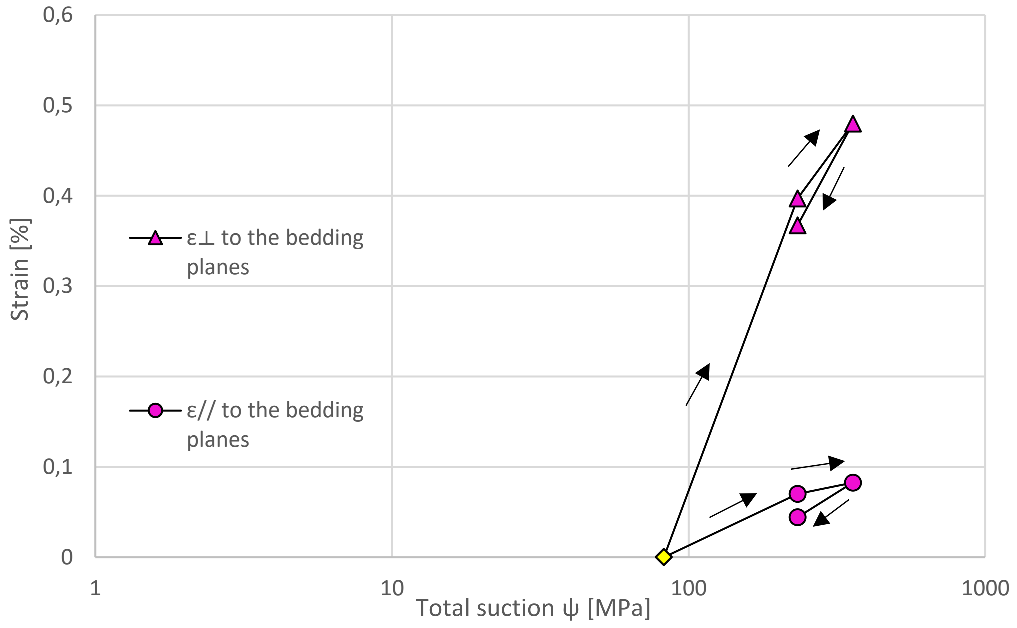

Figure 4-25 Strain determined by total suction changes, Specimen C

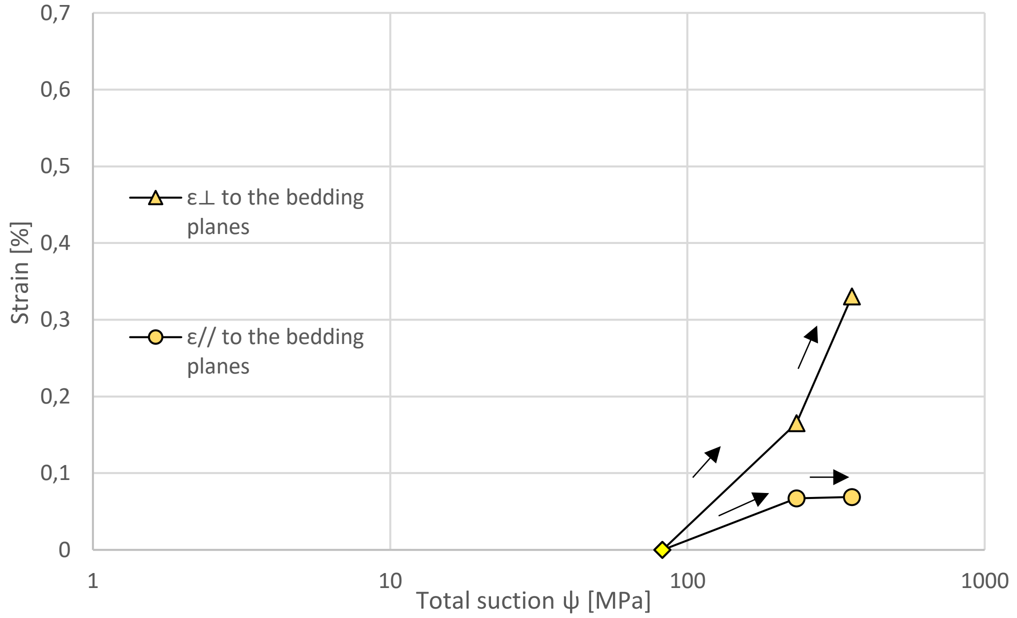

Figure 4-26 Strain determined by total suction changes, Specimen D

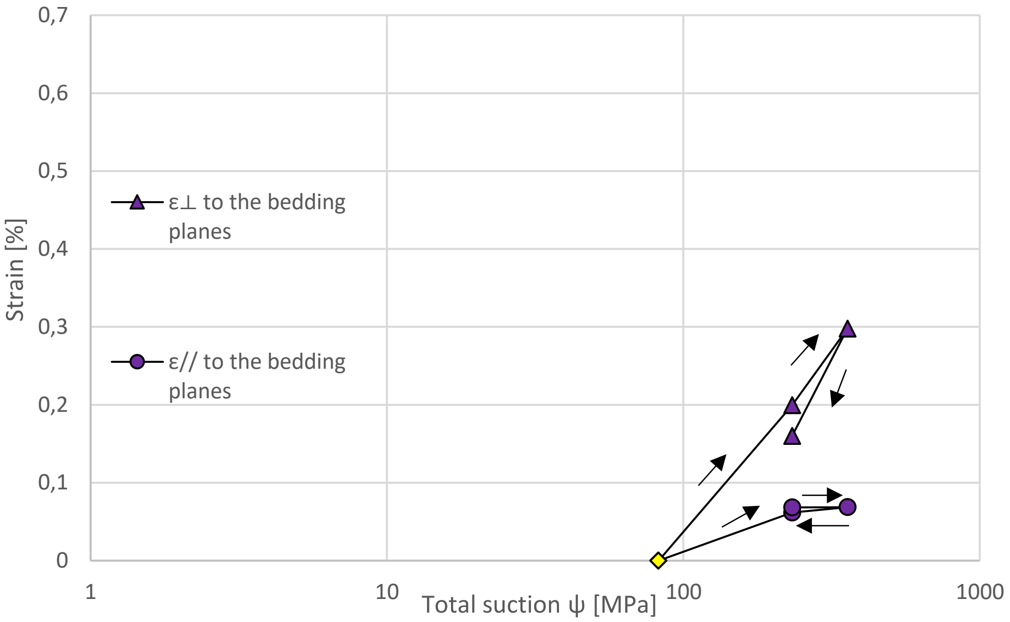

Figure 4-27 Strain determined by total suction changes, Specimen E

The graphs show an amount of strain parallel to the bedding remarkably lower than that in the perpendicular direction both in wetting and drying paths.

In details, the ratio between the strains perpendicular and parallel to the lamination planes is 9 in the wetting paths and 4 in the drying ones.

These difference in the ratio between the deformations, which suggest higher swelling strains can be explained with the opening of the lamination planes in the direction perpendicular to them that allowed and increasing in the permeability in the planar direction.

4.3 Determination of the degree of saturation

As it is highlighted previously, the water retention properties of geomaterials are usually expressed in terms of degree of saturation versus total suction.

The degree of saturation, for each specimen, is computed according to *Equations 2-3* and *3-10,* paying attention for specimen *A* where the volumetric measurements are affected by an error due to its irregular shape, as presented previous in this *Chapter*.

This problem is overcome by using the bulk density at the initial condition of the tested material and the deformation registered at each step in order to compute the evolution of the volume due to the water uptake.

Indeed, even if the volume measurements themselves are affected by an error, as they are computed at each step at the same points on the specimen, the deformations could be considered reliable.

The experimental data for specimen *A* were therefore corrected this way, while no correction was applied to the data of other specimens.

The water retention curve of the tested gas shale in terms of degree of saturation versus total suction is plotted in *Figure 4-28*.

As aforementioned the water retention curve is expressed using on one hand the solid density computed on the intact sample with the Helium pycnometer and on the other the one computed with the Water pycnometer method.

The results are plotted respectively on the left side of the graph in *Figure 4-28* for the degree of saturation "Sr^{He}" computed on basis of the determinations with the Helium pycnometer technique and on the right side for the degree of saturation "Sr^W" on the basis of those with the Water pycnometer technique.

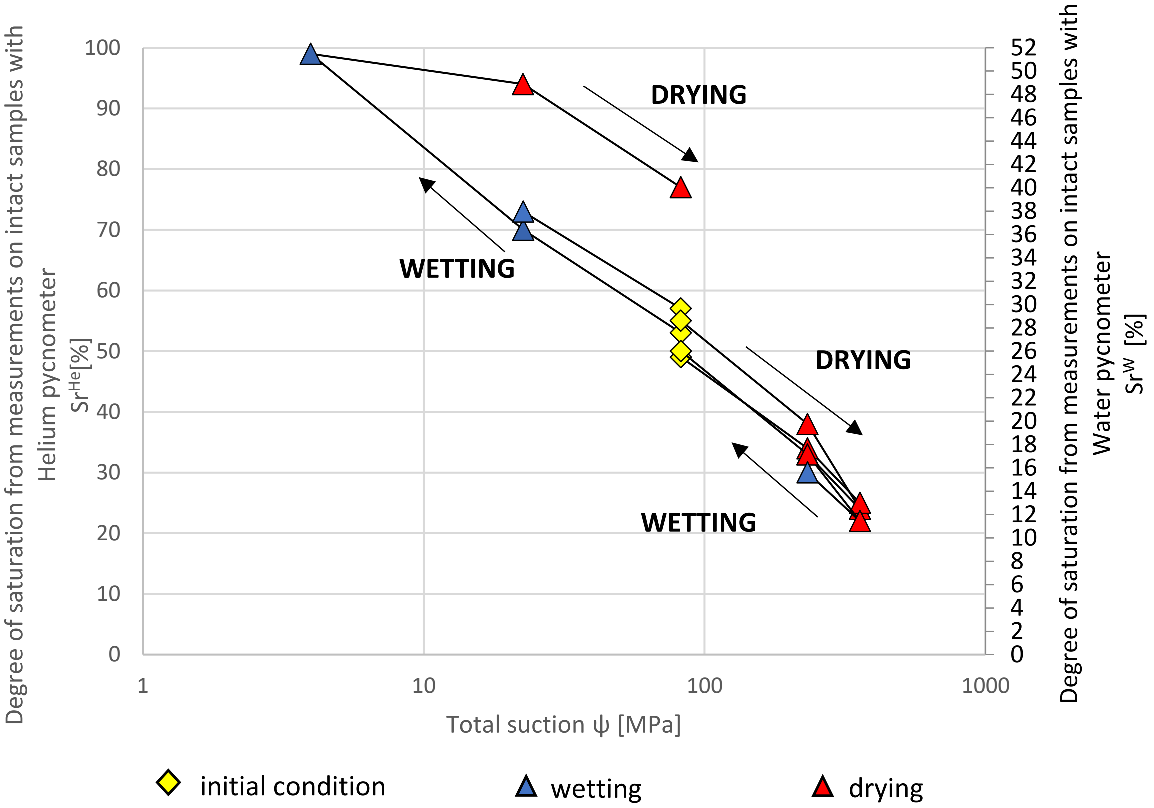

Figure 4-28 Water retention curve in terms of degree of saturation. Y-axis left :side Sr computed with the Helium Pyc solid density(intact). Y-axis right: side Sr computed with the Water Pyc solid density

As it is possible to notice in *Figure 4-28*, using the solid density measured on the intact samples, the degree of saturation of the gas shale at 3,96 MPa reaches the value of 99% versus the value of 52% computed with the solid density measured with the Water pycnometer technique.

4.4 Conclusions

In this chapter all the results obtained on the tested gas shale at the macro scale are presented.

Due to the reduced dimensions of the available specimens a different volume measurement set up it was considered from the previous studies conducted on other shale.

The analyses conducted in order to understand the hydro mechanical behaviour of the tested gas shale exposed in this chapter allowed to determine:

〉 the water retention properties of the tested gas shale in terms of water content and degree of saturation

〉 the swelling and shrinkage response of the tested material upon suction variation, with emphasis on the orientation of the bedding planes that characterize the material, which are the main cause of the anisotropic behaviour of shales.

During the tests conducted it was possible to observe a crack expansion due to the water uptake that capture my attention on the structural characteristics of the tested material, leading me to get further in details by other analyses at the microscale in order to understand the internal behaviour of the specimens upon suction variation, which are presented in the following chapter in thesis.

5 Evolution of the microstructure of the tested shale along wetting and drying paths

During the wetting and drying paths, the tested specimens experienced an increase-decrease in volume. This happened because of water entering or leaving the porous medium.

As a result of the previous experimental studies on the same gas shale, presented in the first chapters of the thesis, an increase in the opening of a natural crack in one of the specimens due to the evolution of the water uptake was observed. This result motivated further investigations on other samples of the same gas shale on another scale, looking inside the specimens.

The evolution of the microstructure of some specimens was studied with micro-CT analyses, with the aim of quantify how microcracks increase or decrease in size upon suction variation in free stress conditions.

The knowledge of cracks geometry within the sample is of primary importance in the prediction of the mechanical and hydraulic behaviour of the tested material (Josh et al. 2012).

5.1 Materials and methods

The developed experimental technique for studying how the microstructure changes due to the water evolution of gas shales is based on a series of tomography images taken at different suctions.

Different hydraulic paths were considered in order to study the response in term of water uptake and volumetric deformation during the wetting and drying episodes.

The following section provides details on the tested material, experimental methodology, tomograph specification and wetting and drying paths applied.

5.1.1 Tested materials

The tested materials are specimens extracted by the 1C core sample at a depth of 3418,149-3418,195 m.

With a mechanical saw, four cylinders with a diameter of 25mm among the length of the core sample were obtained.

When the core was cut in small cylinders perpendicular to the bedding planes of the material, these were divided into smaller cylinders in height by the natural division of them along the bedding planes due to the fissility of the material.

This natural process, leads to obtain samples with irregular shape at the top and at the bottom of the specimens.

In order to do not change further the initial conditions of the specimens, two of them, specimen *2* and specimen *3*, shown in *Figure 5-1* were used without reshape them in order to conduct the experimental analyses at the microscale.

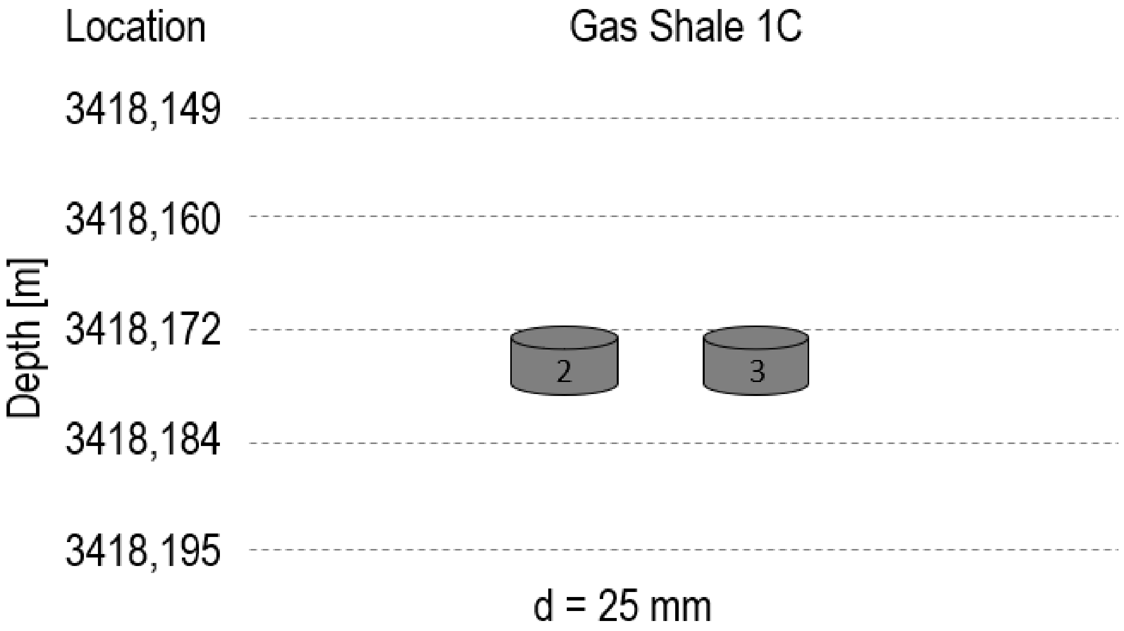

Figure 5-1 Specimens for the microscopic behaviour

The initial properties of the material are reported in *Chapter 3.*

5.1.2 Experimental methodology and testing procedures

As it was observed during the wetting and drying cycle performed on specimen *A*, the gas shale is characterized by an irreversible hydro-mechanical behaviour.

The registered irreversible strains, as discussed in *Section 4.2.2* were attributed to the change in the microstructure of the tested specimen upon suction variation.

This irreversibility has to be taken into account in order to understand how the geomaterial behaves when it is involved in engineering application where the change in water content could happen frequently and some change in microstructure could affect the response of the material.

According to that, a specific laboratory test was set up under free stress conditions, by applying different steps of suction with the vapour equilibrium technique.

The steps applied to specimens *2* and *3* are reported in *Table 5-1* .

These specimens were subjected at a X-ray micro-computed analysis in order to study the experienced change in the microstructure after the wetting and drying steps.

	Steps		
Sample	**#0**	**#1**	**#2**
2	82,50 MPa	22,60 MPa	3,96 MPa
3	82,50 MPa	232,80 MPa	357,42 MPa

Table 5-1 Suction imposed for the micro-analyses

At the end of the step #2 and at the end of all the tomography images, both the specimens were brought back to the first value of suction of ψ = 82,50 MPa, in order to register the hysteretic behaviour of the water content evolution.

As regard the procedure applied in order to get the X-Ray images, at the end of each suction step the samples were weighted and then wrapped into paraffin film to avoid water loss.

The capture of the X-Ray images took about 2 hours, in which the specimens were not stored in a desiccator at a controlled relative humidity but they were protected with the paraffin from the environment conditions.

5.1.3 Tomograph specification

X-Ray micro-computed tomography is a non-invasive technique that allows to investigate the interior of the sample.

In general, the X-rays are directed from a source to the sample and hit the detectors which measure the intensities of the rays. Knowing the intensity of the emitted rays, the detectors are used to calculate the attenuation, which is related to the density.

The principle of tomography analysis is a series of images of the specimens that are taken in a range of angular orientations creating a 2D radiographs that are successively reconstructed in order to observe a three-dimensional visualization of the sample.

The tomograph used in these analyses is the X-Ray Ultratom (RX-solutions, PIXE-EPFL) micro-tomography (μ-CT) system, which is equipped with a Hamamatsu 230kV X-Ray beam source.

The scans performed have a resolution, in terms of Voxel size of 12-15 μm, which indicates the impossibility to investigate at that precision the dimension of the micropores of the tested shale which are in the range of nm. In fact, most of the pores in shales are in the range of nanometre which is below the precision of the microscopy tools.

At the end of the acquisition of the images, in order to post-processing all the data, it is required the use of a RX-solution post-processing software that filters all the collected pictures and the software Avizo Thermo Fisher Scientific which enables users to perform data visualization.

In particular, the software Avizo is used in order to identify the different parts that characterize the material such as the pyrite, the micro-cracks and the matrix in general.

All the components, listed above, are identified by a grey scale threshold that represents the density of the elements inside the material, distinguish from white-light grey the high-density elements such as the pyrite and black the low-density elements such as the microcracks.

All the images, using Avizo are segmented, the components are identified in them and then different layers are created with the aim of better visualize the internal structure of the tested gas shale.

In the graphic results reported below, in blue it is possible to notice the microcracks identified at the initial condition, at the first step of wetting/drying and then at the lowest/highest value of suction imposed.

Moreover, in grey it is highlighted the denser elements, such as pyrite concretions.

Because of a higher density, the pyrite can create artefacts in the tomography, which can be observed as a black part sourranding the bright element in the row data that can be confused with cracks.

5.2 Response along the wetting path

In this section all the results regarding specimen 2 are reported. After the equalization at ψ = 82,50 MPa, this specimen was wetted reaching the value of ψ = 3,96 MPa.

At each step a scan was taken in order to investigate the evolution of the micro-cracks inside the material.

5.2.1 Water uptake

The result reported in this part is the evolution in the water content due to the change in suction performed on specimen 2.

At the end of the lowest value of suction imposed the specimen was then loaded back following the same steps of total suction, as shown in *Figure 5-2*.

At the end it is possible to observe the hysteretic behaviour of the evolution of the water content, registering a value of water content after the last drying process higher than the one observed before at the same value of suctions.

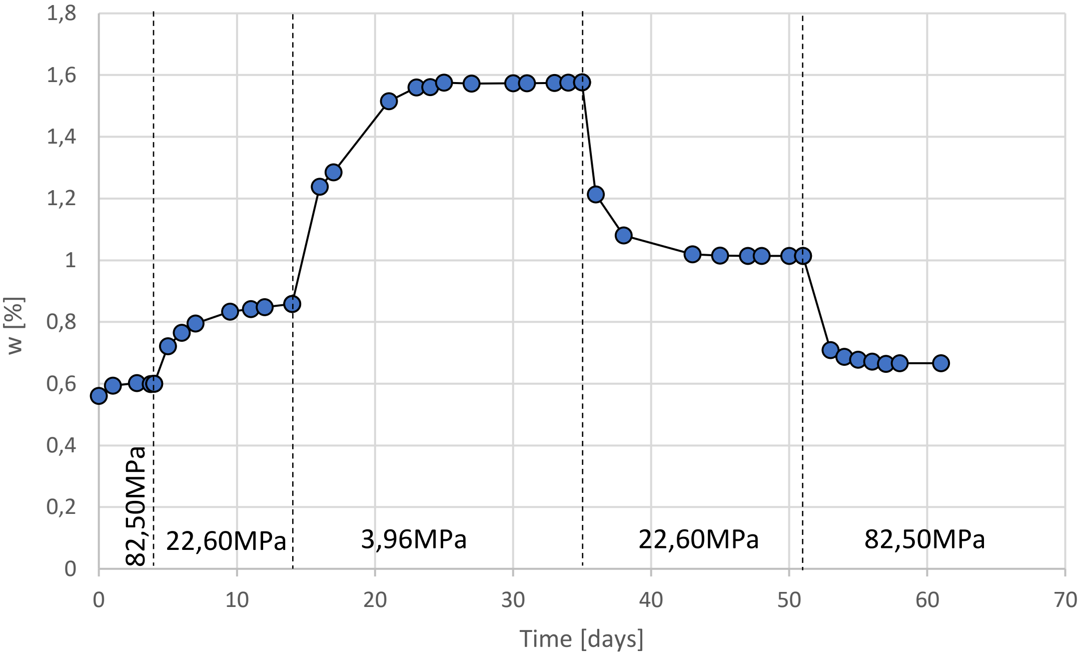

Figure 5-2 Evolution in time of the water content, Specimen 2

5.2.2 Tomographic analysis

The micro-CT analyses conducted on specimen 2 allow to study the internal structure of the specimen.

The extrapolated data, shown in *Figure 5-3,* are the results after the segmentation process conducted using Avizo.

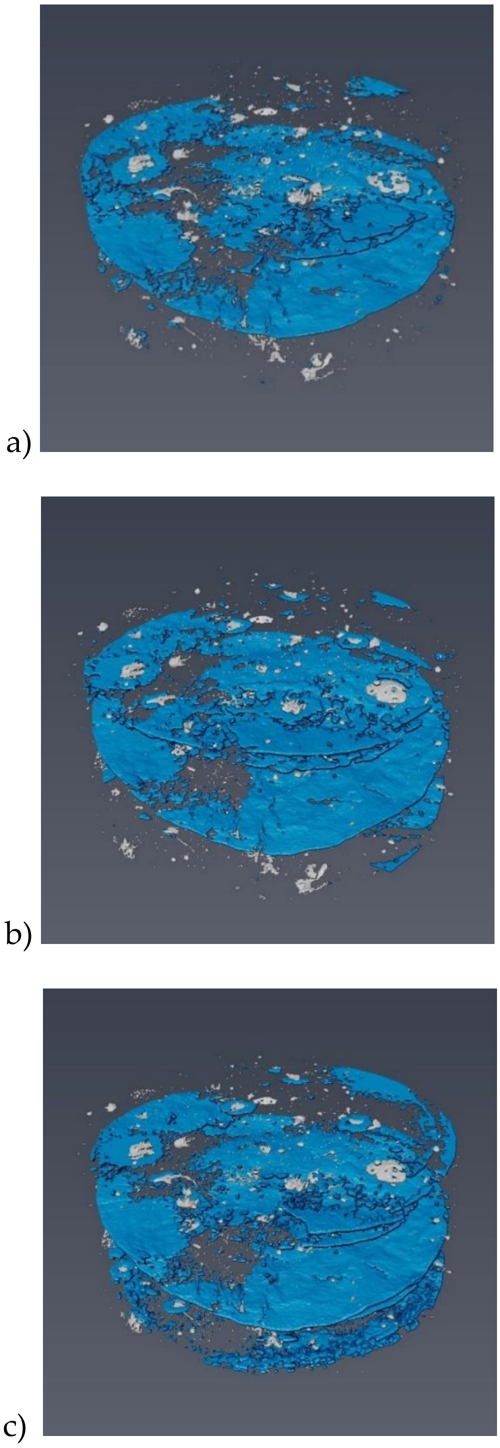

Figure 5-3 Micro-CT analyes on Specimen 2

In particular, in *Figure 5-3a* it is reported the tomography result after the first equalization at ψ = 82,50 MPa; in *Figure 5-3b* the one at ψ = 22,60 MPa and in *Figure 5-3c* at ψ = 3,96 MPa.

At the initial condition the specimen presented a central crack and some thin apertures which are the order of 10-20 micron in thickness.

The orientation of the cracks found at the initial state is comparable with the orientation of the bedding planes of the tested material.

These cracks are probably due to the extraction process of the specimen and the handling of it during the specimen preparation process where the specimen experienced drying.

As it possible to observe in *Figure 5-3*, during the wetting path the cracks identified increase more in volume than in number.

At the last stage the biggest thickness of the aperture registered is about 35-45 micron, two-three times the aperture at the initial conditions.

5.3 Response along the drying path

In this section all the results regarding specimen *3* are reported. After the equalization at ψ = 82,50 MPa, this specimen was dried reaching the value of ψ = 357,42 MPa.

At each step a scan was taken in order to investigate the evolution of the micro-cracks inside the material.

5.3.1 Water uptake

The result reported in this part is the evolution in the water content due to the change in suction performed on specimen 3.

At the end of the highest value of suction imposed the sample is then loaded back following the same steps of total suction, as shown in *Figure 5-4*.

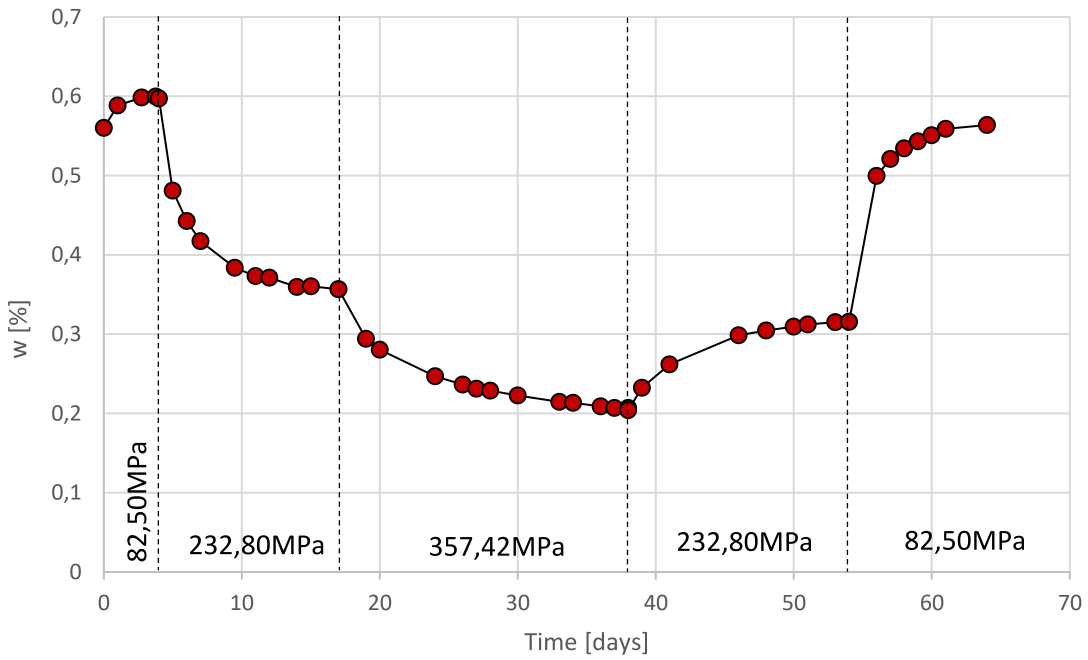

Figure 5-4 Evolution in time of the water content, Specimen 3

At the end it is possible to observe the hysteretic behaviour of the evolution of the water content, registering a value of water content after the desiccation process lower than the one observed before at the same value of suctions.

5.3.2 Tomographic analysis

The micro-CT analyses conducted on specimen *3* allow to study the internal structure of the specimen.

The extrapolated data, shown in *Figure 5-5,* are the results after the segmentation process conducted using Avizo.

In particular, in *Figure 5-5a* it is reported the tomography result after the first equalization at ψ = 82,50 MPa; in *Figure 5-5b* the one at ψ = 232,80 MPa and in *Figure 5-5c* at ψ = 357,42 MPa.

At the initial condition the specimen presented some cracks which are the order of 10-20 micron in thickness.

The orientation of the cracks found at the initial state is comparable with the orientation of the bedding planes of the tested material.

These cracks are probably due to the extraction process of the specimen and the handling of it during the specimen preparation process where the specimen experienced a desiccation path.

As it possible to observe in *Figure 5-5*, during the drying path the cracks identified at the initial condition still remain unchanged.

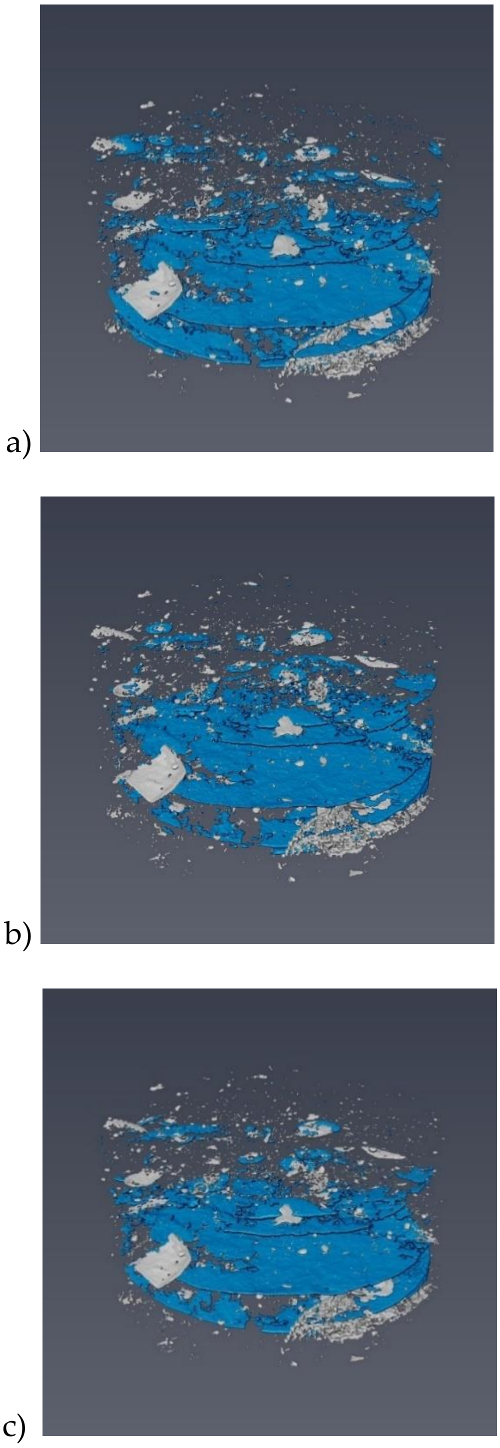

Figure 5-5 Micro-CT analyes on Specimen 3

5.4 Results and conclusions

The tests conducted through the tomograph, allow to understand how the internal structure of the tested gas shale changes upon suction variation.

The tested samples are specimens that came from the same depth of the same core, but despite that some diversities could be found due to the heterogeneities of the shale.

It is important to recall that with the tomography analysis it is possible to measure the entire volume of the tested material with precision.

However, during these analyses it resulted difficult to isolate the border of the specimens from all the images. This is due to the irregular shapes at the top and at the bottom of the samples, which were not reshaped in order to avoid any damage of the material at the initial condition. Moreover, these irregularities are the main cause of artefacts in the images.

According to that, the volume considered was extrapolated by cutting off the edges of the specimens.

The results obtained in terms of volume isolated during the segmentation at the initial condition, ψ = 82,50 MPa, are reported in *Table 5-2* for both the specimens, specifying the class of element considered.

As it possible to notice, at the initial stage the volume of cracks results comparable for both the specimens. What immediately capture the attention is the amount of pyrite concretions of the specimens. In fact, the volume of pyrite inside specimen *3* results four times the value estimated on specimen *2*.

This result highlight the heterogeneties of shales, where from one formation to another, along the depth or as in this case at the same depth and in the same formation the properties could change.

Sample	**Volume of element [mm³]**	
	Pyrite	**Crack**
2	7,7	54,3
3	28,0	52,7

Table 5-2 Measure from the tomography analysis-initial conditions

A high value of pyrite inside the sample leads to a high value of solid density of the material, as the density of the pyrite is two times the density of the clay matrix in which the concretions are immersed.

The following *Table 5-3* shows the quantitative result obtained from specimen 2 upon total suction variation.

Sample	**#0** **82,50MPa**		**#1** **22,60MPa**		**#2** **3,96MPa**	
	Pyrite [mm³]	**Crack [mm³]**	**Pyrite [mm³]**	**Crack [mm³]**	**Pyrite [mm³]**	**Crack [mm³]**
2	7,7	54,3	7,6	73,9	7,6	92,4

Table 5-3 Volume of element, tomography analyses wetting path

The following *Table 5-4* shows the quantitative result obtained from sample *3* upon total suction variation.

Sample	**#0** **82,50MPa**		**#1** **232,80MPa**		**#2** **357,42MPa**	
	Pyrite [mm^3]	**Crack [mm^3]**	**Pyrite [mm^3]**	**Crack [mm^3]**	**Pyrite [mm^3]**	**Crack [mm^3]**
3	28,0	52,7	27,9	52,4	28,0	52,7

Table 5-4 Volume of element, tomography analyses drying path

Comparing the response in wetting and in drying, from *Table 5-3* and *5-4*, it is possible to appreciate the increasing of the cracks volume that occurred during the wetting path, while this remained constant in the drying steps. As regard the quantification of the pyrite, at each step and for each specimen it is observed the same value as expected.

The increasing in crack's aperture which was experienced in the wetting path confirms the macroscopic observation discussed in *Section 4.2.2.*

Moreover, this change in the microstructure due to the change in water content can explain the irreversibility of the macroscopic mechanical behaviour experienced by specimen *A* (see *Section 4.2.2*) and the hysteresis of the water content registered. Indeed, with the increasing of cracks, water can penetrate and be stored in the sample on these "new" cracks surface areas as a result of the adsorption process of clay minerals.

As regard the response observed in the drying path, a significant change in cracks' volume is not registered.

Although a closing in cracks is not observed, the hysteretic behaviour of specimen *3* can be explained with the macroscopic observation of shrinkage in the drying paths (see *Section 4.2.2*). In fact, it is possible that during the desiccation process some micropores on the surface of the samples collapsed and not allow to vapour molecules to enter again in the specimen when it is wetted back to the initial conditions.

The results found in this section demonstrate the importance to consider simultaneously the hydro-mechanical response of the tested material, and the role of microstructure which represents a key factor to predict the shale behaviour, its permeability and sealing capacity.

6 Numerical analysis of vapour equilibrium tests

In this section, a numerical study is presented with the aim of reproducing numerically the results obtained in the laboratory during the experimental tests, regards the change in water content upon total suction variations.

The numerical analyses were implemented in the Finite Element code COMSOL Multiphysics 5.5, allowing to define suitable values of the vapour diffusion coefficient for the tested gas shales.

In particular, the variation of the tortuosity factor with the imposed total suction steps was studied through back analysis.

In order to model the phenomena that are involved in the unsaturated geomaterial, as shale, during the application of the vapour equilibrium technique, it is necessary to describe the partial differential equations (PDEs) that governing the behaviour of this material during the vapour transfer.

Firstly, an overview of several PDEs describing the unsaturated soil behaviour are presented, considering numerous phenomena such as liquid water and water vapour flows that influence the water uptake of a soil, then all the equations considered are simplified in order to get the closed system that governing the phenomena related to the vapour equilibrium technique adding the required assumption, constitutive relationships, soil proprieties and boundary conditions to the problem.

6.1 The use of PDEs to unsaturated geomaterials

With the aim of modelling the unsaturated behaviour, continuum mechanics and differential calculus is required, which is expressed form partial differential equations that refers how the soil state variables change in space and in time (Fredlund et al. 2012).

As known, in saturated problems a lot of analytical solutions were developed, however in the field of unsaturated the partial differential equations, that describe the problem, are more complex and cannot be solved analytically.

According to the continuum mechanics in order to model phenomena in unsaturated soil it is necessary to:

- identify the physical process that occurs and find the “continuum variables” that act in the representative element volume of the soil
- develop field equations making the assumption that the media can be considered as a continuum from a macroscopic point of view, defining:
  - conservation laws, in terms of mass balance equations
  - a final system of well-posed determinate partial differential equations
- define appropriate boundary conditions to the problem
- provide a mathematical solution of the system of PDEs.

According with Fredlund (2005) in order to define the PDEs, some basic assumptions need to be taken:

- soil phases can be described using a continuum mechanic approach
- pore-air (including water vapour) behaves as an ideal gas, following the ideal gas law
- local thermodynamic equilibrium between the liquid water and the water vapour phases exists at all times at any point of the soil
- atmospheric pressure gradients are negligible
- liquid water and soil particles are assumed incompressible
- hysteretic behaviour of the soil-water characteristic curve can be neglected or approximated by taking the logarithmic average between the main drying and the main wetting curves.

6.2 Governing equations in the vapour diffusion mechanism

Porous geomaterial, as shales, can absorb moisture in vapour or in liquid form from the environment and transport it into their matrix, in porous media under the influence of different physical mechanisms.

In order to understand how the material will change the water content, it is important to focused on the gas and vapour transports which are the dominant mechanisms in vapour equilibrium technique making the assumption that the liquid flow is negligible.

When a sample is put in a closed system, in isothermal conditions and under control of the value of relative humidity by using different kinds of solutions, imbibition or desiccation may occur. This is due to a gradient between the water potential of the moisture air in the desiccator and the one inside the pore matrix.

In order to study this phenomenon, it is necessary to consider the total suction applied as a continuum variable and express all the equations that govern the behaviour of shales in terms of it.

6.2.1 Field equations

6.2.1.1 Mass balance equations

Differential equations for the conservation of the mass of water and air in unsaturated geomaterials in three dimensions are obtained equating the flow rates in and out of the REV, representative element volume, and the change of mass storage in the REV with time.

As the material is unsaturated, in order to describe its behaviour, it is important to consider both the liquid phase and the gaseous phase that compose it.

The mass of pore-water or pore-air is conserved assuming that the net flux of inflow and the outflow is equal to the amount of water or air being lost or gained in the elemental volume of soil in *Figure 6-1* (Lu et al. 2004).

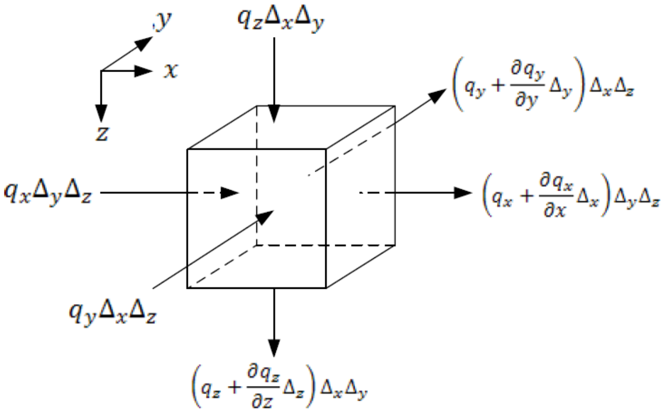

Figure 6-1 Elemental volume of soil and continuity requirements, Lu et al. 2004

Following this approach, it is possible to write the inflow and the outflow as:

$$q_{in} = ({q^{\alpha}}_x \Delta y \Delta z + {q^{\alpha}}_y \Delta x \Delta z + {q^{\alpha}}_z \Delta z \Delta y) \tag{6-1}$$

Equation 6-1 Inflow in REV

$$q_{out} = \left({q^{\alpha}}_x + \frac{\partial {q^{\alpha}}_x}{\partial x}\Delta x\right)\Delta y \Delta z + \left({q^{\alpha}}_y + \frac{\partial {q^{\alpha}}_y}{\partial y}\Delta y\right)\Delta x \Delta z + \left({q^{\alpha}}_z + \frac{\partial {q^{\alpha}}_z}{\partial z}\Delta z\right)\Delta z \Delta y \tag{6-2}$$

Equation 6-2 Outflow in REV

where:

α is the phase, respectively water or air

${q^{\alpha}}_i$ is the flow rate of water or air in the i-directions [M L^{-2} t^{-1}]

Δ_i are the dimensions of the elemental volume of soil in i-direction respectively [L]

In order to get the mass balance equations, it is important to add the concept of storage in the REV.

In fact, the loss or gain in water or air can be expressed as storage, which is the net mass change of water or air in the elemental volume of the soil per rate change of time as follows:

$$\frac{\partial M_\alpha}{\partial t} \tag{6-3}$$

Equation 6-3 Storage in REV

where M_α is the mass of air or water in the REV.

By expressing the mass as:

$$M_\alpha = \rho_\alpha V_\alpha \tag{6-4}$$

Equation 6-4 Mass

where V_α is the volume of the air or the water content in the REV, it is possible to define the mass in *Equation 6-4* as:

$$M_\alpha = \rho_\alpha S_\alpha n V_o \tag{6-5}$$

Equation 6-5 Mass as a function of degree of saturation

where:

ρ_α is the density of water or air respectively [M L^{-3}]

S_α is the degree of saturation of water or air [-]

$$S_\alpha = \frac{V_\alpha}{V_0}\ [-] \tag{6-6}$$

Equation 6-6 Degree of saturation of the a-phase

n is the porosity [-]

$$n = \frac{V_v}{V_o} \ [-] \tag{6-7}$$

Equation 6-7 Porosity

V_o is the referential volume [L^3]

$$V_0 = \Delta x \Delta y \Delta z \ [L^3] \tag{6-8}$$

Equation 6-8 Referential volume

V_v is the volume of voids in the elemental volume [L^3]

By substituting *Equation 6-8* in *Equation 6-5* and then in *Equation 6-3*, the storage function becomes:

$$\frac{\partial M_\alpha}{\partial t} = \frac{\partial}{\partial t} \left(\rho_\alpha S_\alpha n\right) \Delta x \Delta y \Delta z \tag{6-9}$$

Equation 6-9 Storage function

Finally, the governing equation of transient flows through soil can be derived by equalizing the principle of mass conservation with the storage term as follows:

$$-\left(\frac{\partial {q^\alpha}_x}{\partial x} \Delta x \Delta y \Delta z + \frac{\partial {q^\alpha}_y}{\partial y} \Delta y \Delta x \Delta z + \frac{\partial {q^\alpha}_z}{\partial z} \Delta z \ \Delta z \Delta y\right) = \frac{\partial}{\partial t} \left(\rho_\alpha S_\alpha n\right) \Delta x \Delta y \Delta z \tag{6-10}$$

Equation 6-10 Governing equation of transient flow

Simplifying *Equation 6-10*:

$$-\left(\frac{\partial {q^\alpha}_x}{\partial x} + \frac{\partial {q^\alpha}_y}{\partial y} + \frac{\partial {q^\alpha}_z}{\partial z}\right) = \frac{\partial}{\partial t} \left(\rho_\alpha S_\alpha n\right) \tag{6-11}$$

Equation 6-11 Continuity equation of transient flow

Equation 6-11 is known as continuity equation of transient flow.

The continuity equation can be written for pore-water flow and pore-air flow separately as:

- Conservation of mass of pore-water

$$-\left(\frac{\partial q^{w}{}_{x}}{\partial x}+\frac{\partial q^{w}{}_{y}}{\partial y}+\frac{\partial q^{w}{}_{z}}{\partial z}\right)=\frac{\partial}{\partial t}\left(\rho_w S_w n\right) \qquad (6\text{-}12)$$

Equation 6-12 Conservation of mass of pore-water

- Conservation of mass of pore-air

$$-\left(\frac{\partial q^{a}{}_{x}}{\partial x}+\frac{\partial q^{a}{}_{y}}{\partial y}+\frac{\partial q^{a}{}_{z}}{\partial z}\right)=\frac{\partial}{\partial t}\left(\rho_a S_a n\right) \qquad (6\text{-}13)$$

Equation 6-13 Conservation of mass of pore-air

where:

q_{i}^{w} is the total water flow rate in the i-direction across a unit area of the soil [M L^2 t^{-1}]

$$q_{i}^{w}=\rho_w v_i^w \quad [\mathrm{M\,L^2}\,t^{-1}] \qquad (6\text{-}14)$$

Equation 6-14 Total water flow rate

ρ_w is the density of the water [M L^{-3}]

The following expression can be used to relate the mass density of water to the temperature:

$$\rho_w = 1000\left[1-\frac{(T_C+288{,}9414)(T_C-3{,}9863)^2}{508929{,}2\,(T_C+68{,}12963)}\right] \quad [kg/m^3] \qquad (6\text{-}15)$$

Equation 6-15 Water density

T_C temperature [°C]

The density of water generally under isothermal conditions is commonly taken as 1000 kg/m^3 for most of the geotechnical engineering problems.

v_i^w water flow rate in the i-direction across a unit area of the soil [L t^{-1}]

$q_{\underset{i}{a}}$ is the total air flow rate in the i-direction across a unit area of the soil [M L^{-2} t^{-1}]

$$q_{\underset{i}{a}} = \rho_a v_i^a \quad [M\ L^{-2} t^{-1}] \tag{6-16}$$

Equation 6-16 Total air flow rate

ρ_a is the density of air [M L^3]

$$\rho_a = \frac{W_a}{RT_K}\overline{u_a} \quad [kg/m^3] \tag{6-17}$$

Equation 6-17 Air density

W_a molecular weight of air that depends on the composition of the mixture[kg/kmol]   For dry air it is 28,966 kg/kmol

R universal molar gas constant, 8,31432 J/mol K

T_K absolute temperature [K] $T_K = T_C + 273{,}15$

$\overline{u_a}$ absolute air pressure where the overbar indicates absolute pressure [kPa]

$$\overline{u_a} = u_a + u_{atm} \tag{6-18}$$

Equation 6-18 Absolute air pressure

u_a gauge air pressure [kPa]

u_{atm} atmospheric pressure, 101,3 kPa

v_i^a air flow rate in the i-direction across a unit area of the soil [L t^{-1}]

S_w is the degree of saturation of water [-]

$$S_w = \frac{V_w}{V_0}\ [-] \tag{6-19}$$

Equation 6-19 Degree of saturation of water

S_a is the degree of saturation of air [-]

$$S_a = \frac{V_a}{V_0}\ [-] \tag{6-20}$$

Equation 6-20 Degree of saturation of air

n is the porosity [-]

t is the time.

In order to close the coupled system of *Equation 6-12* and *Equation 6-13* is necessary to find other relations that relate the five unknowns, S_a , S_w , v_i^a, v_i^w, n, making the assumption that air density and water density could be constants.

Equation 6-12 and *Equation 6-13* are related together with the restriction that the sum of the degree of saturations is equal to unit:

$$S_w + S_a = 1 \tag{6-21}$$

Equation 6-21 Relationship between degree of saturations,A

Starting from *Equation 6-21* for the rest of the treatment the degree of saturation considered S, will be:

$$S_w = S \tag{6-22}$$

$$S_a = 1 - S$$

Equation 6-22 Relationship between degree of saturations,B

As regards v_i^a, v_i^w, which are the flow rates, they are expressed as flow laws discussed later in this chapter, and simplified in order to consider only the driving potentials that occur in the problem studied.

Before describing the flow laws that govern this problem, it is possible to make another assumption on the air pressure and consider it constant because the vapour equilibrium technique is applied in a closed system where there is no movement of air inside the jar and all the test is done in atmospheric conditions which gradients are considered negligible from the beginning of this treatment (*see Paragraph 6.1*). This leads *Equation 6-16* as a constant value and the left side of *Equation 6-13* equal to zero.

As a consequence, the coupled system of *Equation 6-12* and *Equation 6-13*, becomes only one expression:

$$-\left(\frac{\partial {q^w}_x}{\partial x}+\frac{\partial {q^w}_y}{\partial y}+\frac{\partial {q^w}_z}{\partial z}\right)=\rho_w\frac{\partial}{\partial t}\,(Sn) \tag{6-23}$$

Equation 6-23 Summary of the coupled system

In order to write *Equation 6-23* in terms of total suction ψ, it's possible to apply the chain rule in the right part of the equation as follows:

$$\frac{\partial}{\partial t}\,(Sn)=\ n\frac{\partial S}{\partial t}+S\frac{\partial n}{\partial t}=n\frac{\partial S}{\partial \psi}\frac{\partial \psi}{\partial t}+S\frac{\partial n}{\partial \psi}\frac{\partial \psi}{\partial t} \tag{6-24}$$

Equation 6-24 Chain rule on the mass storage,A

Calling $-n\frac{\partial S}{\partial \psi}=C_w$ specific moisture capacity, which is the slope of the relationship between degree of saturation and total suction and $S\frac{\partial n}{\partial \psi}=A$, which is the slope of the variation of porosity with the total suction, the *Equation 6-24* becomes:

$$\frac{\partial}{\partial t}\,(Sn)=\ n\frac{\partial S}{\partial t}+S\frac{\partial n}{\partial t}=-C_w\frac{\partial \psi}{\partial t}+A\frac{\partial \psi}{\partial t}=(A-C_w)\frac{\partial \psi}{\partial t} \tag{6-25}$$

Equation 6-25 Chain rule on the mass storage,B

Following this approach, substituting *Equation 6-25* in *Equation 6-23* it derives:

$$-\left(\frac{\partial q^{w}{}_{x}}{\partial x}+\frac{\partial q^{w}{}_{y}}{\partial y}+\frac{\partial q^{w}{}_{z}}{\partial z}\right)=\rho_{w}(A-C_{w})\frac{\partial \psi}{\partial t} \tag{6-26}$$

Equation 6-26 Water mass balance equation

The equation above is the water mass balance equation in terms of total suction of an unsaturated soil where the density of the water is considered constant in isothermal conditions.

6.2.1.2 Flow laws of water vapour

There are different flow equations reassumed in *Table 6-1* that are known in order to model unsaturated soil flow behaviour.

Flow laws relate the measure of flow and driving potentials and they have the same format but different proprieties. As shown in *Table 6-1* pore-water can flow in different ways such as liquid water, water vapour diffusing through the free air-phase, or as water vapour carried by moving free air phase.

Type of flow	Flow mechanism	Driving potential	Flow law
Flow of water, v^w	Liquid water, v^{wl}	Hydraulic head h (m)	Darcy's laws
	Water vapour diffusion, v^{vd}	Mass concentration of vapour per unit volume of soil C_v (kg/m^3)	Modified Fick's Law
	Water vapour carried by advection through bulk air flow, v^{va}	Mass concentration of air per unit volume of soil, C_a (kg/m^3)	Modified Fick's law
Interphase liquid-vapour flow	Thermodynamic equilibrium	(*)	Lord Kelvin's equation
(*) local thermodynamic equilibrium assumed , function of the rate of vapour flow			

Table 6-1 Flow laws

Since the aim of this study is to know how the mass of water will change in the geomaterial when the vapour equilibrium technique is applied, it is necessary to focus on the driving potentials that really affect this technique.

The flow of liquid water is described by the Darcy's law. However, since the permeability of shales is very low, this strnsport mechanism is assumed to weak in this cas and it has been neglected compared to the other ones.

The water vapour flow is driven by two different mechanisms, it can flow independently from the pore-air phase driven by a gradient in vapour concentration v^{vd} , or can flow carried by the advection of the bulk pore-air phase as a component of the mix air driven by gradients in the total pore-air pressure v^{va}.

As aforementioned, this last contribution (v^{va}) to the water vapour flow can be not taken into account during this case of study because does not occur during VET where the samples are stored in atmospheric conditions.

As a consequence, the flow of water when the vapour equilibrium technique is applied is due mainly to water vapor diffusion described by vapour concentration as a driving potential.

According with Webb (Pearson, 2000; Gu et al. 1998), the water vapour diffusion v^{vd} follows the Fick's law, which is the most popular and simple approach to evaluate the gas diffusion in clear fluids and not in porous media. In fact, in order to express the formulation of this phenomenon a Modified Fick's law is taken into account (Philip et al. 1957):

$$v_i^{vd} = -\frac{D^v}{\rho_w}\frac{\partial C_v}{\partial i} \quad [L\,t^{-1}] \tag{6-27}$$

Equation 6-27 Modified Fick's law in terms of vapour concentration where:

v_i^{vd} is the pore-water vapour flow rate in the i-direction across a unit area of the soil due to vapour concentration gradients [L t^{-1}]

D^v is the molecular diffusivity of vapour through soil [L^2 t^{-1}]

$$D^v = \tau D_a^v \quad [L^2 t^{-1}] \tag{6-28}$$

Equation 6-28 Molecular diffusivity of vapour through soil

τ is the tortuosity factor of the soil, that describes the tortuosity variable for the diffusion of water vapour through the soil pores (Fredlund et al. 2012)

D_a^v is the diffusion coefficient of vapour in air, which can be expressed as a function of temperature through the relationship:

$$D_a^v = 0{,}229 \cdot 10^{-4} \left(1 + \frac{T_K}{273{,}15}\right)^{1{,}75} \quad [m^2/\,s] \tag{6-29}$$

Equation 6-29 Diffusion coefficient of vapour in air

ρ_w is the density of the water

C^v is the concentration of water vapour in terms of the mass of vapour per unit volume of soil [M L^{-3}]

$$C^v = \rho_v (1 - S) n \quad [M\ L^{-3}] \tag{6-30}$$

Equation 6-30 Concentration of water vapour

ρ_v is the density of the water vapour [M L^{-3}]

$$\rho_v = \frac{W_v p_v}{R T_K} \quad \left[\frac{kg}{m^3}\right] \tag{6-31}$$

Equation 6-31 Density of the water vapour

W_v is the molecular weight of water vapour [kg/kmol], 18,016 kg/kmol

p_v is the partial pressure of water vapour [kPa]

R is the universal gas constant [J/mol K], 8,314J/mol K

T_K is the absolute temperature [K] $T_K = T_C + 273{,}15$

S is the degree of saturation [-]

n is the porosity [-]

By the opportunity substitution the *Equation 6-27* becomes:

$$v_i^{vd} = -\frac{D^{v*}}{\rho_w}\frac{\partial p_v}{\partial i} \quad [L\,t^{-1}] \tag{6-32}$$

Equation 6-32 Modified Fick's law in terms of partial pressure of water vapour

where:

$D^{v*}$is the effective diffusion coefficient of vapour through soil

$$D^{v*} = \frac{\tau\beta D_a^v W_v}{RT_K} \quad [t] \tag{6-33}$$

Equation 6-33 Diffusion coefficient of vapour through soil

β is the cross-sectional area of soil available for vapour flow per total area

$$\beta = (1 - S)n \quad [-] \tag{6-34}$$

Equation 6-34 Cross sectional area of soil available for vapour flow per total area

As aforementioned in the assumptions of the problem, a local thermodynamic equilibrium can be assumed between liquid water and water vapour. This assumption can describe and quantify the mass transfer between the liquid and vapour phase.

This can be expressed by the relation between the total suction and the vapour pressure as:

$$p_v = p_{vsat} e^{\frac{-\psi W_v}{\rho_w R T_K}} \quad [kPa] \tag{6-35}$$

Equation 6-35 Relation between total suction and vapour pressure

where:

p_v is the partial pressure of water vapour [kPa]

p_{vsat} is the saturation vapour pressure of the soil water at temperature T_K [kPa]

This value can be calculated as a function of temperature, follows the Lowe's polynomial equation:

$$p_{vsat} = a_0 + a_1 T_C + a_2 T_C^2 + a_3 T_C^3 + a_4 T_C^4 + a_5 T_C^5 \quad [kPa]$$

$$a_0 = 0{,}6183580754$$

$$a_1 = 0{,}0411427320$$

$$a_2 = 0{,}0017217473$$

$$a_3 = 0{,}0000174108$$

$$a_4 = 0{,}0000003985$$

$$a_5 = 0{,}0000000022$$

T_C= temperature [°C]

ψ is the total suction

W_v is the molecular weight of water vapour (18,016 kg/kmol)

In order to express the *Equation 6-32* in terms of total suction and temperature, is necessary to use the chain rule as follow in *Equation 6-35:*

$$\frac{\partial p_v}{\partial i} = \frac{W_v p_v}{\rho_w R T_K} \left(\frac{\psi}{T_K} \frac{\partial T}{\partial i} - \frac{\partial \psi}{\partial i} \right) \tag{6-36}$$

Equation 6-36 Chain rule on the vapour pressure equation

Assuming that during the vapour equilibrium technique the soil is under isothermal conditions, *Equation 6-36* becomes:

$$\frac{\partial p_v}{\partial i} = -\frac{W_v p_v}{\rho_w R T_K}\left(\frac{\partial \psi}{\partial i}\right) \tag{6-37}$$

Equation 6-37 Gradient of vapour pressure in terms of total suction

In this way, it is possible to express *Equation 6-32* as follow:

$$v_i^{vd} = -\frac{D^{v*}}{\rho_w}\frac{\partial p_v}{\partial i} = \frac{D^{v*}}{\rho_w}\frac{W_v p_v}{\rho_w R T_K}\left(\frac{\partial \psi}{\partial i}\right) \tag{6-38}$$

Equation 6-38 Modified Fick's law in terms of total suction

6.2.2 Partial differential equation for water vapour flow

Combining *Equation 6-14* with *Equation 6-38* and the conservation of pore water in *Equation 6-26,* the PDE that governs this phenomenon in terms of total suction, in 3D dimensions is:

$$-\left(\frac{\partial}{\partial x}\left(\rho_w v_x^{vd} \frac{\partial \psi}{\partial x}\right) + \frac{\partial}{\partial y}\left(\rho_w v_y^{vd} \frac{\partial \psi}{\partial y}\right) + \frac{\partial}{\partial z}\left(\rho_w v_z^{vd} \frac{\partial \psi}{\partial z}\right)\right) = \rho_w (A - C_w)\frac{\partial \psi}{\partial t} \tag{6-39}$$

Equation 6-39 Partial differential equation for water vapour flow

6.2.2.1 Boundary and initial conditions of the problem

In order to set the boundary conditions to the problem, a schematic representation of the 3D dimensions space is shown in *Figure 6-2.*

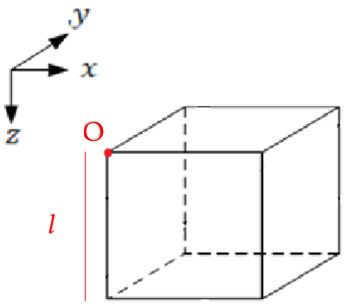

Figure 6-2 Schematic representation of the 3D volume

In *Figure 6-2,* the origin of the axis is set in O and the dimensions of the cube vary form zero to l in each direction. The governing equations of the problem with the set of boundary conditions are listed below:

$$\begin{cases} \rho_w (A - C_w)\dfrac{\partial\psi}{\partial t} = -\nabla\rho_w v_i^{vd} & \\ v_i^{vd} = \dfrac{D^{v*}}{\rho_w}\dfrac{W_v p_v}{\rho_w R T_K}\left(\dfrac{\partial\psi}{\partial i}\right) & \\ & 0 < x < l \quad t = 0 \\ \psi(x,y,z;0) = \psi_{i-1} & 0 < y < l \\ & 0 < z < l \\ & x = 0\,, x = l \quad t > 0 \\ \psi(x,y,z;t) = \psi_i & y = 0\,, y = l \\ & z = 0\,, z = l \end{cases} \tag{6-40}$$

Equation 6-40 Final system for the vapour flow

where:

ψ_{i-1} is the total suction at which the material is equalized from the previous drying or wetting step

ψ_i is the total suction imposed in the jar during the current drying or wetting step

v_i^{vd} is the modified Fick's law in terms of total suction. [L t^{-1}].

6.3 Numerical solution for the water vapour diffusion PDE

In order to provide a mathematical solution of the system of PDEs expressed in *Equation 6-40*, a set of numerical analyses were run, using the Finite Element code COMSOL Multiphysics 5.5.

In particular, the value of tortuosity was studied in order to define a suitable diffusion coefficient for shales upon suction variation through back analysis, expressed as *Equation 6-28*.

6.3.1 Protocol of numerical study

The analyses conducted aim to reproduce numerically the water uptake due to suction variation experienced by specimens *A* and *E*, respectively in wetting and drying.

In particular, different analyses were run change at each hydraulic loading step the value of the tortuosity factor in order to define which one was the best one to fit the experimental data.

The analyses run were divided into different steps, like the experimental tests as shown in *Table 6-2*, where the initial conditions and the boundary conditions applied to the model are summarized:

Specimen	#1	#2
A	$\psi_0 = 82{,}50\ MPa$ $\psi_1 = 22{,}60\ MPa$	$\psi_1 = 22{,}60\ MPa$ $\psi_2 = 3{,}96\ MPa$
E	$\psi_0 = 82{,}50\ MPa$ $\psi_1 = 232{,}80\ MPa$	$\psi_1 = 232{,}80\ MPa$ $\psi_2 = 357{,}42\ MPa$

Table 6-2 Initial conditions and boundary conditions of the numerical analyses

6.3.2 Software specification and numerical model

COMSOL Multiphysics is a Finite Element software for modelling in all fields of engineering and scientific research.

The code is composed by different modules in which there are implemented different equations which are relevant for different engineering fields.

In particular, in this case of study, due to the cylindrical shapes of the specimens, the 2D Axisymmetric space dimension was used, whose implemented coordinates are shown in *Figure 6-3*.

The time dependent analyses were chosen.

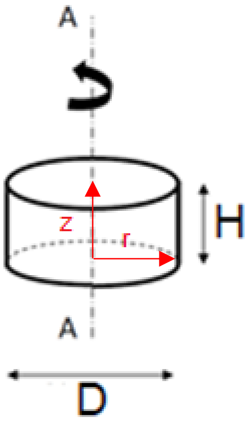

Figure 6-3 Schematic representation of the Axisymmetric space dimension

The COMSOL Multiphysics' module used, was the *Mathematics* one, in particular the *General Form PDE (g)*, in which there were implemented the equations explained previously, adapting the formulas from the cartesian coordinates to the cylindrical ones.

In the model the dependent variable chosen was the total suction ψ defined in Pa.

With the aim of setting up the model, COMSOL Multiphysics required different steps:

- define the geometry in terms of object type, size and shape and position refers to the axis of symmetry, which was oriented perpendicular to the bedding planes, (the value used are summarized in *Table 6-3*)

Specimen	**Object type**	**H [m]**	**D [m]**
A	solid	0,0075	0,0128
E	solid	0,0153	0,0128

Table 6-3 Geometry for the models

- define the input parameters and the input variables that depend on the dependent variable ψ

- define initial values of ψ_1 in the domain, which is the one imposed at the previous step
- define Dirichlet boundary condition as a prescribed value of ψ_2, which is the one imposed at the following step
- mesh the domain as a physics-controlled mesh, in particular the one chosen was the extra fine mesh as shown as an example in *Figure 6-4*

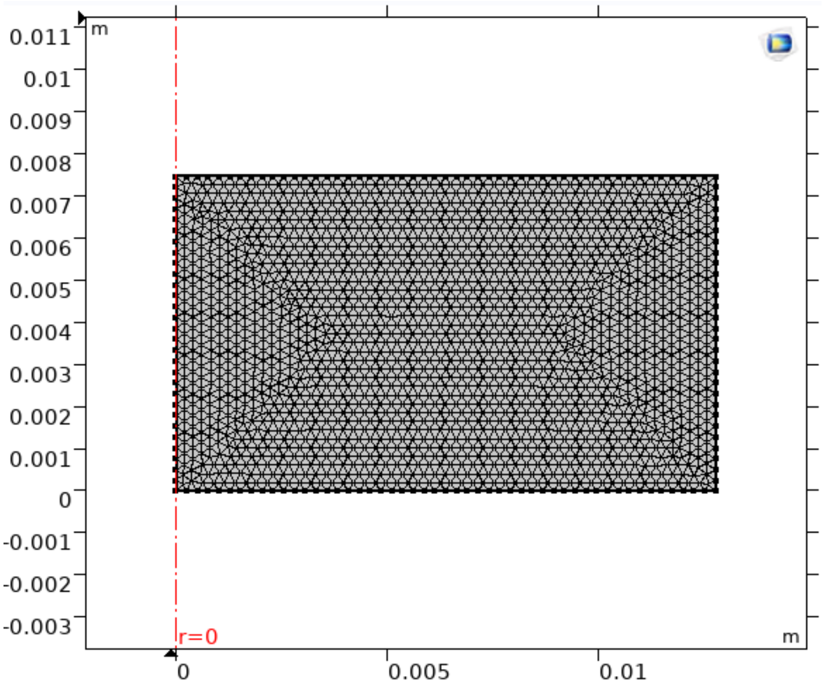

Figure 6-4 Extra fine mesh, from COMSOL model

- define a time step, the one chosen was in day units, from 0 to 25 days by a time step of 0,5 day.
- compute

6.3.3 Input parameter and variables

The parameters required to the model, defined using the previous relationships, are the following shown in *Table 6-4*.

Parameter	Value
ρ_w [kg/m³]	1000
W_v [kg/mol]	0,018016
T_C [°C]	22
T_K [K]	295,15
ρ_s [kg/m³]	2588
D_{av} [m²/s]	8,25E-05
p_{sat} [Pa]	2646,9

Table 6-4 Model's parameters

As regards all the variables that depend on the value of total suction, which is the dependent variable in this study, different relationships were found starting from the experimental data.

In particular, the water retention curve, in terms of total suction ψ and degree of saturation S_r was linearized in the semilogaritmic plane by averaging all the available data as follows:

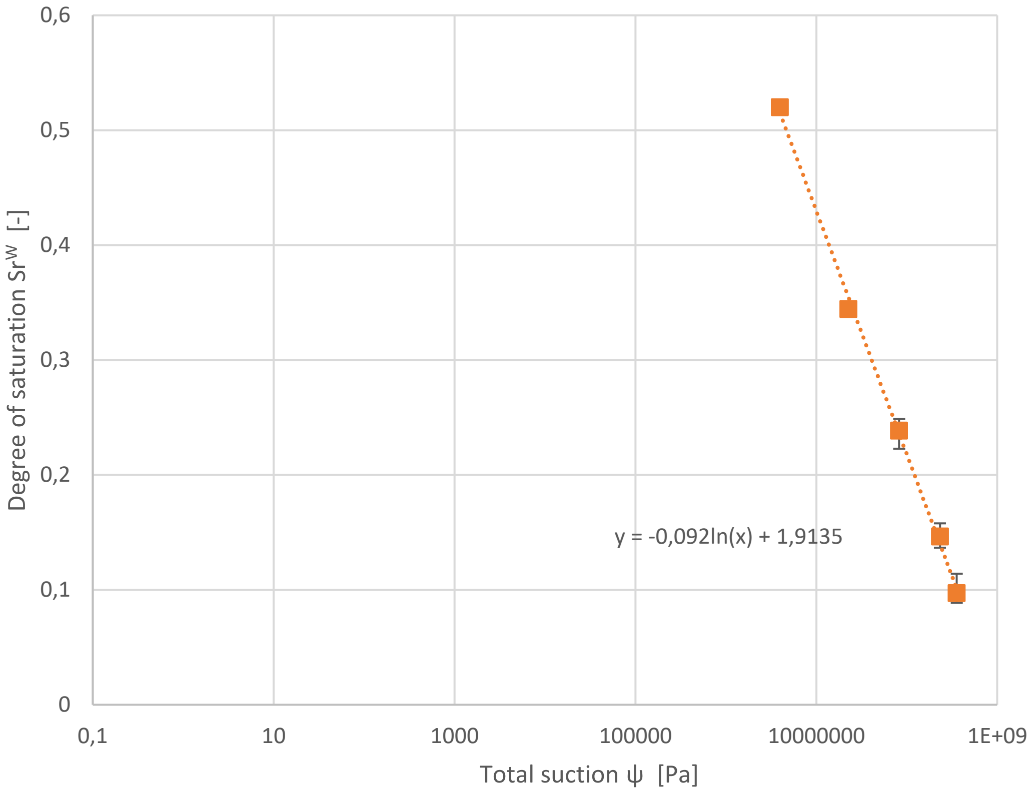

Figure 6-5 Water-Retention Curve used in the simulation

The same procedure was followed also with the aim of define a relationship between the total suction and the porosity, hence the void ratio, as shown in *Figure 6-6* and *6-7*.

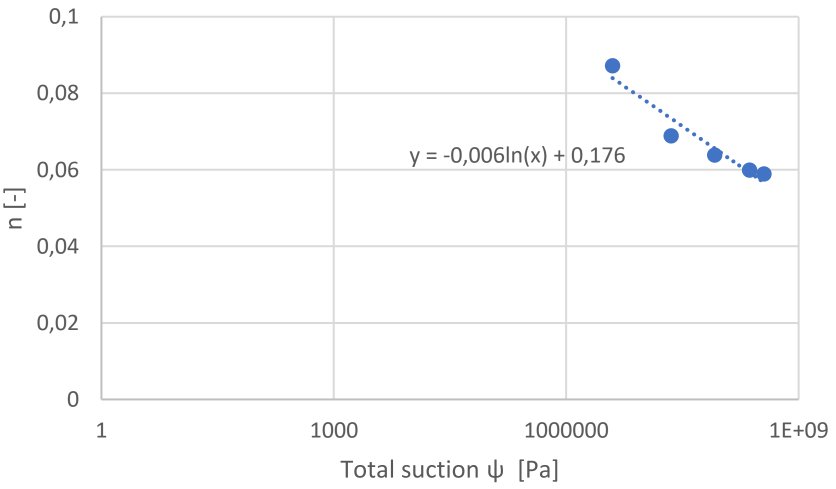

Figure 6-6 Porosity-Suction used in the simulations

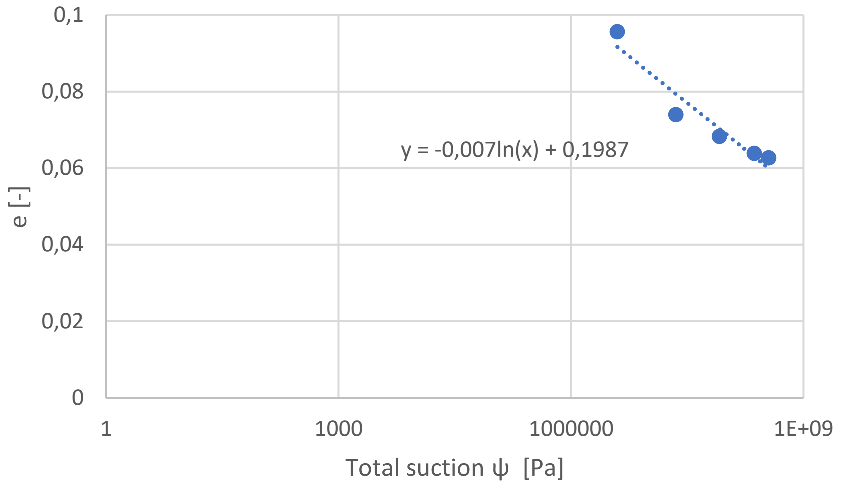

Figure 6-7 Void ratio-suction relationship used in the simulations

As regards the tortuosity factor, with the aim of change it at each study, the *Parametric sweep* tool was used. This tool allows to change systematically a constant value in a range of variation fixed.

Moreover, the diffusion process was considered both isotropic and transversely isotropic among the domain. An anisotropy ratio, ξ, was defined as $\xi = \frac{\tau_z}{\tau_r}$. This anisotropy ratio is set to account for the fact that diffusion of water vapour might be enhanced along the direction of the fissility planes.

In particular, the ratios of anisotropy chosen, referred to z and r directions, were:

- $\xi = 1:1$
- $\xi = 1:5$
- $\xi = 1:10$
- $\xi = 1:100$

In details, the analyses were set to search for the best fitting tortuosity parameter fixed in the r direction while the one in the z direction was defined automatically through anisotropy ratio imposed.

6.4 Numerical results interpretation

The numerical results reported in this section, are referred to an average value over the volume domain of the model for the water content versus time, which allows for comparison with the one determined experimentally.

The results obtained are then normalized as follows:

$$w_{norm} = \frac{w(t) - w(0)}{w(f) - w(0)} \qquad [-] \tag{6-41}$$

Equation 6-41 Normalization of the water content

where :

$w(t)$ is the water content at a generic time

$w(0)$ is the water content at t = 0

$w(f)$ is the water content at the equalization time.

This normalization of the results obtained was done in order to delete the errors related with the linearization of the variables, and by assuming that the initial and final water contents measured experimentally were the only reliable data. The expressions of the water retention curve and the porosity-suction one define a general trend obtained from the experimental data but not the exactly values measured. For this reason the normalization was done in order to focus only in the diffusion process.

6.4.1 Isotropic case

6.4.1.1 Results along the drying paths

The results for the drying paths in isotropic conditions are reported in *Figure 6-8* and *Figure 6-9*, variating the tortuosity factor between 0,001 and 0,009.

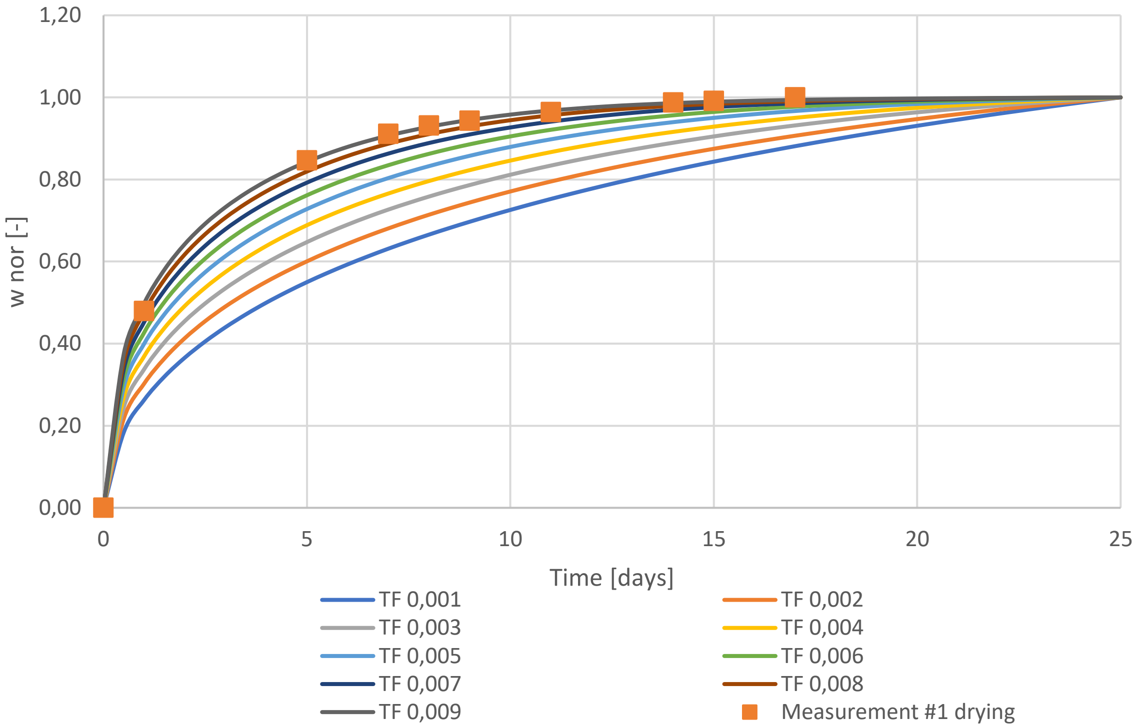

Figure 6-8 Numerical analyses #1drying-τ 0,001-0,009

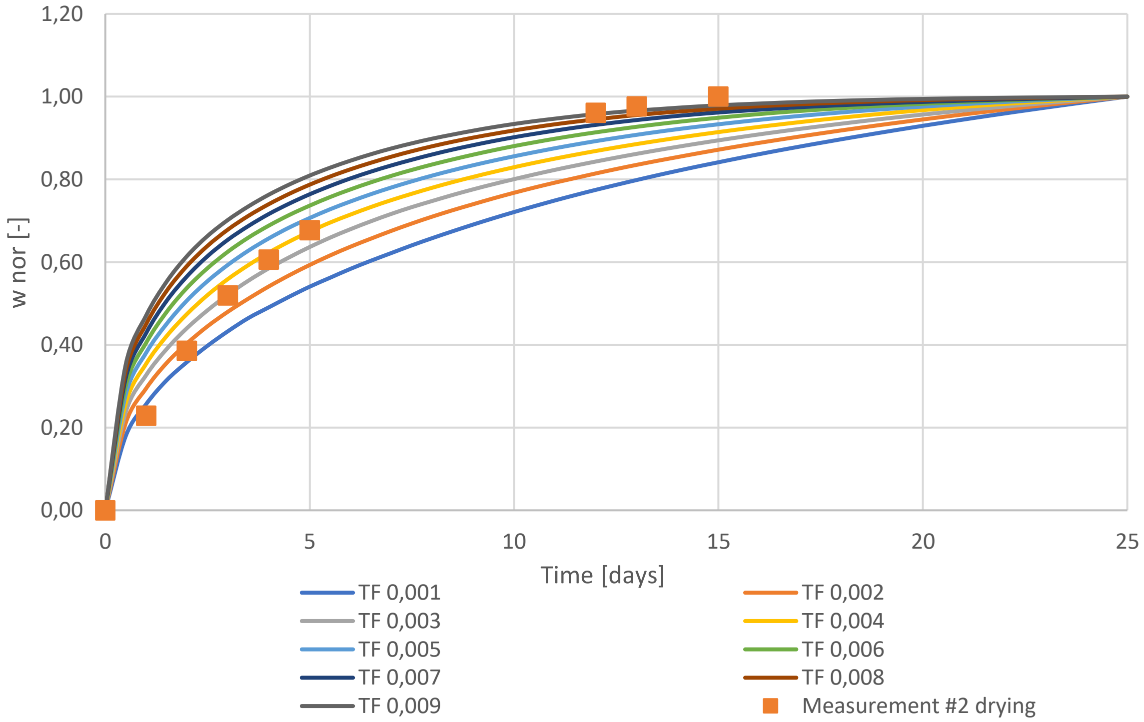

Figure 6-9 Numerical analyses #2drying-τ 0,001-0,009

For the first step of drying, the value of the tortuosity factor that better fits the experimental measurements is the 0,009, as shown in *Figure 6-10*.

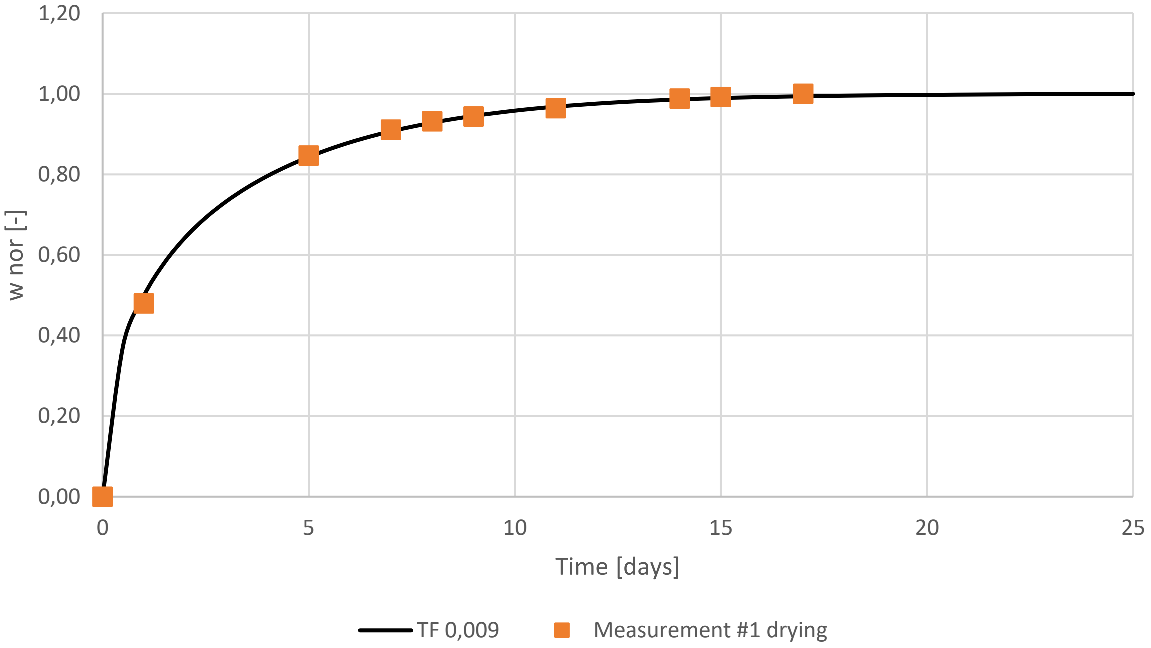

Figure 6-10 Numerical analyses #1drying-τ 0,009

As regard the second step of drying, the value of the tortuosity factor that better fits the experimental measurements is the 0,007, as shown in *Figure 6-11*.

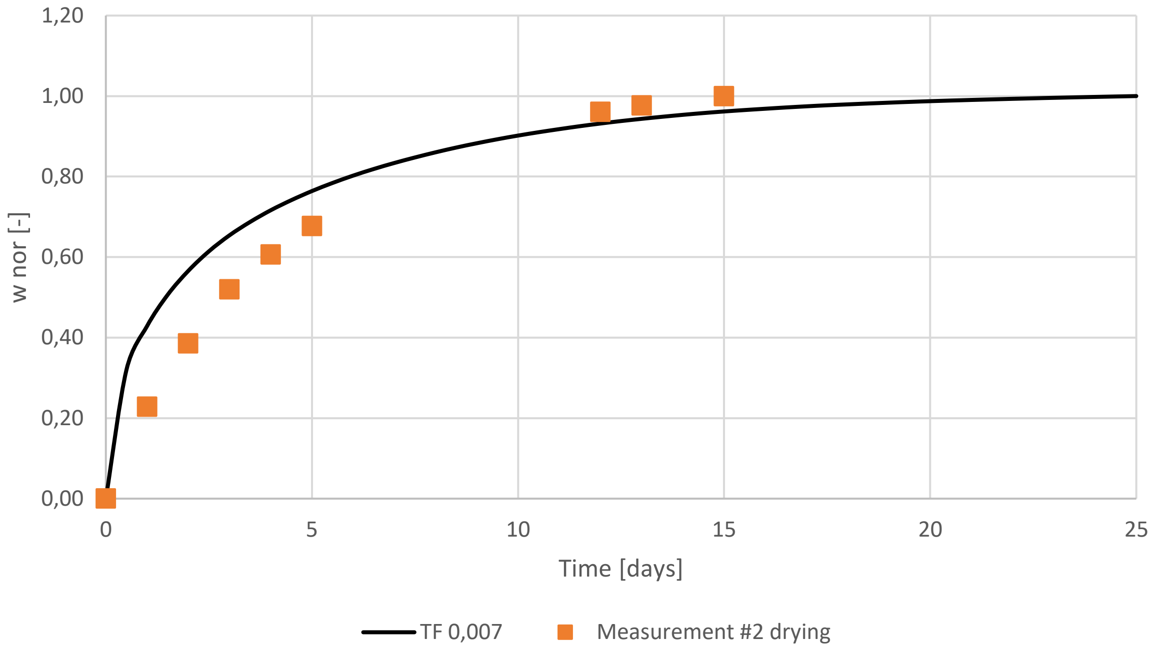

Figure 6-11 Numerical analyses #2drying-τ 0,007

6.4.1.2 Results on the wetting paths

The results for the first step of the wetting paths in isotropic conditions are reported in *Figure 6-12*, variating the tortuosity factor between 0,001 and 0,009 as in the numerical analyses conducted for the drying paths.

As it is possible to notice in *Figure 6-12*, this range of tortuosity factor does not fit the experimental data, because all these values of τ underestimated the rate of the process observed in laboratory.

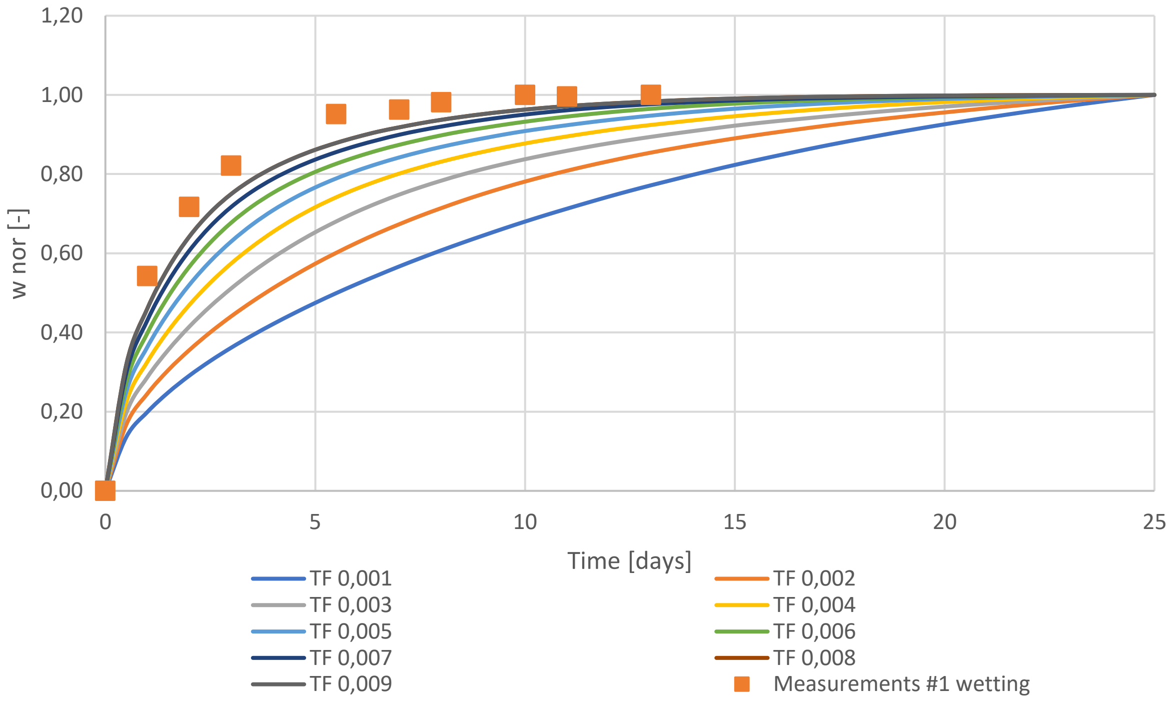

Figure 6-12 Numerical analyses #1wetting-τ 0,001-0,009

This leads to grow up the value of τ in order to accelerate the process, as shown in *Figure 6-13* where the variation of the tortuosity factor was set up between 0,01 and 0,09.

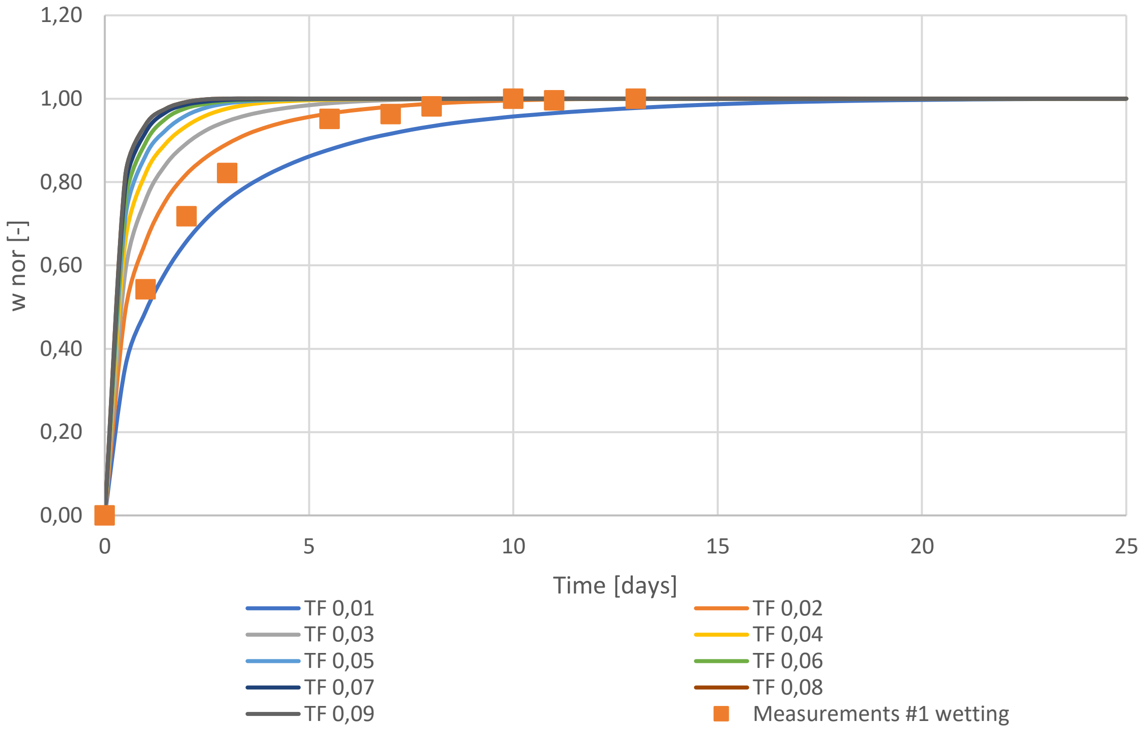

Figure 6-13 Numerical analyses #1wetting-τ 0,01-0,09

For the first step of wetting, the value of the tortuosity factor that better fits the experimental measurements, obtained by further analyses is the 0,015 as shown in *Figure 6-14*.

The results on the second step of wetting in isotropic condition are reported in *Figure 6-15*, variating the tortuosity factor between 0,01 and 0,09.

For the second step of wetting, the value of the tortuosity factor that better fits the experimental measurements, obtained by further analyses is the 0,065, as shown in *Figure 6-16*.

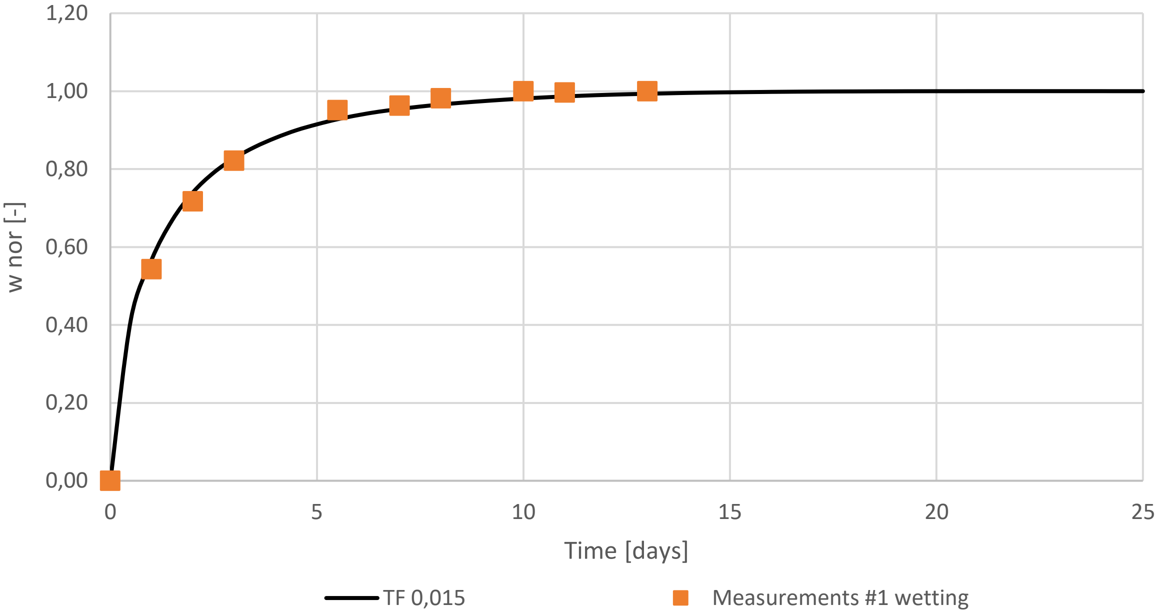

Figure 6-14 Numerical analyses #1wetting-τ 0,015

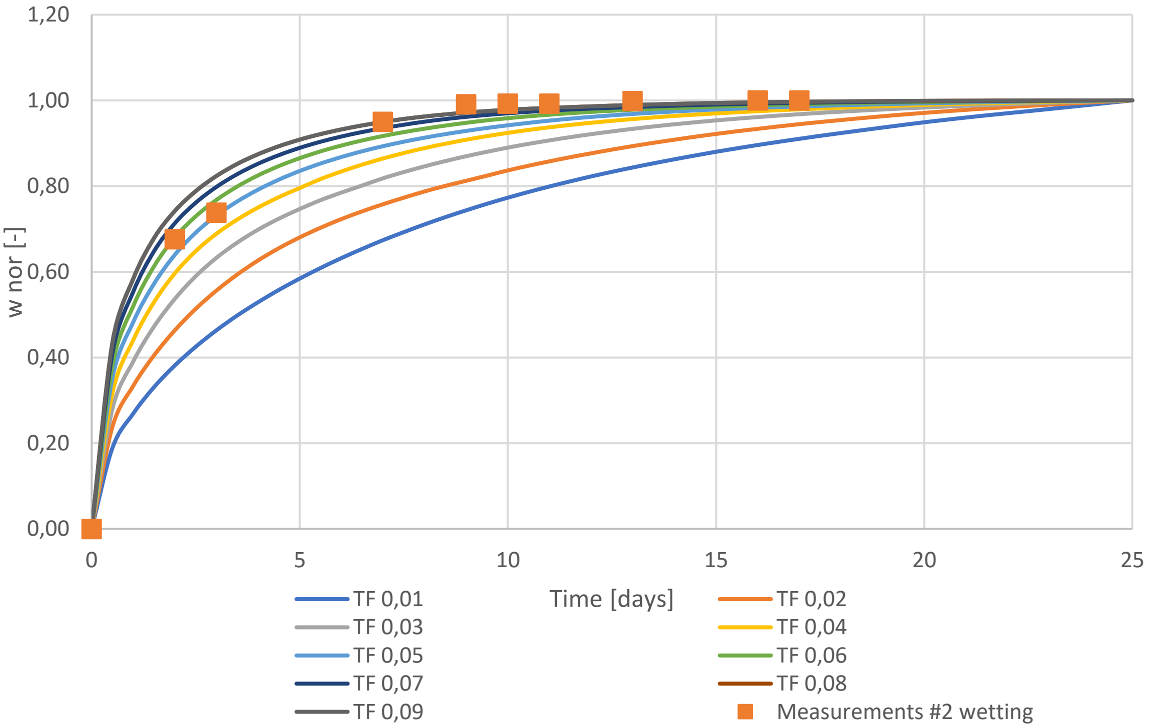

Figure 6-15 Numerical analyses #2wetting-τ 0,01-0,09

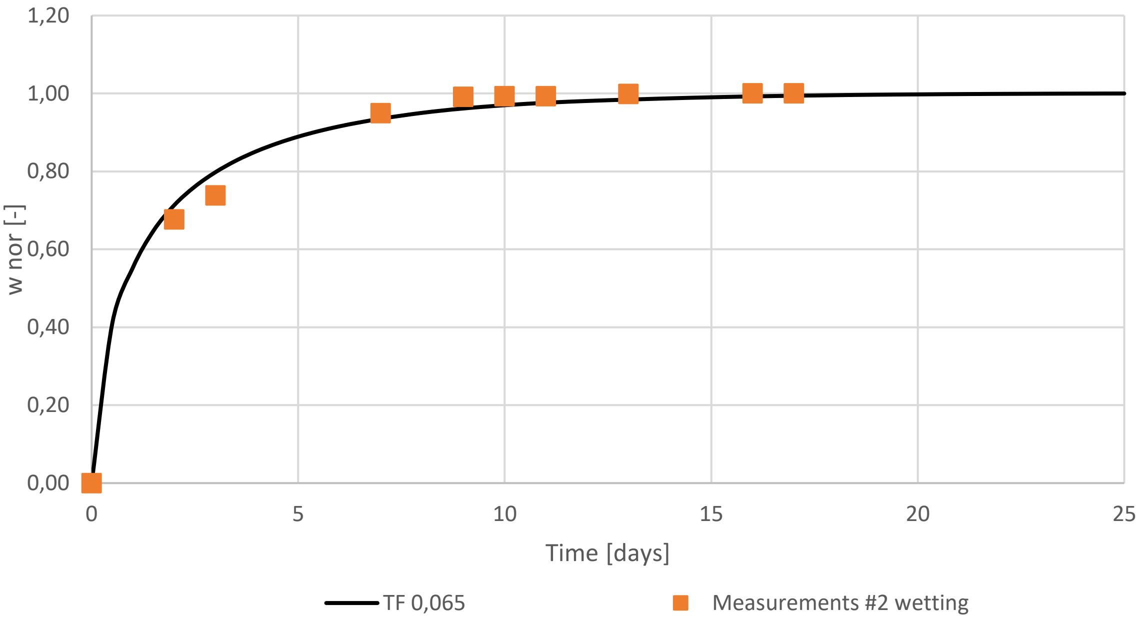

Figure 6-16 Numerical analyses #2wetting-τ 0,065

6.4.1.3 Molecular diffusivity of vapour through shales

The numerical analyses conducted allow to find the values of the tortuosity factor through back analysis for each steps of imposed total suction, by modelling the diffusion process of water vapour in an isotropic medium.

In particular, the results obtained of τ were related with an average value of total suction at each step between the one at the initial condition and the one at the end of the step. The trend of the tortuosity factor was also found in terms of degree of saturation starting from the mean total suction converted with the linearized water retention curve.

The trend of the tortuosity factor versus total suction and degree of saturation are shown in *Figure 6-17* and *6-18*.

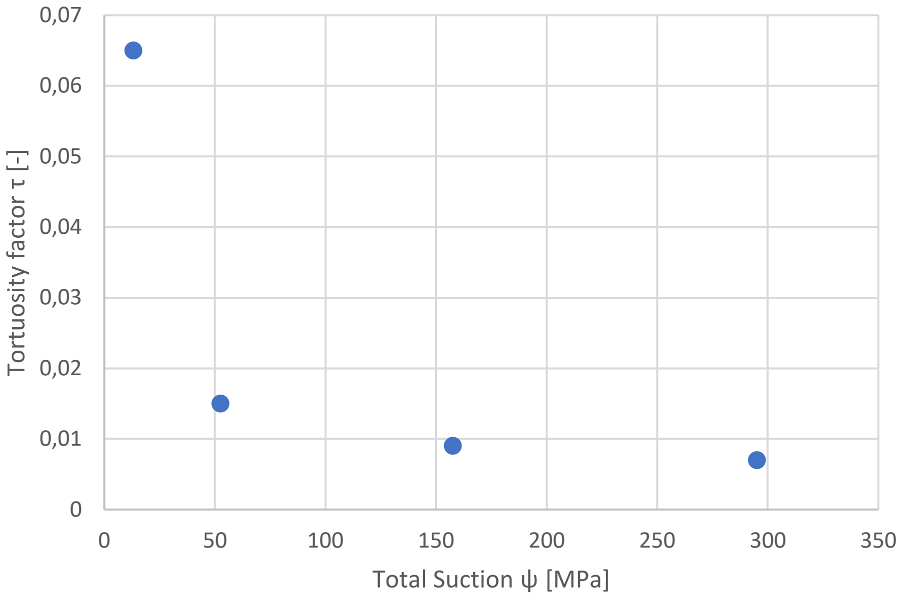

Figure 6-17 Relationship between the total suction and the tortuosity factor

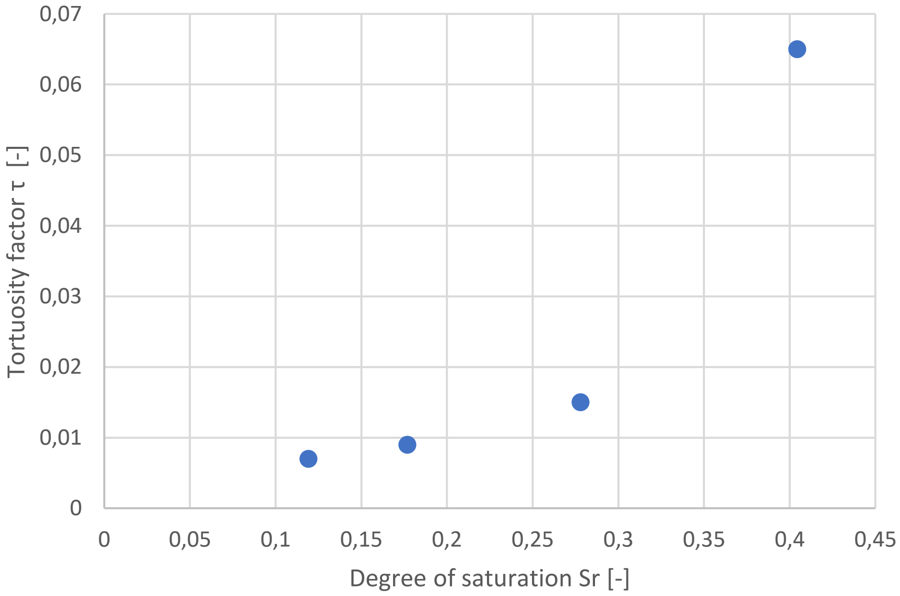

Figure 6-18 Relationship between the degree of saturation and the tortuosity factor

Starting from the tortuosity factors found, it was possible to determine the molecular diffusivity of vapour for the tested gas shales through *Equation 6-28,* which are reported in *Figure 6-19* and *6-20*.

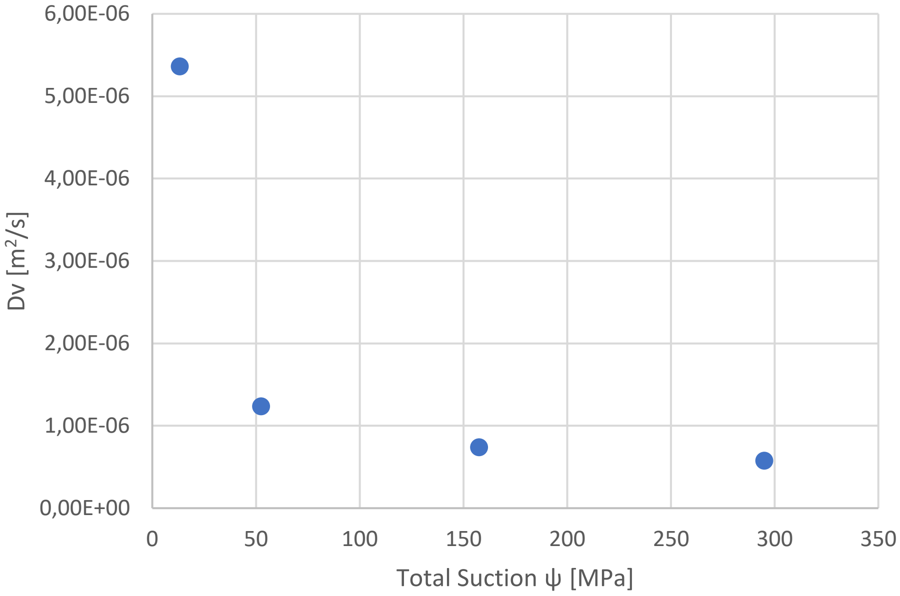

Figure 6-19 Relationship between the total suction and the molecular diffusivity

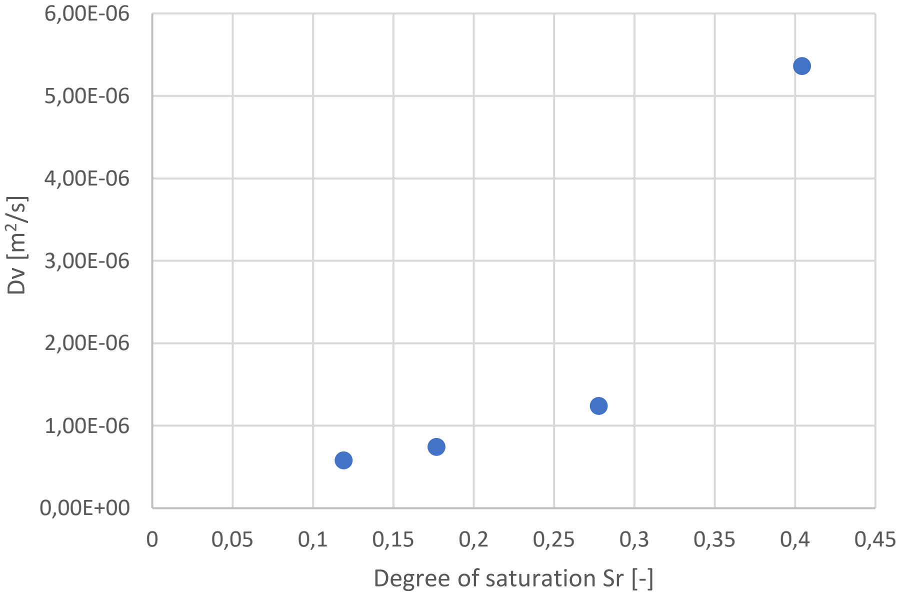

Figure 6-20 Relationship between the degree of saturation and the molecular diffusivity

6.4.2 Anisotropic case with ξ = 1:5

6.4.2.1 Results along the drying paths

The results for the drying paths in anisotropic conditions are reported in *Figure 6-21* and *Figure 6-22*, variating the tortuosity factor in the r direction between 0,01 and 0,09.

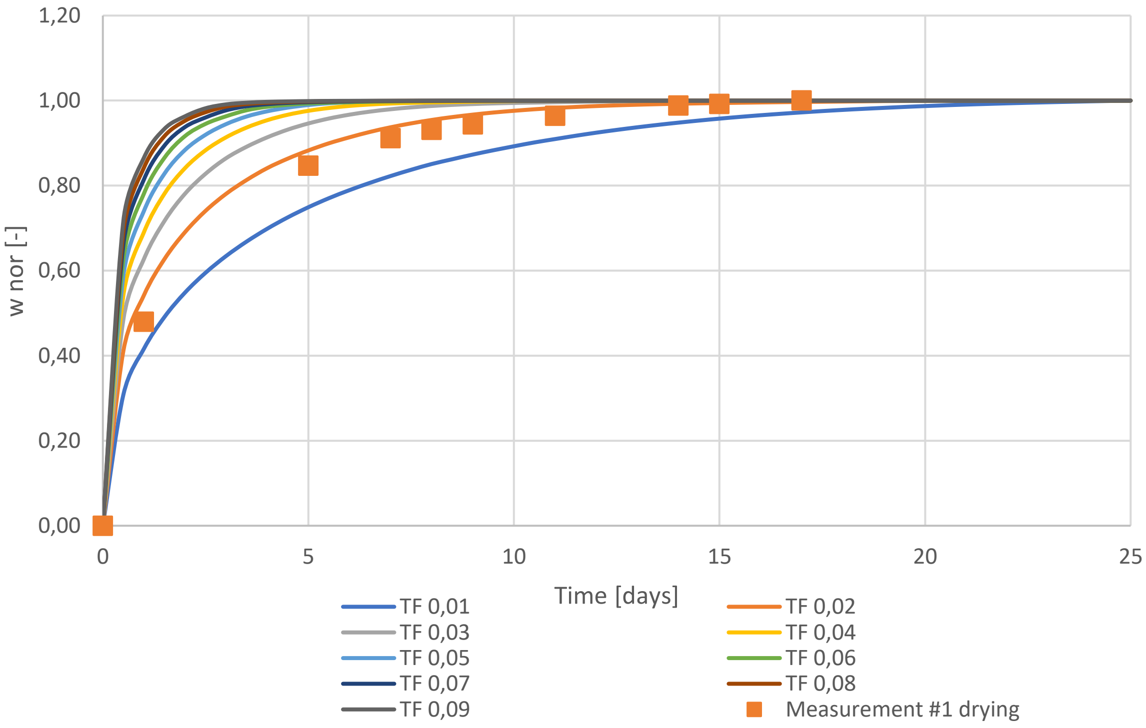

Figure 6-21 Numerical analyses #1drying-τ 0,01-0,09

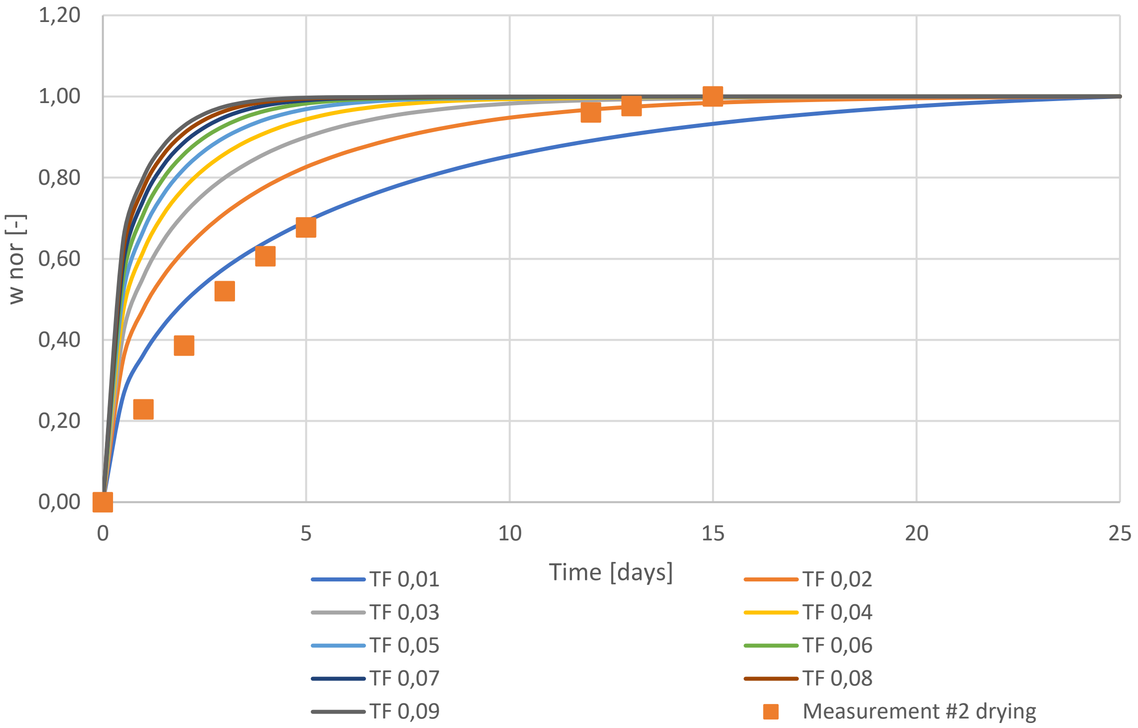

Figure 6-22 Numerical analyses #2drying-τ 0,01-0,09

For the first step of drying, the value of the tortuosity factor in the r direction that better fits the experimental measurements is the 0,02, as shown in *Figure 6-23*.

As regard the second step of drying, the value of the tortuosity factor in the r direction that better fits the experimental measurements is the 0,015, as shown in *Figure 6-24*.

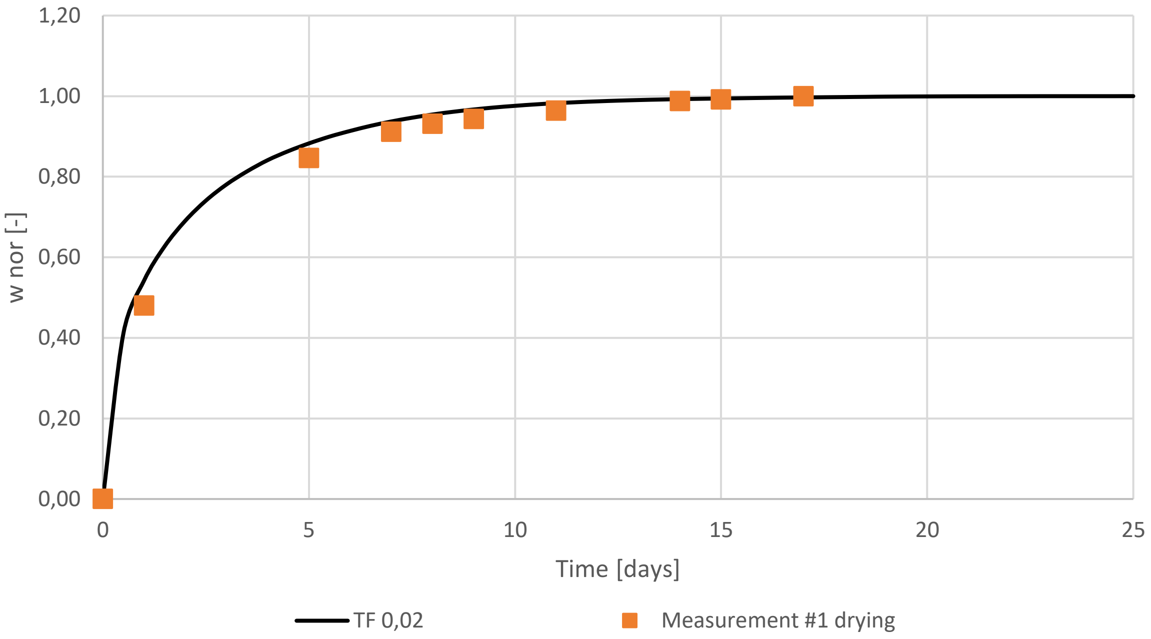

Figure 6-23 Numerical analyses #1drying-τ 0,02

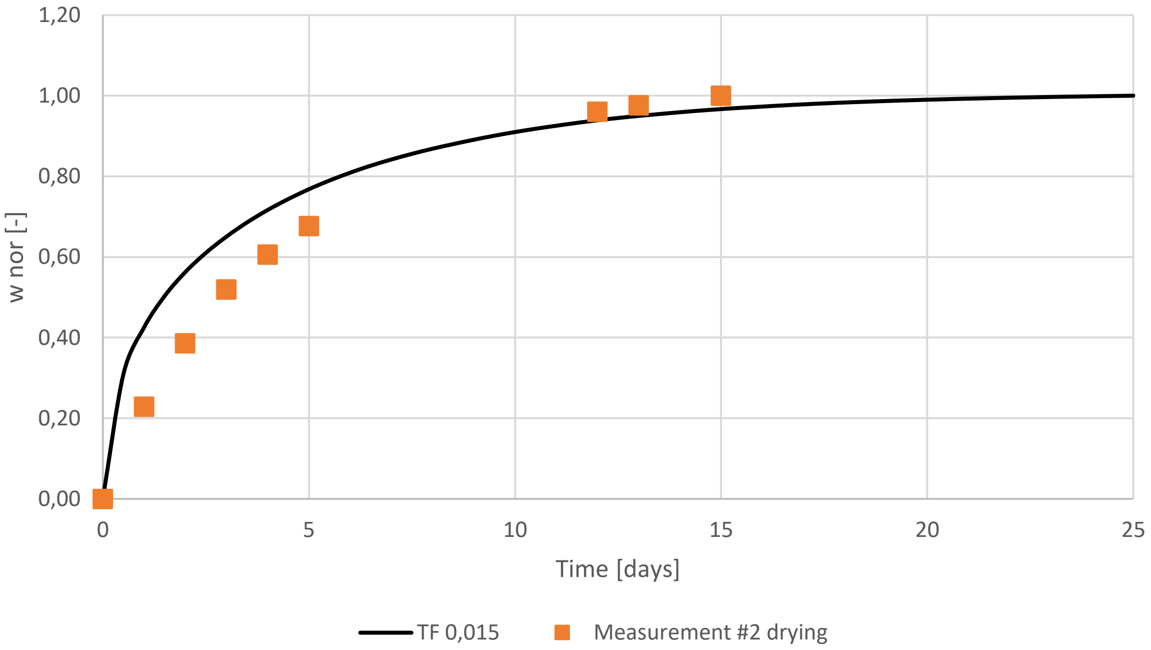

Figure 6-24 Numerical analyses #2drying-τ 0,015

6.4.2.2 Results on the wetting paths

The results for the first step of the wetting paths in anisotropic conditions are reported in *Figure 6-25*, variating the tortuosity factor in the r direction between 0,01 and 0,09 as in the numerical analyses conducted for the drying paths.

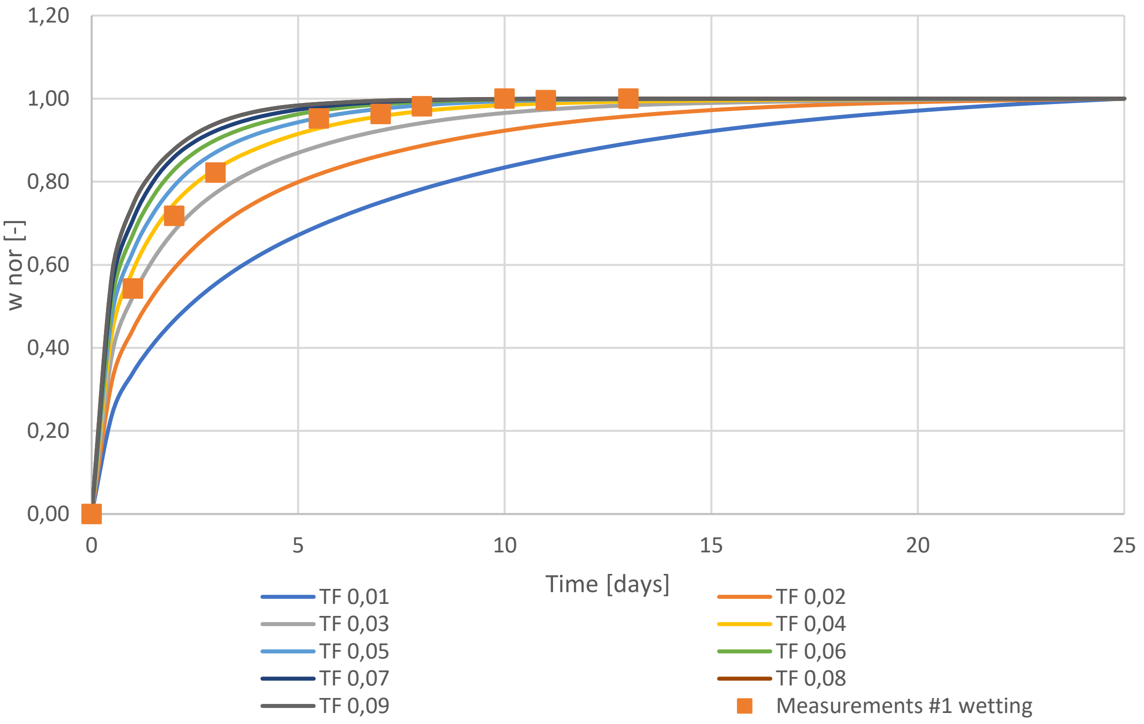

Figure 6-25 Numerical analyses #1wetting-τ 0,01-0,09

The results for the second step of the wetting paths in anisotropic conditions are reported in *Figure 6-26*, variating the tortuosity factor in the r direction between 0,01 and 0,09 as in the numerical analyses conducted for the drying paths.

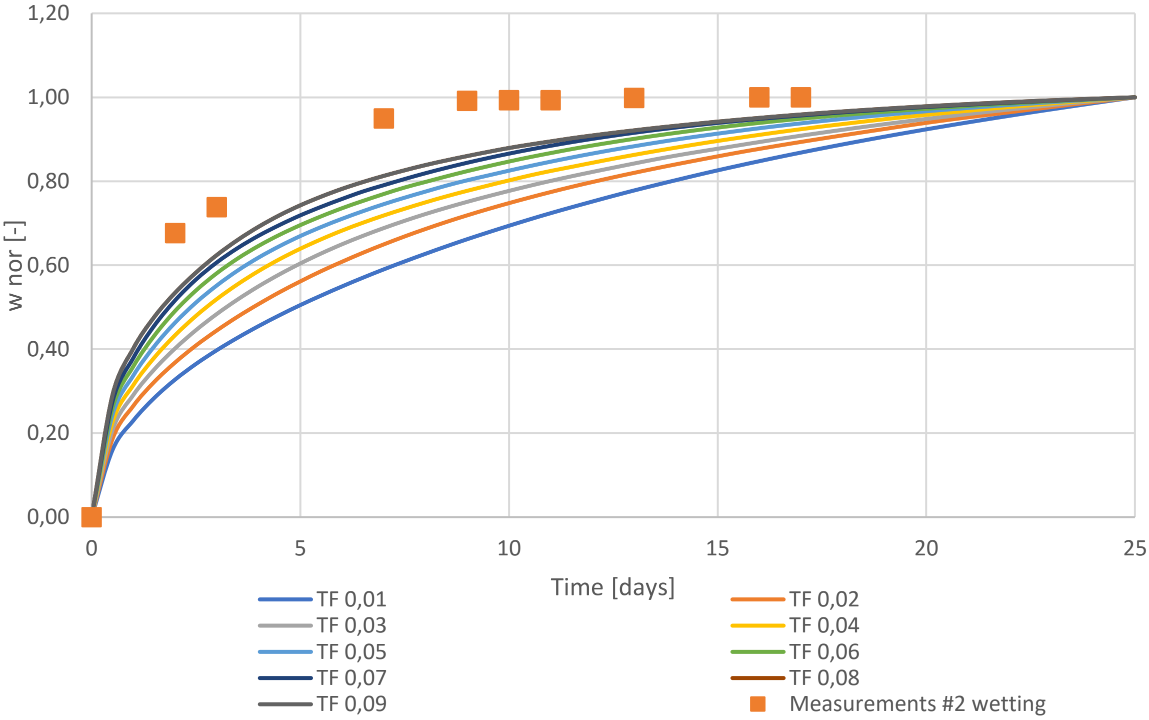

Figure 6-26 Numerical analyses #2wetting-τ 0,01-0,09

As it is possible to notice in *Figure 6-26*, this range of tortuosity factor does not fit the experimental data, because all these values of τ underestimated the rate of the process observed in laboratory.

This leads to grow up the value of τ in order to accelerate the process, as shown in *Figure 6-27* where the variation of the tortuosity factor in the r direction was set up between 0,1 and 0,9.

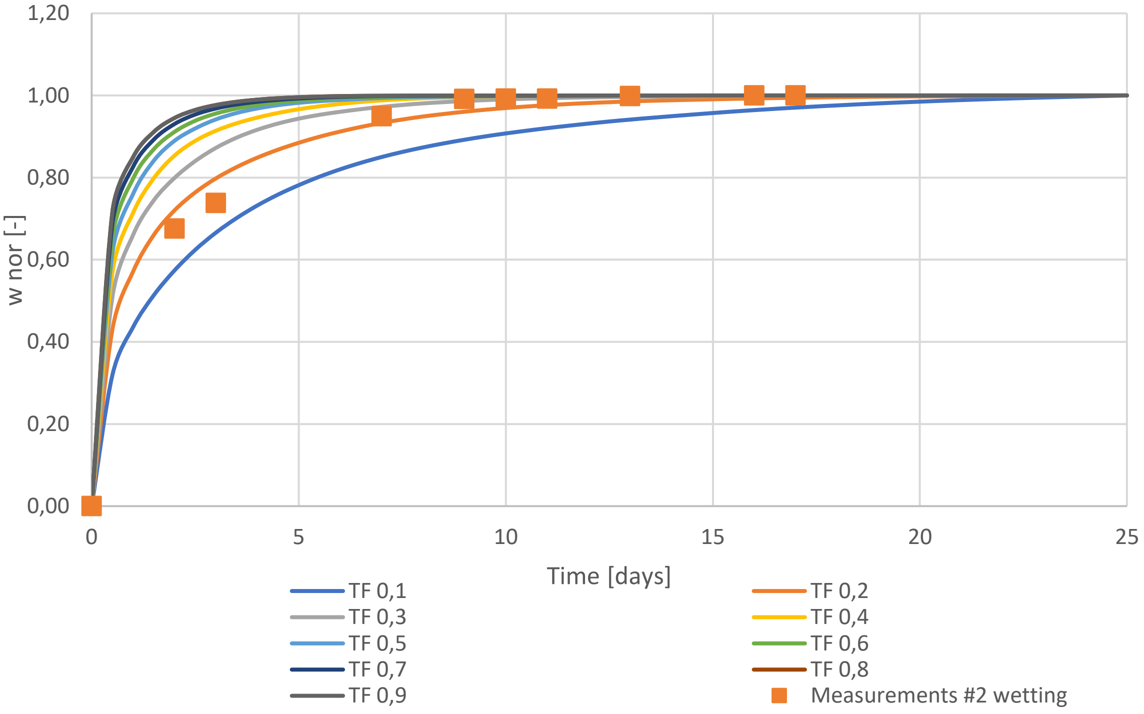

Figure 6-27 Numerical analyses #2wetting-τ 0,1-0,9

For the first step of wetting, the value of the tortuosity factor in the r direction that better fits the experimental measurements, obtained by further analyses is the 0,04 as shown in *Figure 6-28*.

For the second step of wetting, the value of the tortuosity factor in the r direction that better fits the experimental measurements is the 0,2, as shown in *Figure 6-29*.

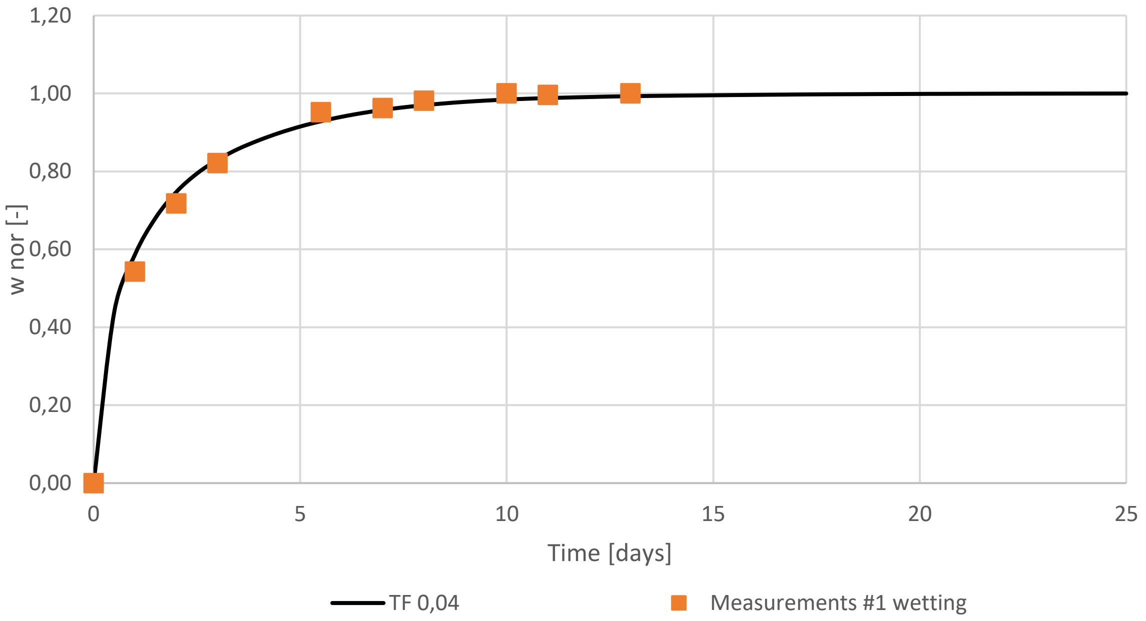

Figure 6-28 Numerical analyses #1wetting-τ 0,04

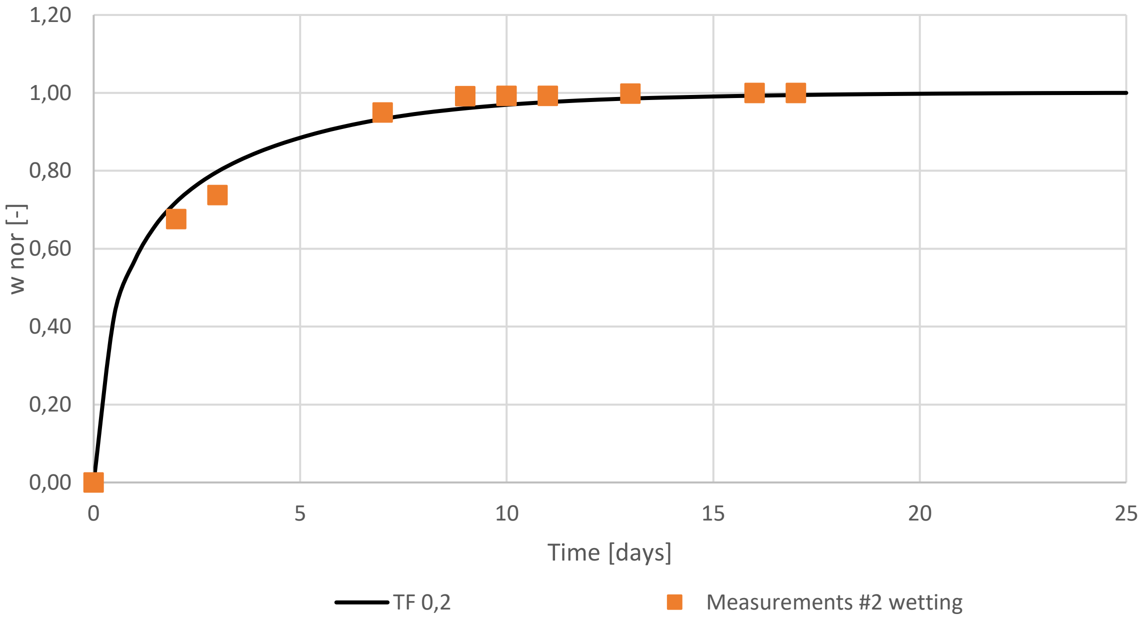

Figure 6-29 Numerical analyses #2wetting-τ 0,2

6.4.2.3 Molecular diffusivity of vapour through shales

The numerical analyses conducted allow to find the values of the tortuosity factor through back analysis for each steps of imposed total suction, by modelling the diffusion process of water vapour in an anisotropic medium.

In particular, the results obtained of τ were related with an average value of total suction at each step between the one at the initial condition and the one at the end of the step. The trend of the tortuosity factor was also found in terms of degree of saturation starting from the mean total suction converted with the linearized water retention curve.

The trend of the tortuosity factor versus total suction and degree of saturation are shown in *Figure 6-30* and *6-31*.

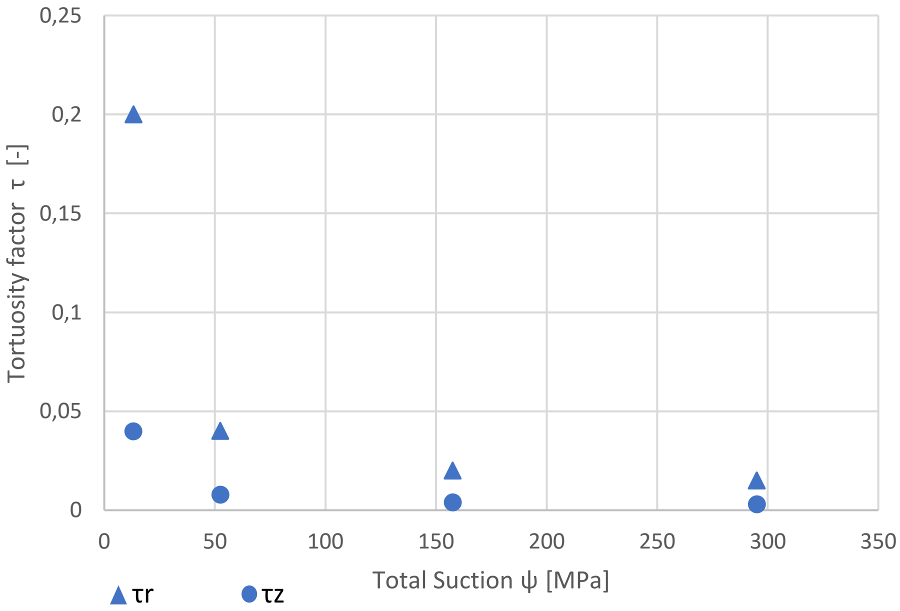

Figure 6-30 Relationship between the total suction and the tortuosity factor

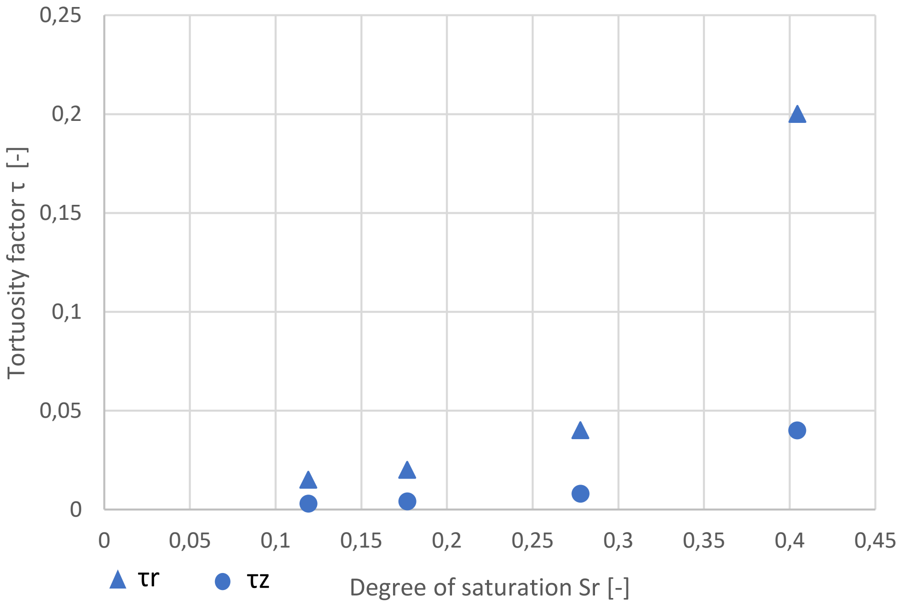

Figure 6-31 Relationship between the degree of saturation and the tortuosity factor

Starting from the tortuosity factors found, it was possible to determine the molecular diffusivity of vapour for the tested gas shales through *Equation 6-28,* which are reported in *Figure 6-32* and *6-33*.

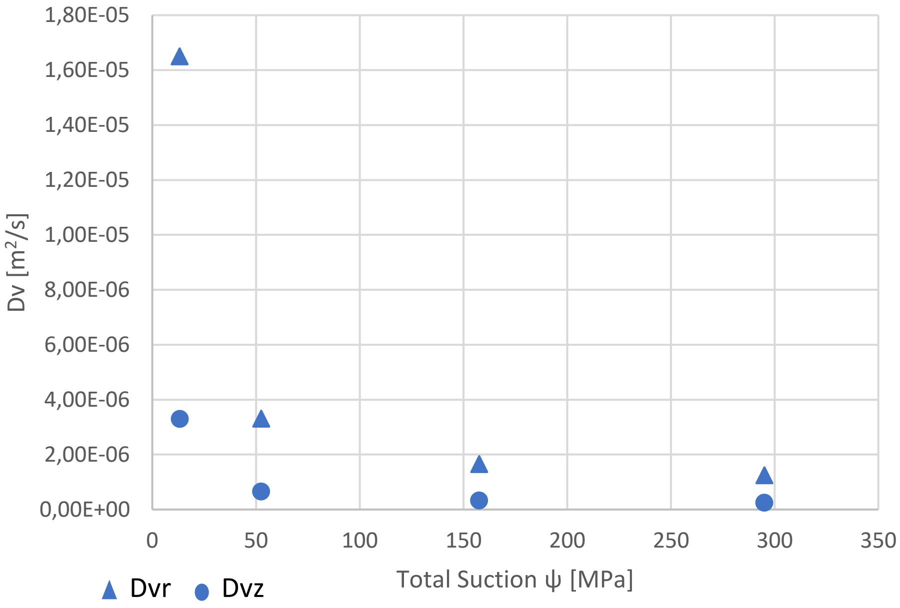

Figure 6-32 Relationship between the total suction and the molecular diffusivity

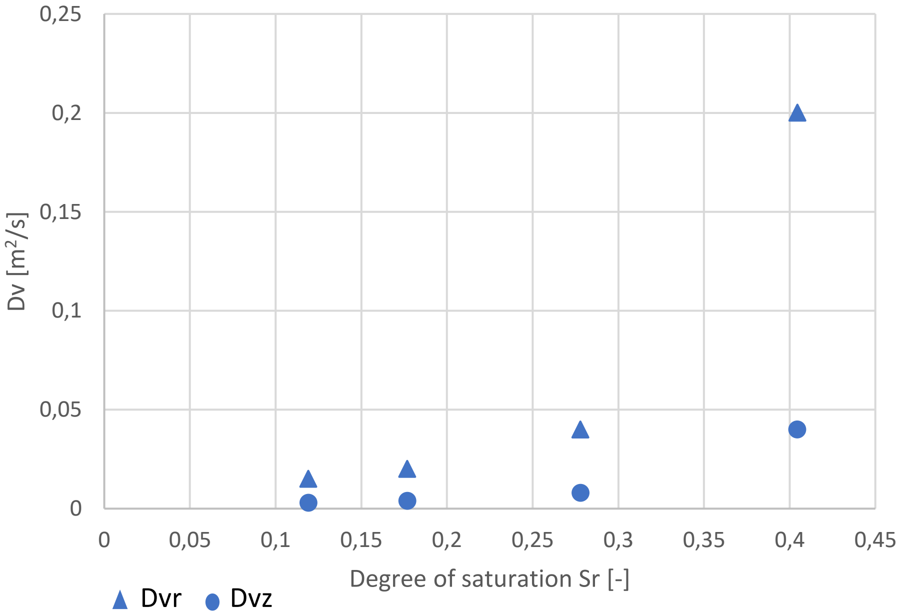

Figure 6-33 Relationship between the degree of saturation and the molecular diffusivity

6.4.3 Anisotropic case with ξ = 1:10

6.4.3.1 Results along the drying paths

The results for the drying paths in anisotropic conditions are reported in *Figure 6-34* and *Figure 6-35*, variating the tortuosity factor in the r direction between 0,01 and 0,09.

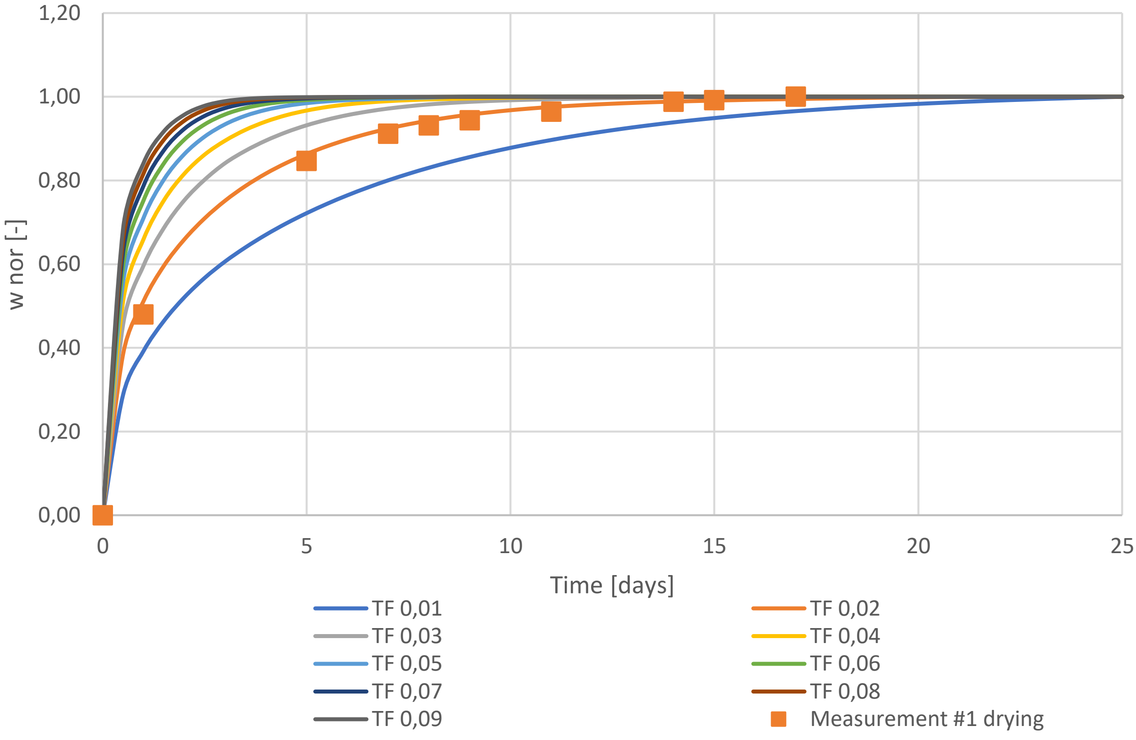

Figure 6-34 Numerical analyses #1drying-τ 0,01-0,09

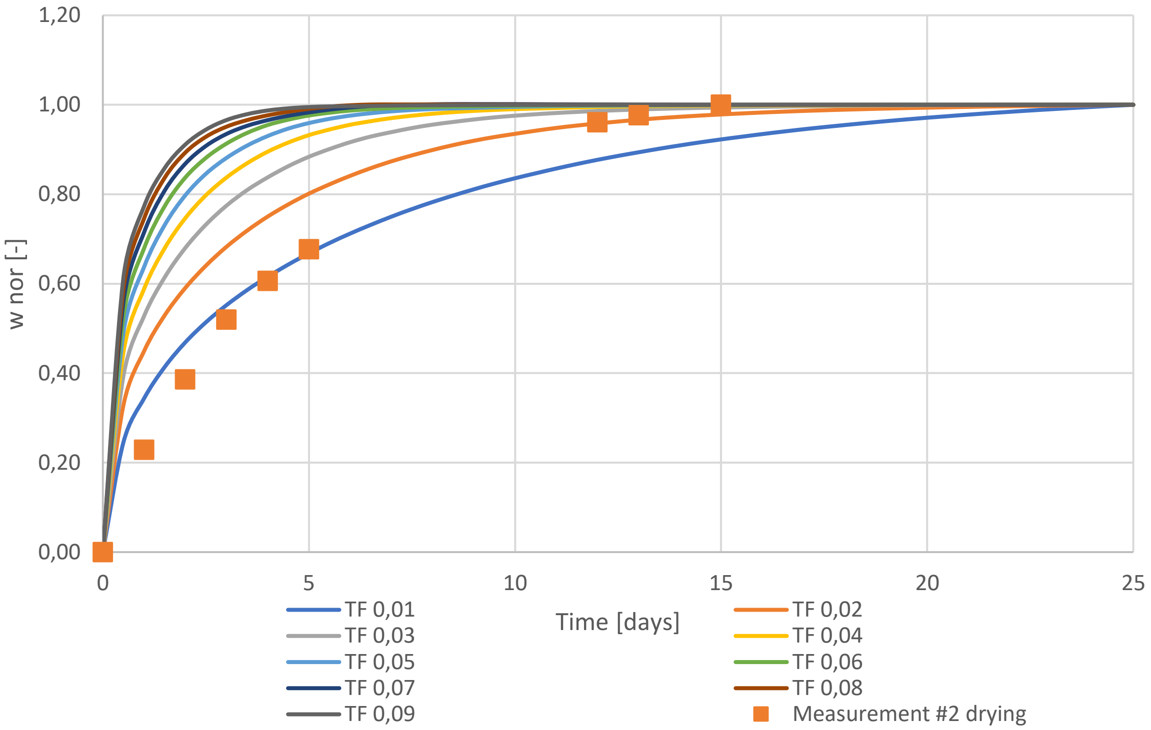

Figure 6-35 Numerical analyses #2drying-τ 0,01-0,09

For the first step of drying, the value of the tortuosity factor in the r direction that better fits the experimental measurements is the 0,02, as shown in *Figure 6-36*.

As regard the second step of drying, the value of the tortuosity factor in the r direction that better fits the experimental measurements is the 0,015, as shown in *Figure 6-37*.

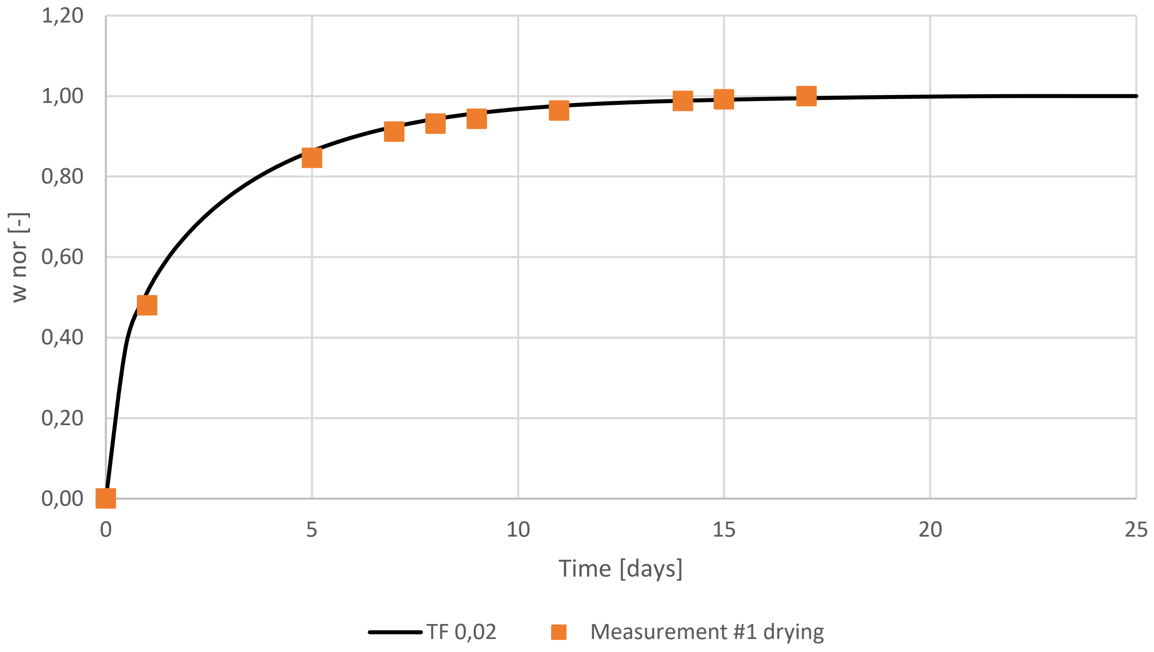

Figure 6-36 Numerical analyses #1drying-τ 0,02

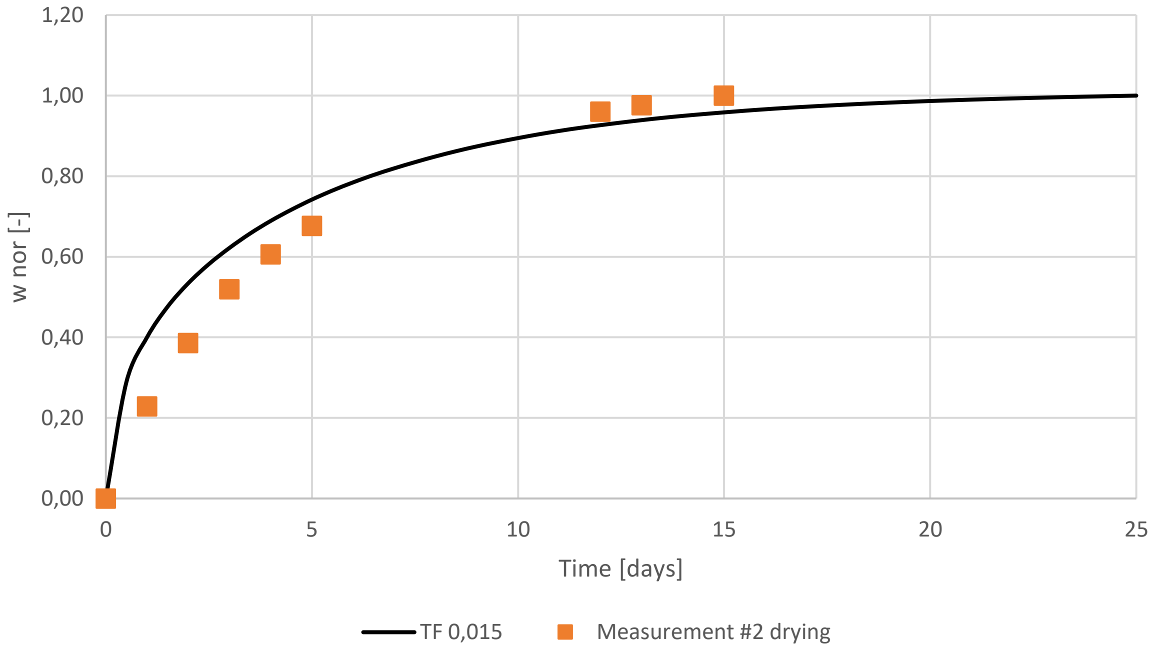

Figure 6-37 Numerical analyses #2drying-τ 0,015

6.4.3.2 Results on the wetting paths

The results for the first step of the wetting paths in anisotropic conditions are reported in *Figure 6-38*, variating the tortuosity factor in the r direction between 0,01 and 0,09 as in the numerical analyses conducted for the drying paths.

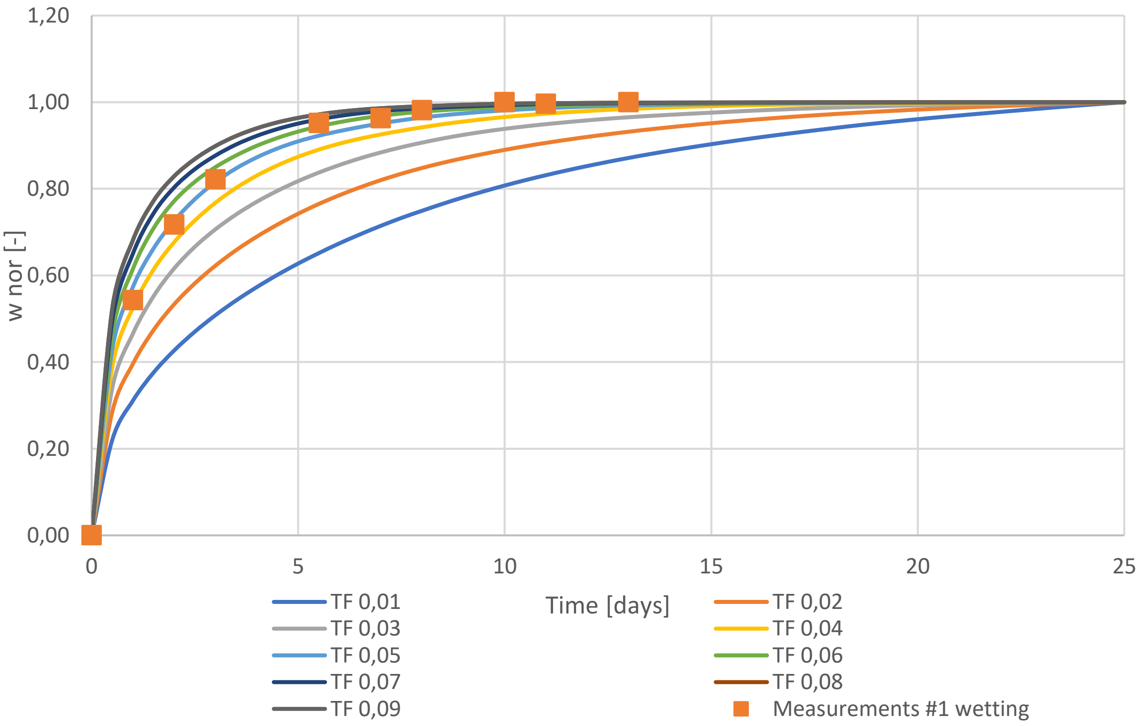

Figure 6-38 Numerical analyses #1wetting-τ 0,01-0,09

The results for the second step of the wetting paths in anisotropic conditions are reported in *Figure 6-39*, variating the tortuosity factor in the r direction between 0,1 and 0,9

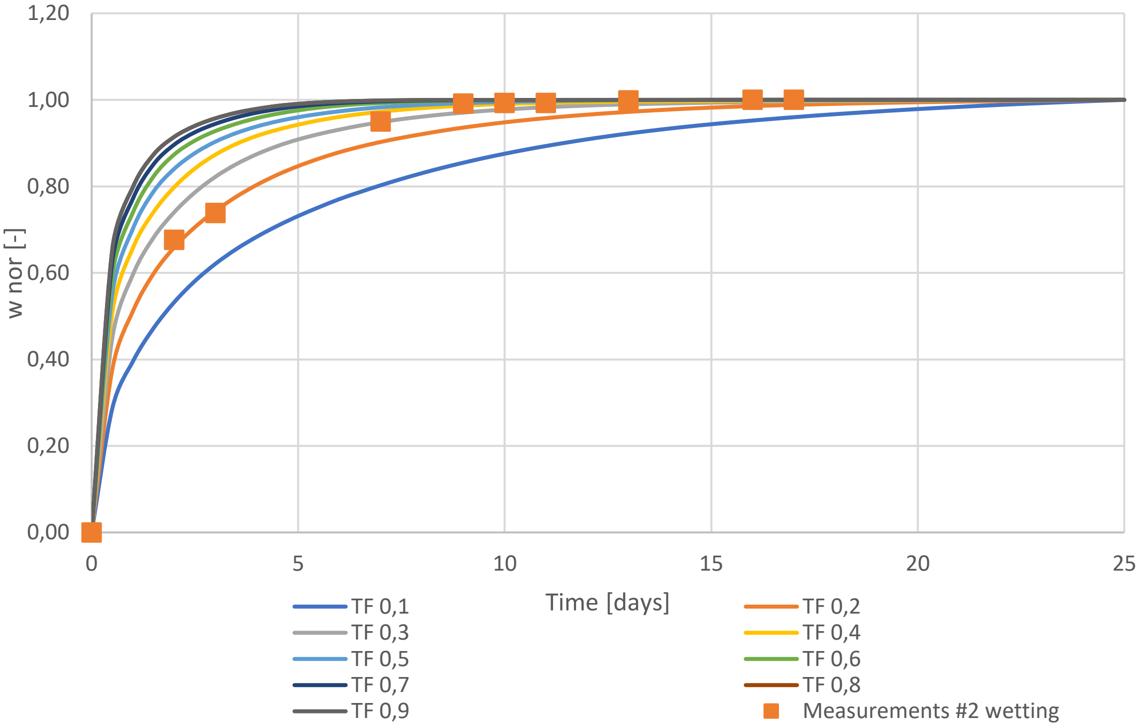

Figure 6-39 Numerical analyses #2wetting-τ 0,1-0,9

For the first step of wetting, the value of the tortuosity factor in the r direction that better fits the experimental measurements, obtained by further analyses is the 0,05 as shown in *Figure 6-40*.

For the second step of wetting, the value of the tortuosity factor in the r direction that better fits the experimental measurements is the 0,25, as shown in *Figure 6-41*.

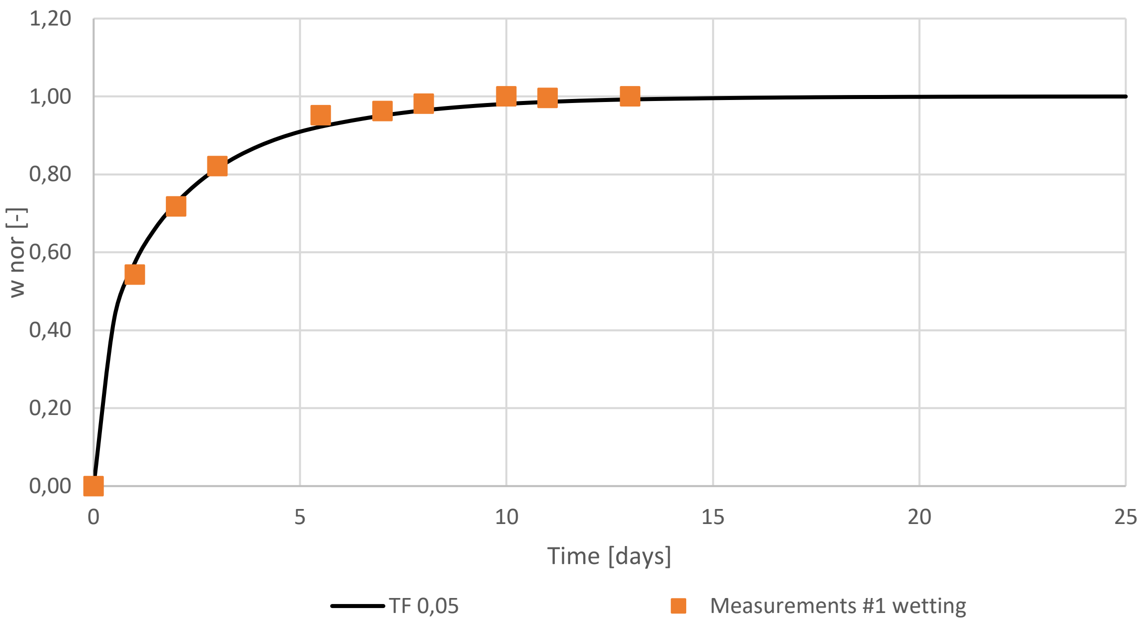

Figure 6-40 Numerical analyses #1wetting-τ 0,05

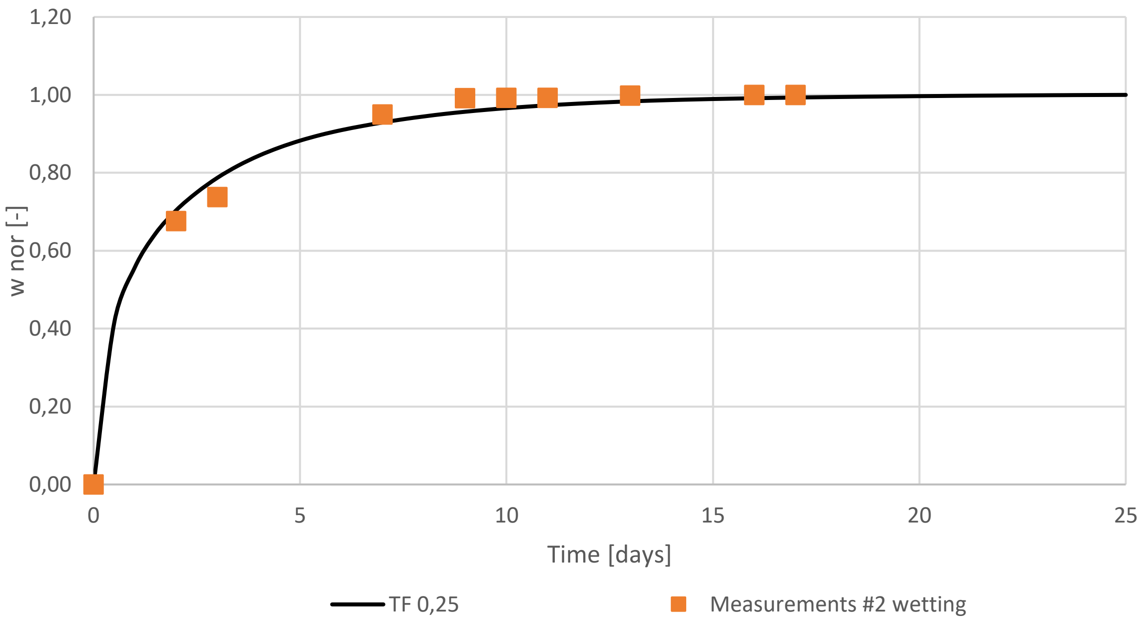

Figure 6-41 Numerical analyses #2wetting-τ 0,25

6.4.3.3 Molecular diffusivity of vapour through shales

The numerical analyses conducted allow to find the values of the tortuosity factor through back analysis for each steps of imposed total suction, by modelling the diffusion process of water vapour in an anisotropic medium.

In particular, the results obtained of τ were related with an average value of total suction at each step between the one at the initial condition and the one at the end of the step. The trend of the tortuosity factor was also found in terms of degree of saturation starting from the mean total suction converted with the linearized water retention curve.

The trend of the tortuosity factor versus total suction and degree of saturation are shown in *Figure 6-42* and *6-43*.

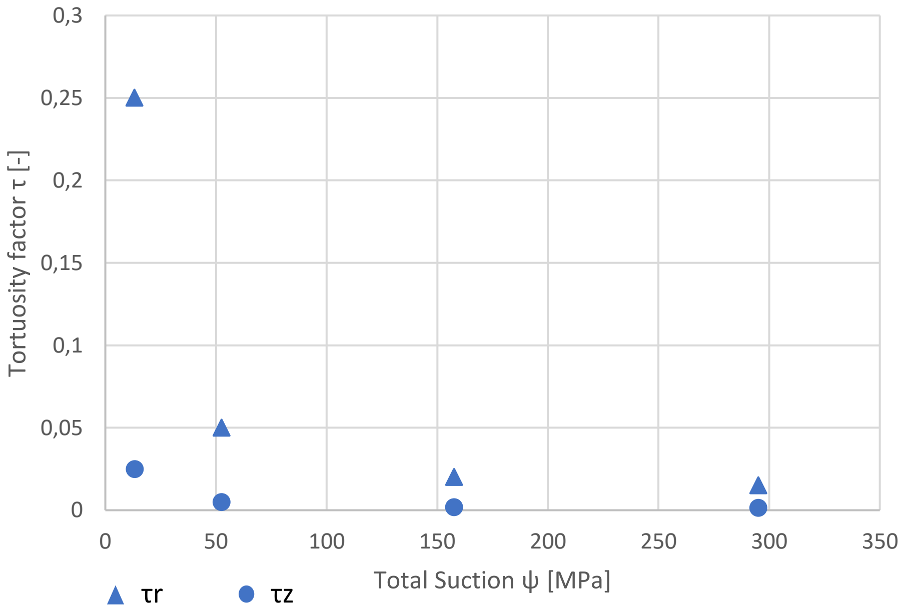

Figure 6-42 Relationship between the total suction and the tortuosity factor

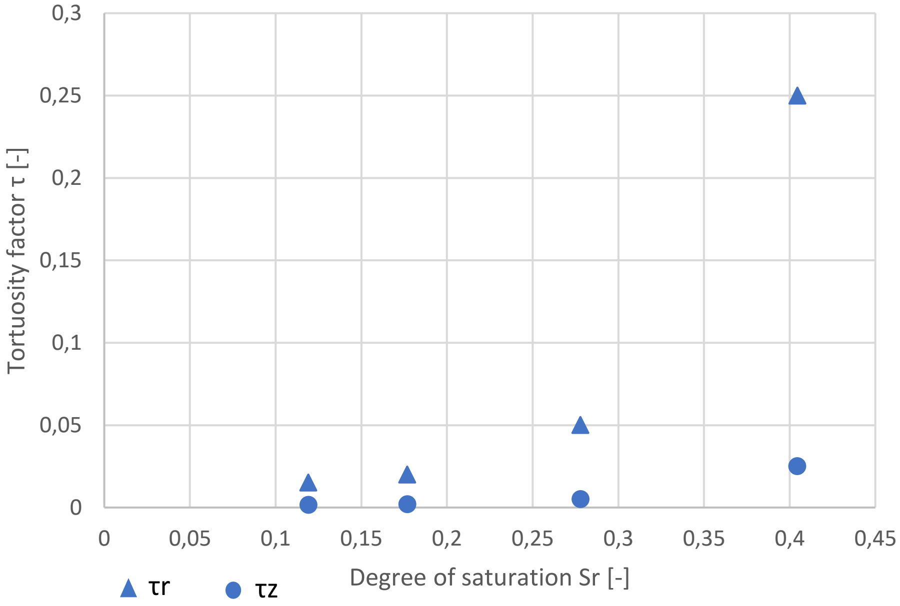

Figure 6-43 Relationship between the degree of saturation and the tortuosity factor

Starting from the tortuosity factors found, it was possible to determine the molecular diffusivity of vapour for the tested gas shales through through *Equation 6-28,* which are reported in *Figure 6-44* and *6-45*.

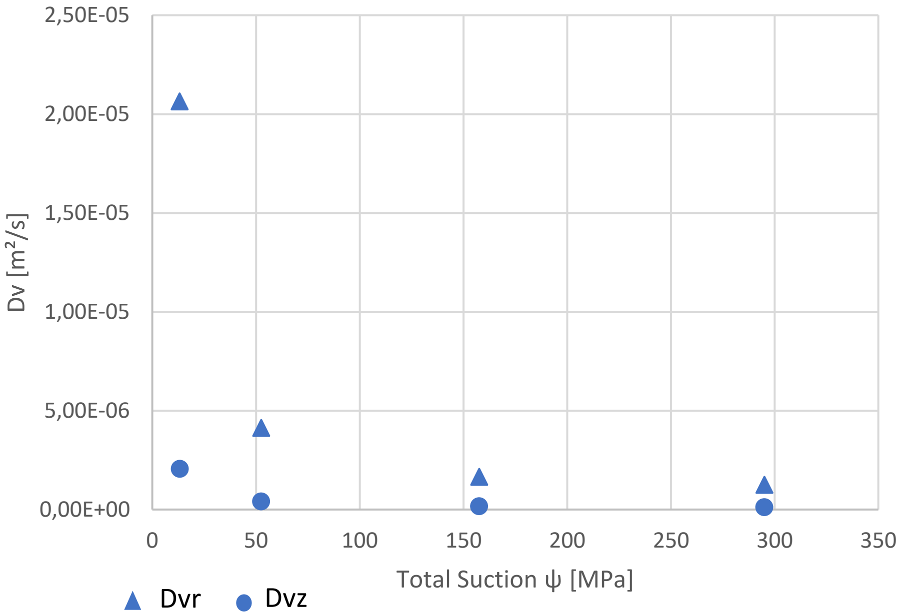

Figure 6-44 Relationship between the total suction and the molecular diffusivity

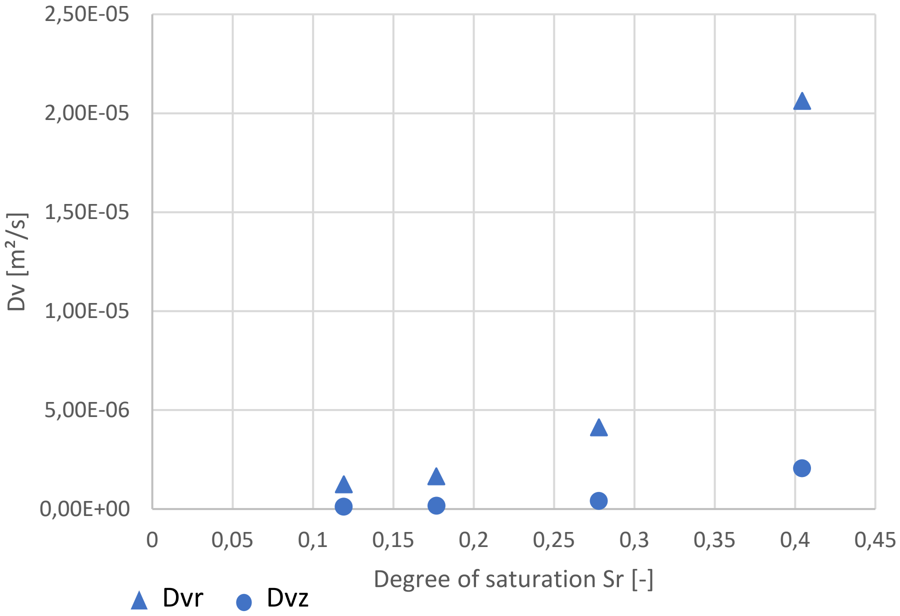

Figure 6-45 Relationship between the degree of saturation and the the molecular diffusivity

6.4.4 Anisotropic case with ξ = 1:100

6.4.4.1 Results along the drying paths

The results for the drying paths in anisotropic conditions are reported in *Figure 6-46* and *Figure 6-47*, variating the tortuosity factor in the r direction between 0,01 and 0,09.

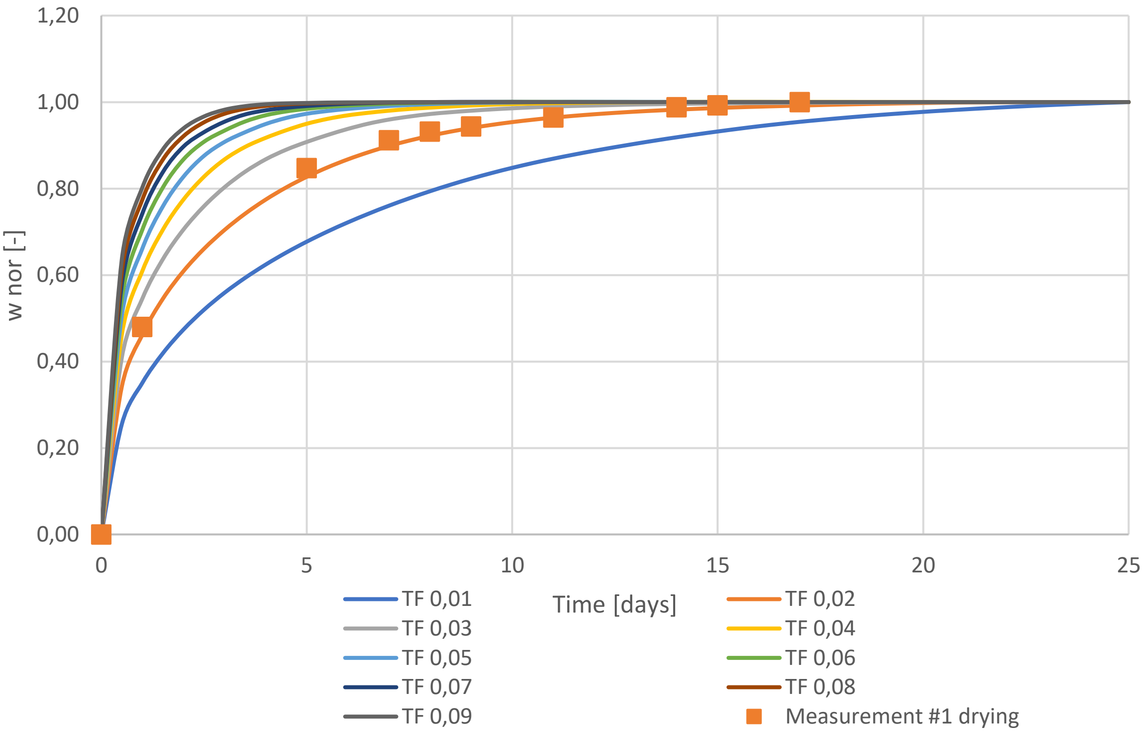

Figure 6-46 Numerical analyses #1drying-τ 0,01-0,09

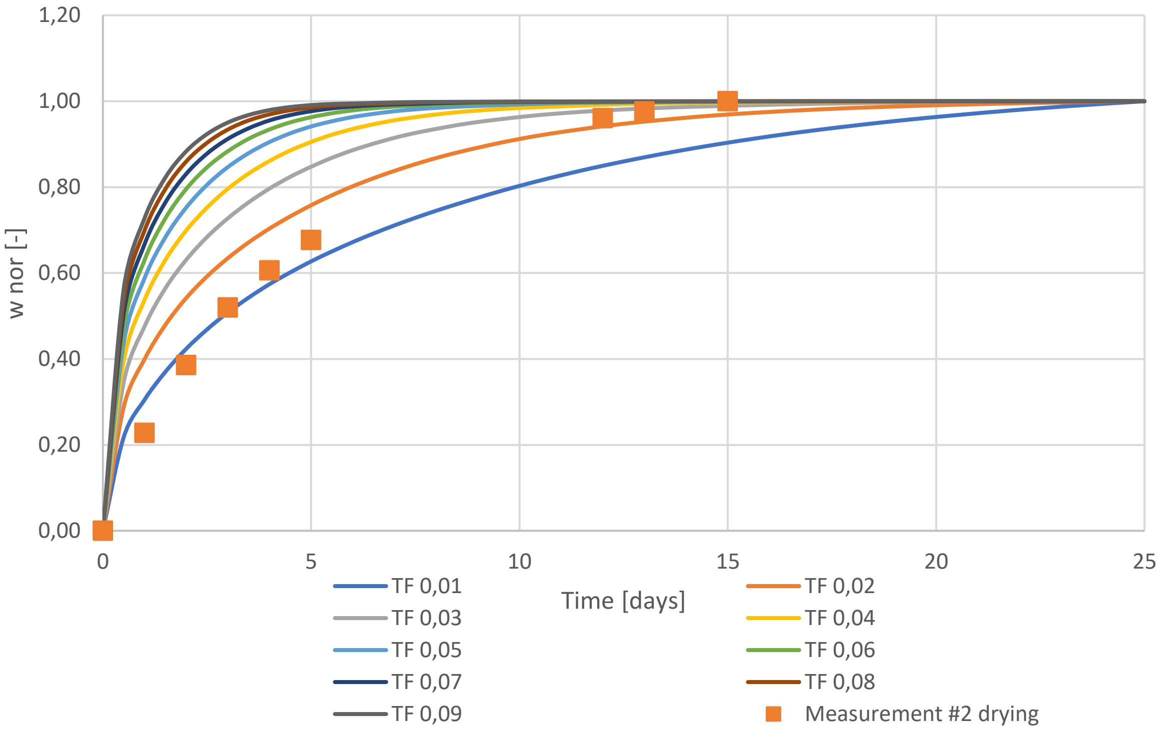

Figure 6-47 Numerical analyses #2drying-τ 0,01-0,09

For the first step of drying, the value of the tortuosity factor in the r direction that better fits the experimental measurements is the 0,02, as shown in *Figure 6-48*.

As regard the second step of drying, the value of the tortuosity factor in the r direction that better fits the experimental measurements is the 0,015, as shown in *Figure 6-49*.

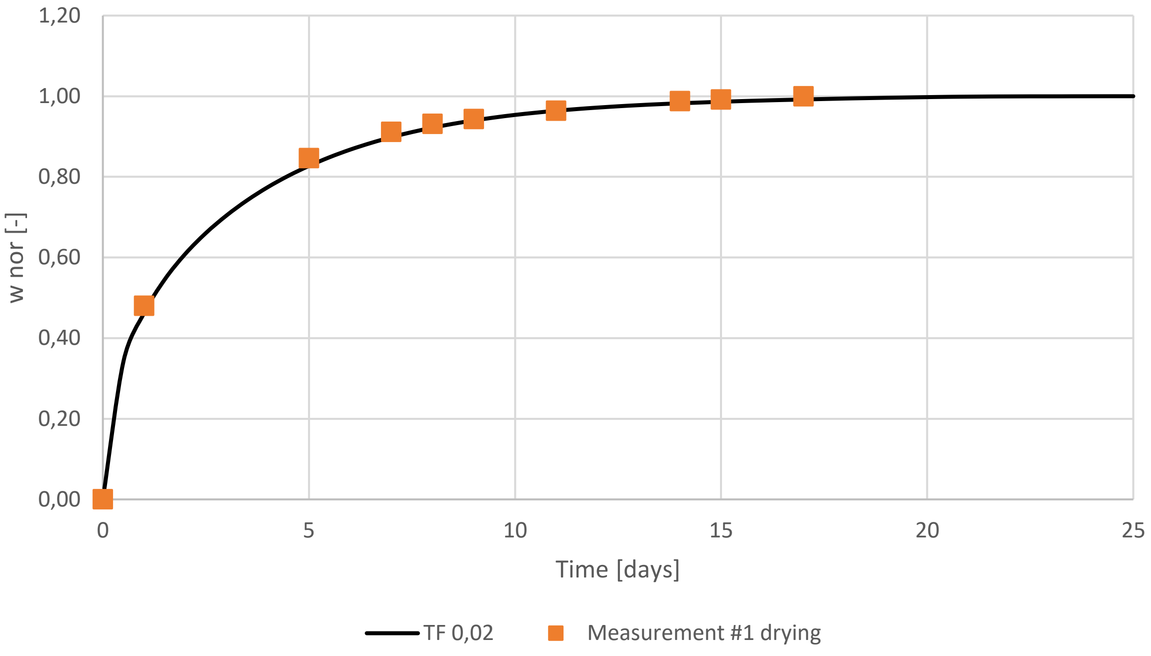

Figure 6-48 Numerical analyses #1drying-τ 0,02

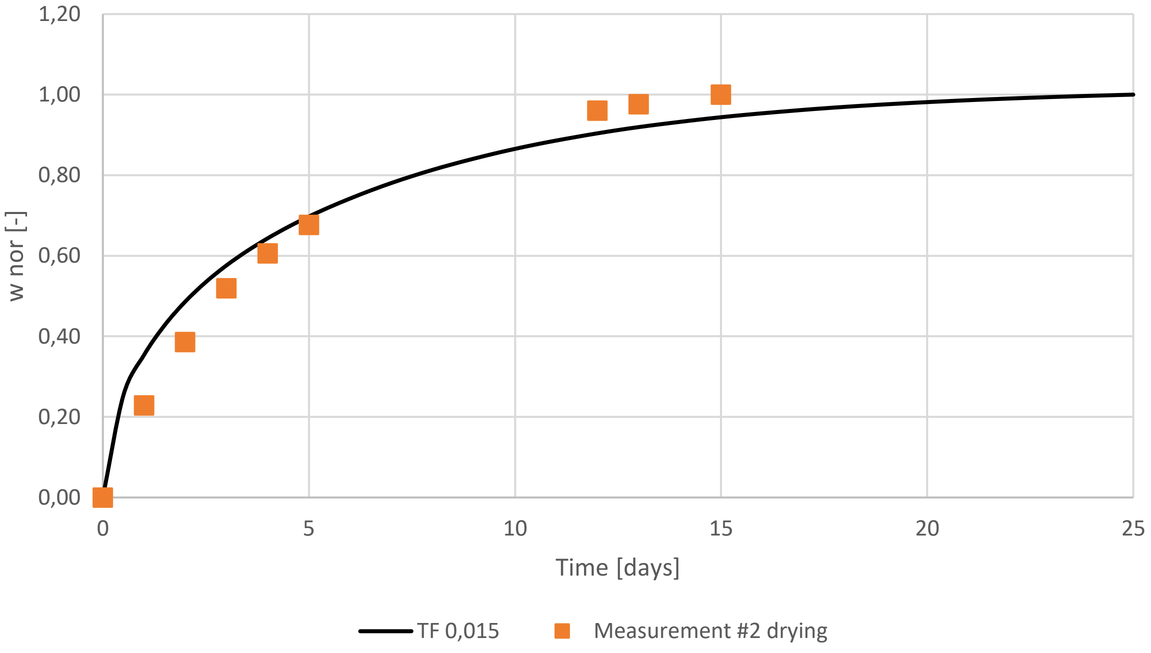

Figure 6-49 Numerical analyses #2drying-τ 0,015

6.4.4.2 Results on the wetting paths

The results for the first step of the wetting paths in anisotropic conditions are reported in *Figure 6-50*, variating the tortuosity factor in the r direction between 0,01 and 0,09 as in the numerical analyses conducted for the drying paths.

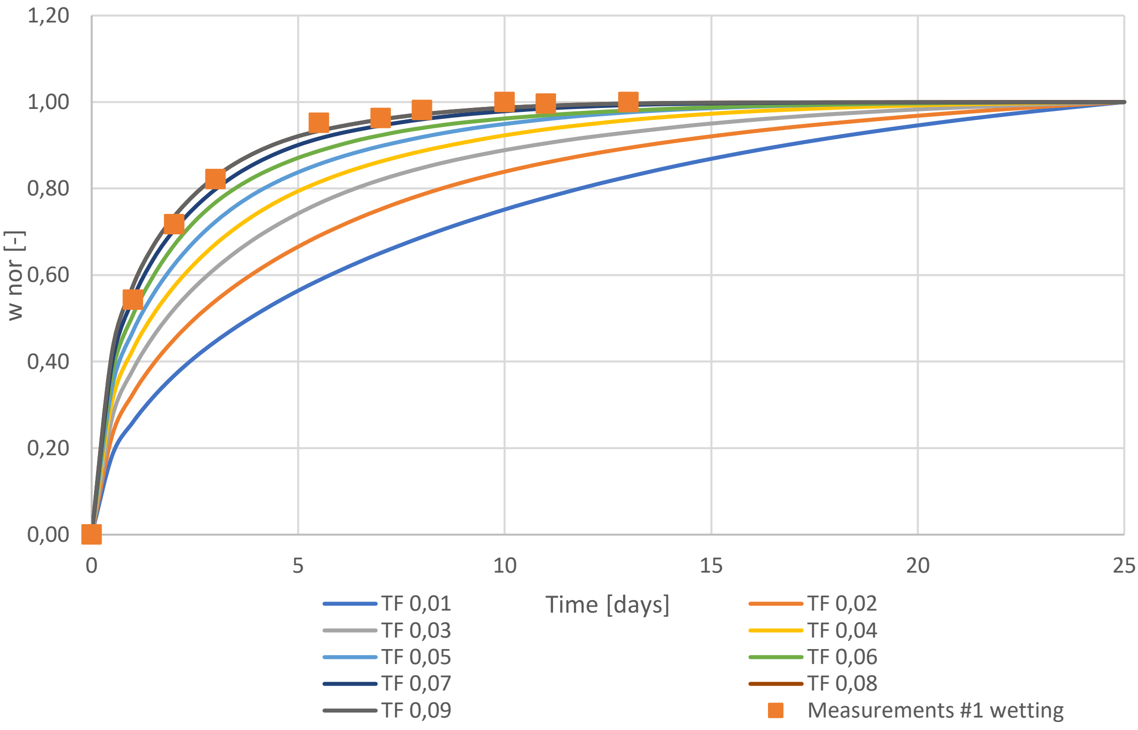

Figure 6-50 Numerical analyses #1wetting-τ 0,01-0,09

The results for the second step of the wetting paths in anisotropic conditions are reported in *Figure 6-51*, variating the tortuosity factor in the r direction between 0,1 and 0,9.

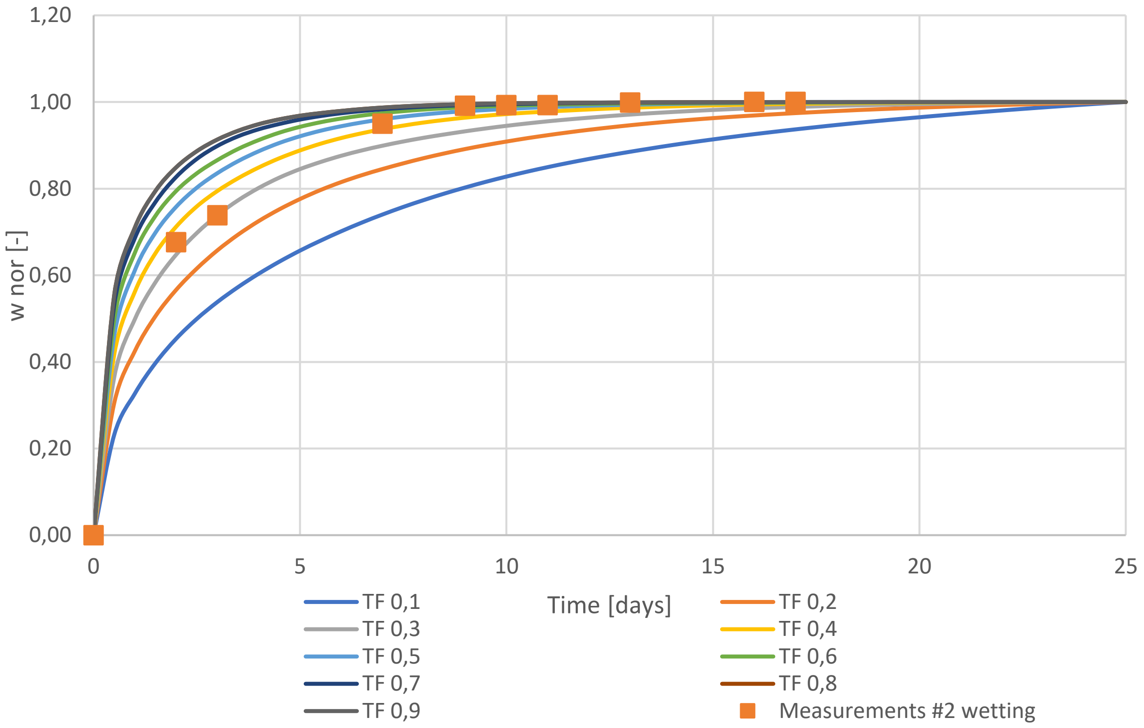

Figure 6-51 Numerical analyses #2wetting-τ 0,1-0,9

For the first step of wetting, the value of the tortuosity factor in the r direction that better fits the experimental measurements, obtained by further analyses is the 0,09 as shown in *Figure 6-52*.

For the second step of wetting, the value of the tortuosity factor in the r direction that better fits the experimental measurements is the 0,4, as shown in *Figure 6-53*.

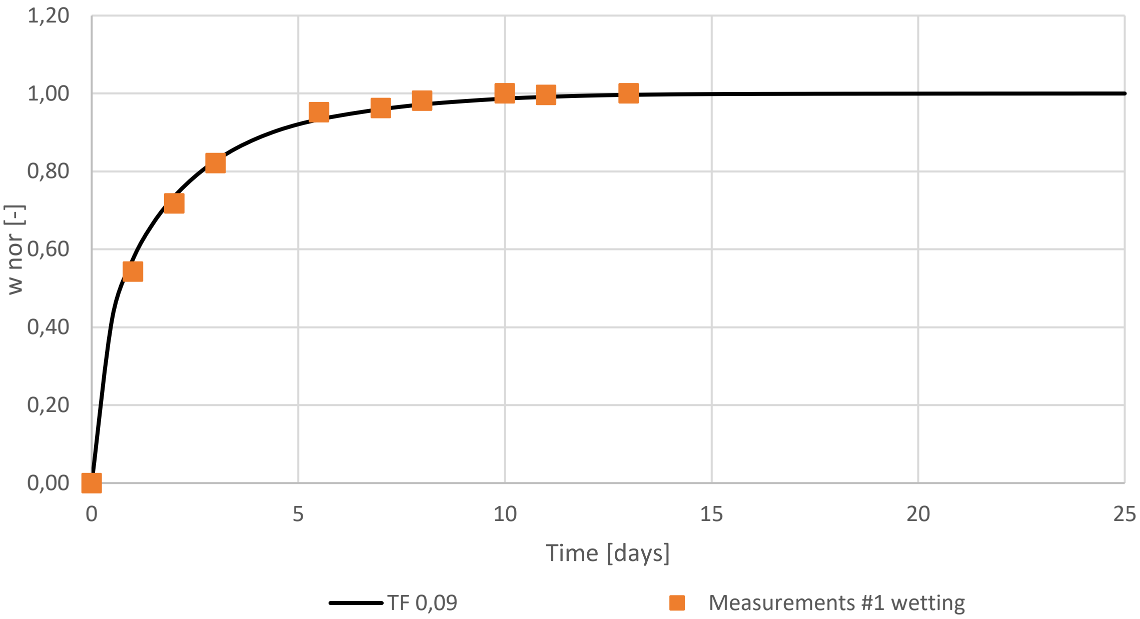

Figure 6-52 Numerical analyses #1wetting-τ 0,09

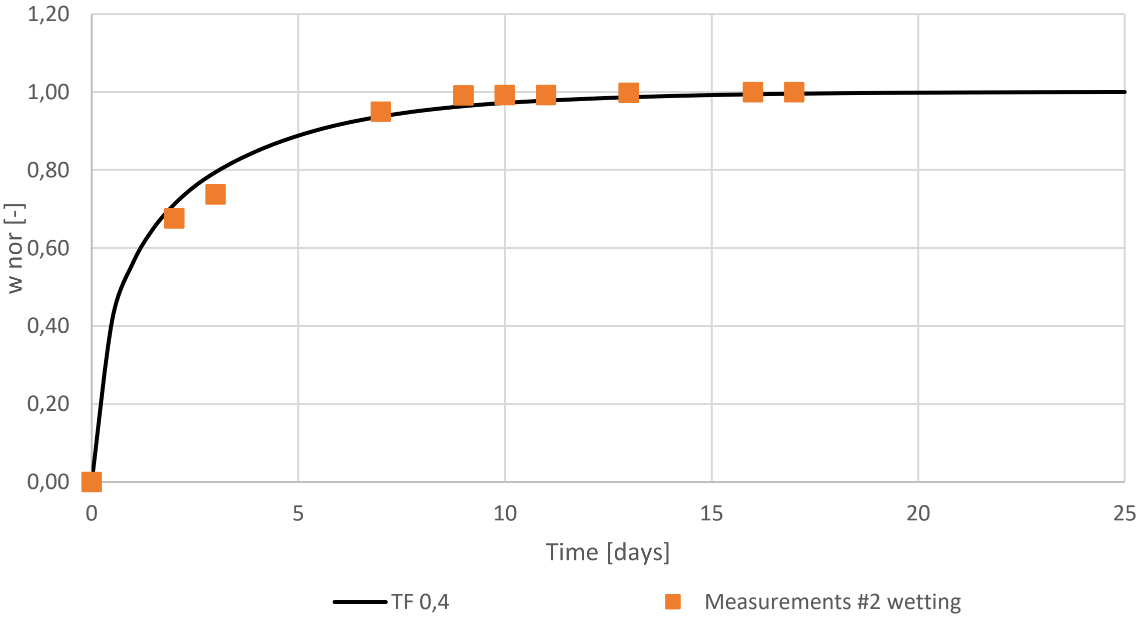

Figure 6-53 Numerical analyses #2wetting-τ 0,4

6.4.4.3 Molecular diffusivity of vapour through shales

The numerical analyses conducted allow to find the values of the tortuosity factor through back analysis for each steps of imposed total suction, by modelling the diffusion process of water vapour in an anisotropic medium.

In particular, the results obtained of τ were related with an average value of total suction at each step between the one at the initial condition and the one at the end of the step. The trend of the tortuosity factor was also found in terms of degree of saturation starting from the mean total suction converted with the linearized water retention curve.

The trend of the tortuosity factor versus total suction and degree of saturation are shown in *Figure 6-54* and *6-55*.

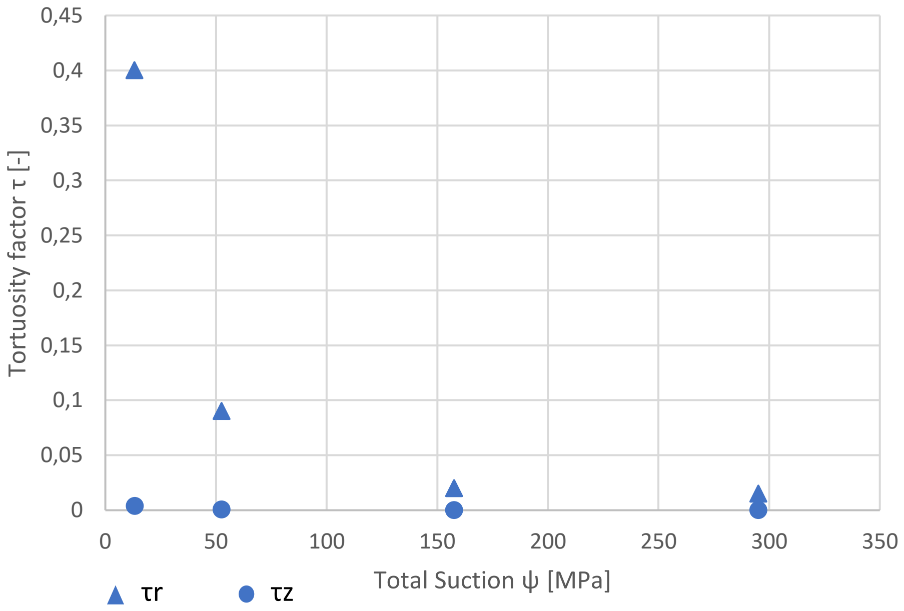

Figure 6-54 Relationship between the total suction and the tortuosity factor

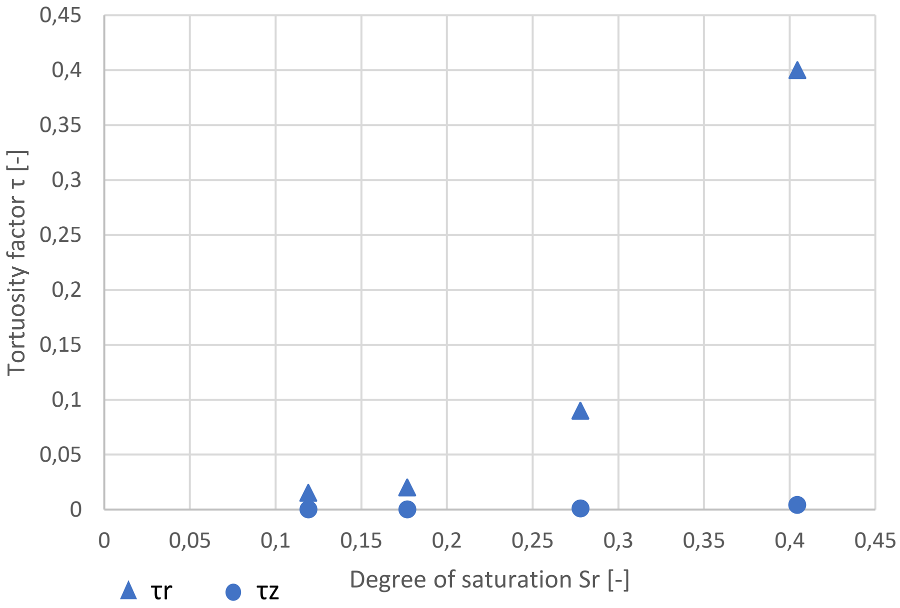

Figure 6-55 Relationship between the degree of saturation and the tortuosity factor

Starting from the tortuosity factors found, it was possible to determine the molecular diffusivity of vapour for the tested gas shales through *Equation 6-28,* which are reported in *Figure 6-56* and *6-57*.

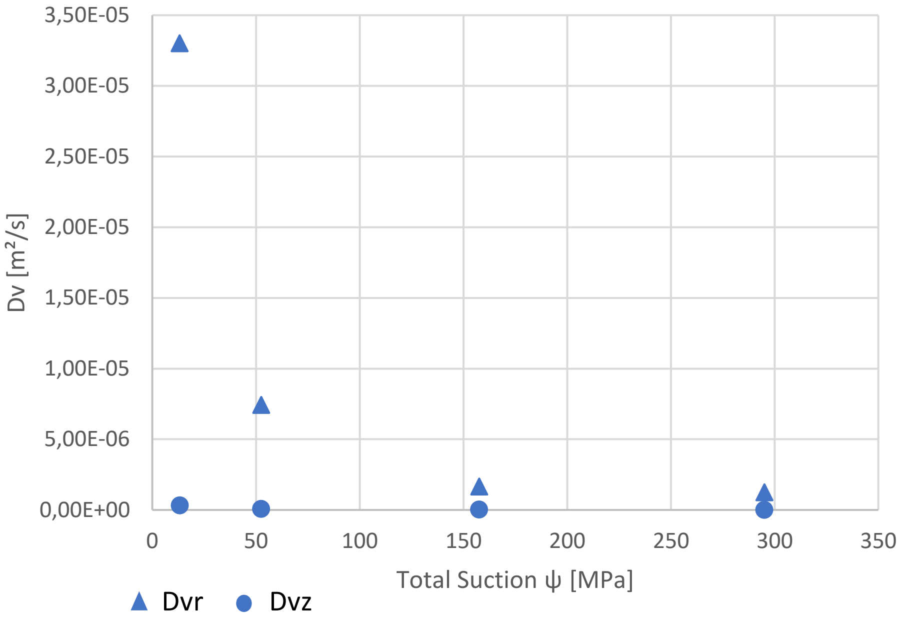

Figure 6-56 Relationship between the total suction and the molecular diffusivity

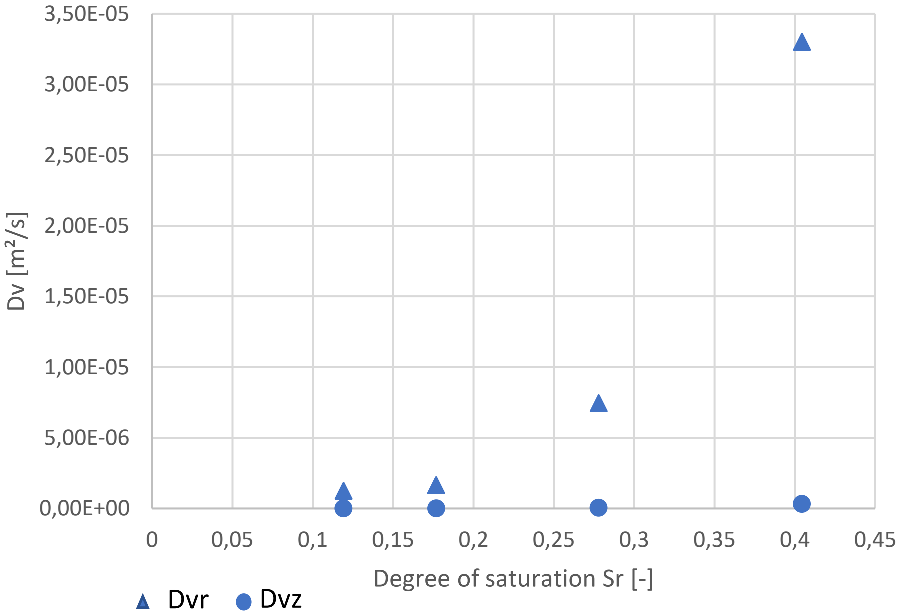

Figure 6-57 Relationship between the degree of saturation and the molecular diffusivity

6.5 Conclusions

All the results obtained of τ and Dv are reported in *Table 6-5*.

		wetting				**drying**			
		#1		**#2**		**#1**		**#2**	
anisotropy		**r**	**z**	**r**	**z**	**r**	**z**	**r**	**z**
5:1	τ	0,04	0,008	0,2	0,04	0,02	0,004	0,015	0,003
	Dv	3,30E-06	6,6E-07	1,65E-05	3,3E-06	1,65E-06	3,3E-07	1,24E-06	2,48E-07
10:1	τ	0,05	0,005	0,25	0,025	0,02	0,002	0,015	0,0015
	Dv	4,13E-06	4,13E-07	2,06E-05	2,06E-06	1,65E-06	1,65E-07	1,24E-06	1,24E-07
100:1	τ	0,09	0,0009	0,4	0,004	0,02	0,0002	0,015	0,00015
	Dv	7,43E-06	7,43E-08	0,000033	3,3E-07	1,65E-06	1,65E-08	1,24E-06	1,24E-08
1:1	τ	0,015	0,015	0,065	0,065	0,009	0,009	0,007	0,007
	Dv	1,2375E-06	1,24E-06	5,36E-06	5,36E-06	7,43E-07	7,43E-07	5,78E-07	5,78E-07

Table 6-5 Numerical analyses results

With the numerical study conducted and the implemented model, it was possible to reproduce the transient process of the water vapour diffusion observed during the experimental tests.

The value of the tortuosity factor could not be imposed in the simulations, as the anisotropy of the tested shales, referred to the diffusion process, is not known a priori.

Despite that, as it is possible to notice in *Table 6-5* the molecular diffusivity of vapour through shales decreases with the increase in the total suction and increses with the increase of the degree of saturation for each anisotropy tested.

The obtained trend, for each anisotropy taken into account, is not constituent with the expected behaviour of a single porosity medium. Due to the increase in the degree of saturation, the water uptake in the pore structure for a single porosity medium occludes the paths to the water vapour molecules. In these circumstances the available interconnected pore space for the vapour transport decreases with the increase of the water content at a macroscale. This make the vapour transport process to occur with some resistance.

When observing this phenomenon from a microscale prospective, the decrease in moisture diffusivity is also expected due to the expansion of clay grains that causes the closure of the space between grains.

However, in addition to this phenomenon the cracks' aperture has also been observed in the tomographic analyses along the wetting path.

The difference in the trend of the moisture diffusivity obtained to the one expected could be associated hence with the aperture of cracks. In fact, the cracks' aperture becomes a preferential path to the vapour molecules to enter in porous media as shales and represents a more effective channel for the vapour transport process, overshadows the clay swelling capacity process. According to that, the reason why the tortuosity factor increases with the increase of the degree of saturation could be appointed to the change in microstructure experienced from the geomaterial along the wetting.

The numerical analyses conducted leads to consider the importance of the role of crack aperture on the equilibration times as a result for the diffusion process.

7 Conclusions and further developments

The study conducted in this thesis leads to improve the knowledge of the behaviour of partially water saturated shales involved in the gas extraction by analysing the change in water content and in volume upon suction variation under free stress conditions. It focused on the behaviour of a gas shale core sample from south America.

In this chapter, all the research outcomes obtained, in terms of experimental results and numerical results, are reported.

Starting from some considerations, further research developments on gas shales are presented at the end of this chapter.

7.1 General conclusions

7.1.1 Experimental results

Initially the basic geotechnical characterization of the deep gas shale was conducted, highlighting some difficulties experienced during the experimental tests due to the peculiar features of shales.

In particular, the biggest uncertainty found was related to the grain density of the material, which was investigated using two different available techniques: the Helium pycnometer and the Water pycnometer technique. The impossibility to compare the results obtained with available data in literature, leads to consider both the values directly measured of ρ_s and compute with them, using given phase correlations, the other initial parameters such as the void ratio, porosity and the initial degree of saturation.

The following primary outcomes from the geotechnical characterization were obtained:

- the material presents a high value of TOC (TOC =5,51%) which is a reflection of the dark colour of the material and confirms the suitability of the material to be involved in the petroleum engineering field
- the material presents low value of initial water content (w = 0,54%) with respect to other soils, low porosity (n = 2,8-6,6%) and low value of void ratio (e = 0,029-0,071)
- in their native state, gas shales are partially water-saturated due to the presence of natural gas trapped in their pore space. The degree of saturation at the initial conditions was computed ranging between Sr = 20-46%.

The hydro-mechanical behaviour of the gas shales was investigated by advanced experiments with the aim of characterizing the material from a macro scale to a micro scale.

Different values of total suction were imposed to the material using the vapour equilibrium technique.

Due to the irregular shape of the specimens, it was necessary to prepare them using sand papers, paying attention to expose them to the lab environment less time as possible in order to avoid any water exchange between the specimens and the environment. Moreover, during the specimens' preparation it was observed the fissility of the material along the bedding planes.

In contrast to previous researches on other gas shales, the reduced dimensions of the tested specimens made impossible to glue the strain gauges in order to register the strain evolution upon suction variation. In fact, the deformations were measured using a micrometre.

The results obtained of the hydro-mechanical behaviour of the tested gas shales at a macroscale, reveal:

- the water retention capacity of the material in terms of water content and degree of saturation
- the swelling capacity and shrinkage capacity of the material due to wetting and drying
- the irreversibility in the behaviour of the gas shales in terms of water content and volumetric deformation
- the anisotropy of shales in terms of axial and radial deformations due to the orientation of the bedding planes. In details, the amount of strain parallel to the bedding observed is remarkably lower than that in the perpendicular direction both in wetting and drying paths.

During the tests conducted it was possible to observe a crack expansion due to the water uptake. This observed phenomenon leads to get further in details by other analyses at the microscale in order to understand the internal behaviour of the specimens upon suction variation.

The micro structural analyses of the tested gas shales were studied by micro-CT topographies. The tests conducted through the tomograph, allow to understand how the internal structure of the tested gas shale, changes upon suction variations.

The main outcomes from the investigation of the microstructural behaviour of the specimens reveal:

- the heterogeneities of shales in terms of different pyrite content for specimens that come from the same depth
- the shrinkage capacity in the drying path with no significant change in cracks' volume
- the swelling capacity associated with the increase of the cracks' volume during the wetting path. In particular the thickness of the cracks' aperture increases two-three times the value at the initial condition along the wetting path (from 10-20 μm to 35-45 μm). This change in microstructure explains the irreversible mechanical behaviour of the tested shales and the hysteresis of the water content registered.

The results found in this section demonstrate the importance to consider simultaneously the hydro-mechanical response of the tested material, and the role of microstructure which represents a key factor to predict the shale behaviour, its permeability and sealing capacity.

7.1.2 Numerical results

A preliminary model was developed in order to reproduce the experimental results in terms of changes in water content, due to suction variations, with time.

The numerical analyses were implemented in the Finite Element code COMSOL Multiphysics 5.5, allowing to define suitable values of the vapour diffusion coefficient for the tested gas shales.

Modelling the media as an isotropic continuum and transversally isotropic one, the diffusion process of water vapour was studied.

The trend of the diffusion coefficient versus total suction found leads to consider the importance of the role of cracks' aperture on the equilibration times. In fact, it increases with the decrease of total suction, which is not the one expected for a single porosity medium.

However, the trend obtained could be explained with the cracks' aperture that becomes a preferential path to the vapour molecules to enter in porous media as shales and represents a more effective channel for the vapour transport process.

7.2 Further developments

These further investigations proposed in this chapter could be useful in order to understand the behaviour of the tested material when it is exploited in the engineering fields. Further developments are proposed in order to understand the behaviour of shales in situ and at the laboratory scale.

The free stress conditions investigated in this research study, even if revealed important information about the response of the material, are not representative of the in situ conditions at which shales are found.

According to that, further investigation under confined conditions are suggested. What is expected is that under confined pressure, the volumetric response of the material and its cracks ′aperture will be lower than the one measured under free stress conditions.

Furthermore, it could be interesting to apply the strain gauges to the material under confined conditions and in free stress conditions in order to register the evolution of the deformative response of the material continuously.

With the aim of improving the results of the diffusion coefficient and how it varies due to the changes in total suction, from an experimental point of view, it could be set up a different protocol of study for the application of the VET. In details, smaller steps of total suction could be applied. This could be done in order to link the tortuosity factor found through back analysis with an average total suction which is not far from the initial conditions of the tested specimens at each step.

Moreover, the numerical model could be improved modelling also the swelling and shrinkage behaviour of the material, the presence of the bedding planes and defining the scale of anisotropy of the material.

References

Bashir H.; Wang Y. and Abbas A. 2016. “On Void Volume Determination in Clay Rich Shale.” *International Journal of Latest Trends in Engineering and Technology (IJLTET).*

Bear J. and Cheng A.H.-D. 2010. "Modeling Groundwater Flow and Contaminant Transport." *Modeling Groundwater Flow and Contaminant Transport*. Springer.

Blatz J; Cui Y. J. and Oldecop L. 2008. “Vapour Equilibrium and Osmotic Technique for Suction Control.” *Geotechnical and Geological Engineering*.

Boosari S. S. H.; Aybar U. and Eshkalak M.O. 2015. “Carbon Dioxide Storage and Sequestration in Unconventional Shale Reservoirs.” *Journal of Geoscience and Environment Protection*.

Chen F. H. 1988. “Foundations on Expansive Soils in Mexico.” *Elsevier*.

Deen, R. C. 1981. “Need for a schema for the classification of transitional (Shale) materials.” *Geotechnical Testing Journal*.

Delage P.; Cui Y.J. and Tang A. M. 2010. “On Radioactive Waste Disposal.” *Journal of rock mechanics and geotechnical engineering*.

Ewy R. T. 2014. “Shale Swelling/Shrinkage and Water Content Change Due to Imposed Suction and Due to Direct Brine Contact.” In: *Acta Geotechnica* 9.

Ferrari A.; Favero V.; Marschall P. and Laloui L. 2014. “Experimental Analysis of the Water Retention Behaviour of Shales.” *International Journal of Rock Mechanics and Mining Sciences*.

Ferrari A.; Minardi A.; Ewy R. T. and Laloui L. 2018. “Gas Shales Testing in Controlled Partially Saturated Conditions.” *International Journal of Rock Mechanics and Mining Sciences*.

Fisher L.; Gamble R. and Middlehurst J. 1981. “The Kelvin Equation and Capillary Condensation.” In: *Nature* 290(April): 575–76.

Fredlund D. G. and Rahardjo H. 1993. "Soil Mechanics for Unsaturated Soils." *Soil Mechanics for Unsaturated Soils*. John Wiley & Sons, Inc.

Fredlund D. G.; Rahardjo H. and Fredlund M.D. 2012. "Unsaturated Soil Mechanics in Engineering Practice" *Unsaturated Soil Mechanics in Engineering Practice*. John Wiley & Sons, Inc.

Gu L.; Ho C.K; Plumb O.A and Webb S.W. 1998. "Diffusion with condensation and evaporation in porous media" *American Society of Mechanical Engineers.*

Hammes U.; Hamlin H. S. and Ewing T. E. 2011. “Geologic Analysis of the Upper Jurassic Haynesville Shale in East Texas and West Louisiana.” *AAPG Bulletin*.

Heller R. and Zoback M. 2014. “Adsorption of Methane and Carbon Dioxide on Gas Shale and Pure Mineral Samples.” *Journal of Unconventional Oil and Gas Resources*.

Ingram R. L. 1953. “Fissility of Mudrocks.” *Bulletin of the Geological Society of America*.

Josh M.; Esteban L.; Delle Piane C.; Sarout J.; Dewhurst, D. N. and Clennell, M. B. 2012. “Laboratory Characterisation of Shale Properties.” *Journal of Petroleum Science and Engineering*.

Liu D.; Li Y.; Yang S. and Agarwal R.K. 2019. “CO 2 Sequestration with Enhanced Shale Gas Recovery.” *Energy Sources, Part A: Recovery, Utilization, and Environmental Effects*.

Liu X.; Zeng W.; Liang L. and Xiong J. 2016. “Experimental Study on Hydration Damage Mechanism of Shale from the Longmaxi Formation in Southern Sichuan Basin, China.” *Petroleum*.

Lu N. and Likos W. J. 2004 "Unsaturated soil mechanics". *Unsaturated soil mechanics*.John Wiley & Sons, Inc.

Makhanov K.; Dehghanpour H. and Kuru E. 2012. “An Experimental Study of Spontaneous Imbibition in Horn River Shales.” *Society of Petroleum Engineers - SPE Canadian Unconventional Resources Conference 2012, CURC 2012,*.

Minardi A.; Crisci E.; Ferrari A. and Laloui L. 2016. “Anisotropic Volumetric Behaviour of Opalinus Clay Shale upon Suction Variation.” In: *Geotechnique Letters*.

Minardi A. 2018. “Hydro-Mechanical Characterization of Gas Shales and Opalinus Clay Shale in Partially Saturated Conditions PAR.” 8315.

Molfetta A. and Sethi R. 2012. "Ingegneria degli acquiferi" *Ingegneria Degli Acquiferi*. Springer.

Monson P. A. 2008. “Simple Molecular Model.” *Adsorption Journal Of The International Adsorption Society*.

Pearson J.R. 2000 "Theory and Application of Transport in Porous Media" *Journal of Fluid Mechanics.*

Péron H.; Hueckel T. and Laloui L. 2007. "An Improved Volume Measurement for Determining Soil Water Retention Curves." *Geotechnical Testing Journal*.

Pham Q. T.; Vales F.; Malinsky L.; Nguyen M.D and Gharbi H. 2007. "Effects of Desaturation-Resaturation on Mudstone." *Physics and Chemistry of the Earth*.

Philip J.R. and De Vries D.A. 1957. "Moisture movement in porous materials under temperature gradients" *Eos, Transactions American Geophysical Union.*

Pintado X.; Lloret A. and Romero E. 2009. "Assessment of the Use of the Vapour Equilibrium Technique in Controlled-Suction Tests." *Canadian Geotechnical Journal*.

Rawls W. J.; Pachepsky, Y. A.; Ritchie, J. C.; Sobecki, T. M. and Bloodworth, H. 2003. "Effect of Soil Organic Carbon on Soil Water Retention." *Geoderma* 116.

Romero E. 2001. "Controlled Suction Techniques." In: *4º Simpósio Brasileiro de Solos Nâo Saturados.*

Tarantino A. 2013. "Basic Concepts in the Mechanics and Hydraulics of Unsaturated Geomaterials." In: *Mechanics of Unsaturated Geomaterials*. Wiley-ISTE.

Underwood L. B. 1966. "Classification of Shales." *Journal of soil mechanics and foundations division* 91(117): 295–316.

Wan M.; Delage P.; Tang A. M. and Talandier J. 2013. "Water Retention Properties of the Callovo-Oxfordian Claystone." *International Journal of Rock Mechanics and Mining Sciences*.

Wentworth C. K. 1922. “A Scale of Grade and Class Terms for Clastic Sediments.” *The Journal of Geology*.

Yagiz S. 2001. “Overview of Classification and Engineering Properties of Shales for Design Considerations.” *Construction and Materials Issues 2001*: 156–65.

Acknowledgments-Ringraziamenti

Is this the end? I'm not sure, but this stop is amazing!

I would like to deeply thank you all the LMS and LEMR teams for giving me the opportunity to develop my master thesis in a dynamic environment, helping me in the laboratory during my activities and supporting me with all my struggles during my stay in Lausanne. A special thank you goes to Jinu who shared with me his research plan and introduced me in the "shale's world"; Patrick who tough me all the lab secrets and Gary who helped me with the tomographic analyses, spending with me hilarity moments during the Avizo's loading. I would like to thank you my LMS ladies, la mia Salvatrice Eleonora, un mix perfetto tra una sorella maggiore e un'insegnante paziente e sempre disponibile; Angelica per essere stata la certezza nei mei weekend in laboratorio and Eleni, who was always ready to motivate me during my study. But Lausanne would not have been the same without my favorite PhD students: Federica, Salvatore and Chiara, my special officemate Salma, and my sweet friend Antonia, I sincerely have to thank you a lot guys!

Un immenso grazie va anche ai miei colleghi al mio ritorno al Politecnico, per avermi accolto nello stesso luogo che ho frequentato per anni, permettendomi di viverlo sotto un'altra chiave e soprattutto per avermi aiutato nella stesura conclusiva del mio lavoro.

E anche se la tesi racchiude un po' tutto il percorso, il cammino per la laurea ammetto non è stato facile, e per me si può riassumere in tre 3S: scleri, sacrifici e soddisfazioni.

Un grazie infinito va a chi ha iniziato con me questa nuova avventura: ai "miei ragazzi" e Giorgia, che hanno rappresentato in tutti questi anni la mia famiglia "torinese"; ad Antonio, coscienza dei miei giorni e Fabio piacevole scoperta di casa in campo nordico.

Un rapido sguardo all'indietro mi riporta su quel treno cancellato il giorno del test di ingresso al Poli, che come dire..era un segno divino che non ho colto ai tempi; eppure oggi ringrazio sia la mia testardaggine nell'essere arrivata a questo traguardo che i miei due fedeli compagni di viaggio, senza i quali non ce l'avrei mai fatta. Con loro dentro e fuori l'università ne abbiamo passate tante e non smetterò mai di ringraziare Ciccio per avermi insegnato a credere in me stessa e nelle mie capacità e per essere quell'amico dalla risposta pungente ma sempre schietta e sincera e Giorgia, per avermi mostrato che le cose condivise a volte possono sembrare più leggere e per essere così diversa da me eppure cosi vicina da abbattere qualsiasi ostacolo.

Grazie a Giammarco, Simone, Daniele e alla fotocopia della mia persona, Laura, per aspettarmi sempre al mio ritorno, o accogliermi in altri stati, ma soprattutto per tenere viva un'amicizia decennale preziosissima.

Il più grande grazie va alla mia famiglia, soprattutto alle mie sorelle Anna e Lisa che mi hanno sempre appoggiato ed incoraggiato nelle mie scelte. Voi due siete il mio punto di riferimento più grande, che supera tempo e distanza.

Infine voglio ringraziare la mia terza sorella, Babbi, per essere sempre al mio fianco, per aver condiviso la scelta dell'università, il trasferimento, la casa ed ogni gioia e dispiacere in tutti questi anni. Grazie per essere il ponte tra quella che ero e quella che sto diventando, con te ogni cambiamento è più dolce e facile.

So, right now, is this the end? Final chapter, final page, final destination of this journey, tomorrow I will leave again.

"There's gotta be more

I know there's more, there's always more

One day I'll decide to roll with the tide

And I'm gonna see

(Moana stand tall)

I will cross the divide, I will ride

I will see what's on the other side

(Moana stand proud)

With the ocean as my guide, on the tide

I will go where no one's ever been before

There's always more "

Moana

from "Moana-Disney"